Titre: Title:	Rotary power flow controller (RPFC) performance in asymmetrical operation of power system
Auteur: Author:	Tao Peng
Date:	2004
Type:	Mémoire ou thèse / Dissertation or Thesis
Référence: Citation:	Peng, T. (2004). Rotary power flow controller (RPFC) performance in asymmetrical operation of power system [Master's thesis, École Polytechnique de Montréal]. PolyPublie. https://publications.polymtl.ca/7297/

UNIVERSITÉ DE MONTRÉAL

ROTARY POWER FLOW CONTROLLER (RPFC) PERFORMANCE IN ASYMMETRICAL OPERATION OF POWER SYSTEM

TAO PENG
DÉPARTEMENT DE GÉNIE ÉLECTRIQUE
ÉCOLE POLYTECHNIQUE DE MONTRÉAL

MÉMOIRE PRÉSENTÉE EN VUE DE L'OBTENTION
DU DIPLÔME DE MAÎTRISE ÈS SCIENCES APPLIQUÉES
(GÉNIE ÉLECTRIQUE)
Janvier 2004

Your file Votre référence
ISBN: 0-612-90853-4
Our file Notre référence
ISBN: 0-612-90853-4

UNIVERSITÉ DE MONTRÉAL

ÉCOLE POLYTECHNIQUE DE MONTRÉAL

Ce mémoire intitulé:

ROTARY POWER FLOW CONTROLLER (RPFC)
PERFORMANCE IN ASYMMETRICAL OPERATION OF POWER SYSTEM

Présenté par: PENG Tao

En vue de l'obtention du diplôme de : Maîtrise ès sciences appliquées

a été dûment accepté par le jury d'examen constitué de :

M. ROY Gilles, président

M. OLIVIER Guy, membre et directeur recherche

M. BA Amadou-Oury, Ph.D., ing., membre et co-directeur recherche

M. MARCEAU Richard, Ph.D., ing., membre

DÉDICACE

À ma très chère femme

À mes chers parents

À mon très cher fils

ACKNOWLEDGEMENT

Ce mémoire a été réalisé grâce à un projet de l'Institut de Recherche d'Hydro-Québec (IREQ). Mes remerciements vont particulièrement à mon co-directeur, M. Amadou-Oury BA de l'IREQ.

Special thanks to Mr. Amadou-Oury BA, a friendly and generous gentleman, who has given me plenty of help and support through the whole project, and an opportunity to work as a trainee at IREQ so that I could apply what I have learned to the real world and get more familiar with Hydro-Québec.

Also thanks to Mr. Alpha Oumar BARRY from IREQ, who gave me a great and valuable helps in effectively and correctly using Simulation-Power-System (SPS).

Thanks to Mr. Xuan-Dai DO of the Electrical Department of École Polytechnique de Montréal for his academic and partial financial support.

Thanks to Mr. Guy OLIVIER of Electrical Department of École Polytechnique de Montréal for his partial financial support.

I am very grateful to the members of the jury for their comprehensive review of this Master dissertation.

At last, I would like to thank my wife, HE, Zhizhen, and my cute son, Harry, and my parents in China, for their continuous encouragement and support.

RÉSUMÉ

La nécessité croissante d'accroître la capacité de transit de puissance à travers les réseaux est un problème actuellement aigu, non seulement à cause des problèmes relatifs au *droit de passage* de nouvelles lignes ou à la congestion des lignes existantes, mais aussi à cause de la difficulté relative à la répartition des responsabilités économiques dans l'actuelle situation de déréglementation de l'énergie électrique.

Aussi, l'utilisation du Régulateur de Puissance Rotatif (RPR), un compensateur dont le temps de réponse est moins rapide que celui du UPFC mais de loin moins cher que ce dernier, devient une intéressante alternative pour augmenter la capacité de transit de puissance, comparativement à la construction de nouvelles lignes ou à l'installation de la compensation classique. De plus, il a été prouvé que l'exploitation asymétrique de corridors formés de lignes électriques, dont le principal atout est de prendre avantage des défauts, contribue aussi à l'accroissement de capacité et des limites de sécurité du réseau.

Ce présent mémoire de maîtrise est consacré à l'étude, en régime permanent, des performances du RPR dans des conditions d'exploitations symétriques et asymétriques d'un corridor de transport constitué de deux lignes. On y propose tout d'abord le circuit équivalent et un modèle macroscopique du RPR formé de deux transformateurs conventionnels (un shunt l'autre série) et de deux transformateurs déphaseurs rotatifs (TDR), pour ensuite simuler le modèle du RPR ainsi que le réseau qui lui est associé, à l'aide du logiciel SPS/Matlab (Simulation-Power-System) développé à IREQ (l'Institut de Recherche d'Hydro-Québec) et du logiciel Matlab/Simulink.

Les résultats des simulations ont montré l'utilité du RPR pour l'accroissement du transit de puissance aussi bien dans le cas de l'exploitation symétrique que celui de l'exploitation asymétrique du corridor de transport. Enfin, les courbes obtenues dénotent de la sensibilité des débuts de transitoires par rapport au nombre de paire de pôles, et

prouvent la possibilité de la diminution du temps de réponse du RPR avec l'augmentation du nombre de paires de pôles. Le mémoire propose enfin quatre recommandations pour la poursuite de travaux futurs dans ce domaine.

CONDENSÉ EN FRANÇAIS

0.1 Introduction

Le réglage du transit de puissance à travers un corridor formé de N lignes de transport peut être réalisé en faisant varier soit:

- l'amplitude de la tension de l'extrémité de départ des lignes;
- l'amplitude de la tension de l'extrémité d'arrivée des lignes;
- l'écart des angles des tensions des extrémités de départ et d'arrivée;
- l'impédance des lignes de transport;
- toute combinaison des paramètres cités ci-dessus.

Grâce à la technologie des FACTS (Flexible Alternating Current Transmission Systems), une panoplie de dispositifs de compensation et de régulateurs de puissance ont été développés pour permettre un réglage flexible de la puissance en vue d'une l'exploitation adéquate des réseaux. Comme le transformateur déphaseur conventionnel, le transformateur déphaseur rotatif (ou communément appelé transformateur à fréquence variable) est classé parmi les régulateurs séries.

Ce mémoire est consacré à l'étude de performances, dans des conditions d'exploitation symétrique et asymétrique du réseau, du Régulateur de Puissance Rotatif (RPR) dont la composante fondamentale est constituée de deux unités identiques de transformateurs déphaseurs rotatifs (TDR) (figure 3.2). Le mémoire introduit tout d'abord, dans le chapitre 2, à la stratégie de *l'exploitation asymétrique* d'un réseau électrique pour consacrer le chapitre 3 à l'établissement des schémas équivalents des différentes composantes du RPR. Elle propose ensuite, dans le chapitre 4, un modèle en régime permanent du RPR ainsi que son système de commande implanté dans l'environnement SPS développé à l'IREQ. Enfin, les chapitres 5 et 6 sont respectivement consacrés à la simulation des performances du RPR dans les conditions d'exploitation *symétrique et asymétrique du réseau.*

0.2 Introduction à l'exploitation asymétrique du réseau

Lorsqu'un réseau électrique est exploité par la stratégie symétrique qui est basée sur la règle de coupure de toute la ligne triphasée indépendamment de la nature de contingences (défaut monophasé, biphasé ou triphasé, etc.), la capacité, la sécurité, la fiabilité, la flexibilité et l'économie de ce dernier sont réduites.

Du point de vue exploitation, toute solution permettant de transporter la puissance sans aucune détérioration de l'intégrité du réseau de transport est recommandable. En effet, faire transiter de l'énergie de manière sécuritaire à travers une ligne dont l'une des trois phases est hors tension (à cause d'un défaut), conduit à un gain de capacité de transit au profit de la stratégie d'exploitation en jeu. Cela signifie que chaque fois qu'une ligne, incapable être symétriquement exploitée comme une seule entité formée de trois circuits non séparés, pouvait être exploitée en tant que trois entités distinctes mises ensemble, de manière à alimenter les charges de la phase non saine pendant la durée de l'élimination du défaut, cela se traduirait en un considérable gain en capacité de transport, flexibilité et économie.

Le travail de recherche [20] a déjà montré, pour l'exploitation asymétrique, qu'un nombre de deux (au moins) lignes parallèles formant un corridor est suffisant pour que les séquences inverses et homopolaires des déséquilibres dus à l'ouverture d'une seule phase (par exemple la phase A) d'une ligne soient considérées comme négligeables. C'est pourquoi, le schéma de compensation proposé est relatif au seul courant de séquence positive circulant dans la phase non saine (phase A) du corridor, ce qui signifie qu'il est possible d'exploiter une ligne triphasée ayant une phase non disponible (ouverte), sans compromettre l'intégrité du réseau : c'est ce que l'on définie par l'*exploitation asymétrique (E.A)* d'un réseau. Le concept de l'E.A. du réseau considère le système triphasé comme trois indépendants circuits monophasés fonctionnant de manière individuelle et

découplée. Cela signifie que l'on peut transférer au schéma triphasé, les résultats des travaux obtenus des trois schémas monophasés. Ainsi, les déséquilibres dus à l'exploitation asymétrique sont confinés par filtrage au sein de la même ligne, grâce à l'action d'une adéquate compensation placée aux deux extrémités du corridor.

À cet effet, la technologie des devient utile à l'exploitation asymétrique du réseau. Il existe deux types de stratégies de mise en œuvre associées à l'exploitation asymétrique : la stratégie globale (ou de système) et la stratégie ponctuelle (ou localisée) [20]. Dans ce mémoire, la stratégie de type système a été retenue, c'est-à-dire que les compensations série et shunt sont respectivement représentées par une source de tension et une source de courant qui pourraient être issues de dispositifs sans ou à base d'électrique de puissance. Dans le cadre de ce travail, un dispositif électromagnétique (formé de machines-transformateurs) dépourvu d'électronique de puissance a été retenue pour produire la source de tension, alors que la source de courant est obtenue à partir de simples condensateurs.

Du point de vue compensation, ces sources de tension et de courant pourraient être placées soit à l'extrémité de départ, soit à l'extrémité d'arrivée du corridor constitué des lignes, dont celle incluant la phase en défaut. Pour ce travail, on a retenu l'extrémité de départ du corridor comme emplacement des sources de tension et de courant; la valeur de la compensation (en courant et tension) est évaluée de telle manière à préserver les mêmes conditions de l'écoulement de puissance durant les périodes avant et pendant contingence.

Il va sans dire que l'exposé ci-dessus présenté dans le cadre de l'approche asymétrique peut être aussi bien tenu pour le cas de l'exploitation symétrique (E.S.) du réseau qui correspond à la perte des trois phases d'une même ligne du corridor; dans ce dernier cas la compensation serait appliquée aux trois phases symétriques en défaut.

0.3 Le circuit équivalent du régulateur de puissance rotatif (ou RPR)

Le RPR est constitué de deux transformateurs (l'un shunt et l'autre série) et deux identiques unités de transformateurs déphaseurs rotatifs (TDR, RPST en anglais) opérant en mode arrêt (ou de rotor bloqué) [12,13].

L'enroulement primaire du transformateur shunt est connecté à la ligne alors que son secondaire alimente les rotors des deux TDR dont les enroulements rotoriques sont connectés en parallèle et les statoriques en série. Ces enroulements statoriques alimentent le secondaire du transformateur série dont le primaire est branché en série avec la ligne. La tension de sortie de chacun des TDR est fonction du rapport des nombres de spires et du décalage angulaire entre le rotor et le stator. De ce fait, on pourrait contrôler l'écoulement de puissance du réseau par simple injection d'une tension ajustable du secondaire du transformateur série.

Le schéma équivalent monophasé du TDR (RPST) a été représenté par le circuit équivalent du classique transformateur dont le secondaire est ramené au primaire (ou le rotor ramené au stator) ayant un rapport de transformation et un angle de déphasage correspondant au déphasage électrique entre le rotor et le stator (i.e. produit du nombre de paire de pôles par l'angle mécanique du rotor par rapport au stator) (voir figure 3.5). C'est pourquoi, un TDR, avec un nombre élevé de paire de pôles, produirait un plus grand angle électrique malgré un faible angle de rotation.

Ensuite, le schéma équivalent de l'ensemble des deux TDR, dont les bobines rotoriques sont en parallèle et les statoriques en série, a été établi comme celui d'un moteur à induction, opérant en mode de rotor bloqué, et dont les rapports de transformation, l'angle de déphasage et l'impédance équivalente (ramené au primaire) sont exprimés en fonction des décalages angulaires des rotors des TDR (cf. figures 3.6 à 3.7).

Enfin, le schéma équivalent du RPR (cf. figure 3.9) a été représenté par celui du moteur à induction, opérant en mode de rotor bloqué, et dont le rapport de transformation, le déphase angulaire et l'impédance équivalente sont fonctions des positions angulaires des rotors des deux TDR: ces différents grandeurs sont déterminées à partir des paramètres du RPR.

0.4 Modélisation du RPR

Etant donné que le RPR est relié à la ligne en deux endroits: en série via le secondaire du transformateur série, et en parallèle à travers le primaire du transformateur shunt, alors le modèle du RPR correspond à celui d'un dispositif à connexion shunt-série, tels le UPFC (Unified Power Flow Controller), le transformateur déphaseur, etc.

Si la branche série du RPR a été représenté par une source de tension avec sa propre impédance interne en série avec la ligne, la branche shunt a été modélisée par une source de courant en parallèle. Aussi, la source de tension réagit comme une compensation série alors le courant inductif réagit comme une compensation shunt inductive qui va absorber la puissance réactive du réseau (voir figure 4.1). C'est pourquoi il faudrait prévoir une source de puissance réactive capable d'au moins compenser la branche shunt (cf. figure 4.2).

La conception du système de régulation du RPR se ramène au réglage des positions angulaires des deux TDR, selon la valeur désirée de la source de tension à injecter en série. La valeur de tension a été déterminée à partir des conditions initiales.

Le système de régulation du RPR est constitué de deux entrées et deux sorties (figure 4.3). Une des entrées correspond à la différence entre la valeur efficace de la tension désirée, injectable via le transformateur série, et celle de la tension mesurée sur la ligne; et la seconde entrée représente l'écart entre la phase de la tension désirée et celle de la

tension de mesure. Les deux sorties correspondent aux angles rotoriques des deux TDR. Chacune de ces entrées passe par un correcteur PI (proportionnel/intégral) et chacune des sorties provient d'un régulateur (le régulateur du RPR) dont l'entrée correspond aux sorties des contrôleurs PI qui opèrent mathématiquement. Il est crucial de trouver les bonnes valeurs de ces paramètres. Le modèle du RPR ainsi que son système de régulation ont été développés et programmés dans l'environnement Matlab/Simulink/SPS.

0.5 Simulations des performances du RPR dans le cas d'exploitation symétrique

Le réseau simulé correspond à un corridor de transport constitué de deux lignes triphasés en parallèle aux extrémités desquelles sont branché des groupes alternateur/transformateur. Le départ du corridor est, via un transformateur élévateur, alimenté par une machine synchrone fonctionnant en régime génératrice; alors que l'extrémité d'arrivée est connectée au second groupe formé d'un transformateur abaisseur et d'une machine synchrone en régime moteur. Le RPR est enfin branché en connexion shunt-série, côté départ, entre le transformateur élévateur et la barre de départ du corridor (voir figures 5.1 et 5.2).

Dans tout ce travail, le terme '*exploitation symétrique*' réfère au mode d'opération du réseau dans lequel le RPR et la compensation shunt triphasée capacitive sont en service, avec l'indisponibilité permanente de la première ligne triphasée du corridor de transport.

Deux cas de simulations ont été effectués dans les conditions de l'exploitation symétrique : le cas n°1 (voir pages 58 à 69) correspond à l'utilisation d'un RPR ayant un nombre de paire de pôles égal à 1, et le cas n°2 (voir pages 69 à 80) représente l'utilisation d'un RPR avec un nombre de paires de pôles égal à 6.

Ces deux cas de simulations ont conduit aux résultats ci-dessous.

- L'utilisation du RPR et de la compensation shunt capacitive permet de recréer les conditions de l'écoulement de puissance de la situation de pré-contingence.
- Les parties initiales (0.4~1s) des transitoires des grandeurs électriques simulées sont sensibles à la position du rotor du TDR doté du nombre de paire de pôle élevé.
- Plus le nombre de paires de pôles du TDR est élevé, moins importants sont les déplacements des rotors.
- Le nombre de paires de pôles n'affecte pas les régimes permanents des courbes des grandeurs électriques du réseau simulé.

0.6 Simulations des performances du RPR dans le cas d'exploitation asymétrique

Pour l'exploitation asymétrique, le réseau simulé correspond à celui du cas symétrique, avec la seule différence qu'ici, le défaut étant monophasé, les applications du RPR et de la compensation shunt capacitive sont monophasées (et placées sur la phase non saine) (cf. figures 6.1 et 6.2).

Dans tout le travail, le terme '*exploitation asymétrique*' réfère au mode d'opération du réseau dans lequel le RPR et la compensation shunt monophasée sont en service sur l'unique phase en défaut (phase A), avec la permanente non disponibilité de la phase A de la première ligne du corridor de transport.

Aussi, deux cas de simulations ont été réalisés dans les conditions de l'exploitation asymétrique : le cas n° 3 (pages 90 à 103) pour lequel le RPR utilisé a un nombre de paires de pôles égal à 1, et le cas n° 4 (pages 104 à 118) où le RPR a un nombre de paires de pôles égal à 6. Ainsi, on a porté une particulière attention non seulement sur le fonctionnement du RPR comme un ensemble, mais aussi sur l'impact du nombre de paires de pôles sur les grandeurs électriques.

Enfin, ces deux cas de simulations ont abouti aux résultats ci-dessous.

- Dans la stratégie asymétrique, l'utilisation du RPR et de la compensation shunt capacitive monophasée permet de recréer les conditions de l'écoulement de puissance de la situation pré-contingence, par simple filtrage des courants et tensions de séquences négatives et homopolaires.
- Les parties initiales (0.4~1s) des transitoires des grandeurs électriques simulées sont sensibles à la position du rotor du TDR doté du nombre de paire de pôle élevé.
- Plus le nombre de paires de pôles du TDR est élevé, moins importants sont les déplacements des rotors.
- Le nombre de paires de pôles n'affecte pas les régimes permanents des courbes des grandeurs électriques du réseau simulé.

0.7 Conclusions

Puisque que le système triphasé peut être considéré comme un système formé de trois circuits monophasés pouvant fonctionner de manière individuelle et découplée, les résultats de simulations ont prouvé que l'exploitation asymétrique d'un réseau de transport procure des solutions pratiques et économiques non seulement sur le plan de la flexibilité d'exploitation mais surtout du point de vue accroissement de la capacité de transit de puissance d'un réseau de transport. En effet, lorsqu'une phase est non disponible (à cause d'un défaut), les résultats corroborent le fait qu'il est possible de continuer à transiter les mêmes puissances, grâce aux mesures correctives prévues dans le mode d'exploitation asymétrique.
La théorie développée a été utilisée pour déterminer les conditions dans lesquelles est préservé le critère de conservation des amplitudes et phases des grandeurs électriques (courants, tensions, puissances), en présence de perte d'une phase ou d'une ligne entière.

Il a été démontré que le RPR, en tant que source de tension série injectée, peut être utilisé non seulement dans les conditions d'exploitation symétrique, mais aussi dans celles de l'exploitation asymétrique. D'ailleurs, pour cet effet, le RPR a été modélisé comme une source de tension injectée en série avec la ligne et une source de courant en parallèle. Enfin, avec le RPR associé à la compensation capacitive, on est arrivé à conserver les valeurs (en amplitudes et phases) des courants et tensions aux deux barres d'extrémités, malgré les défauts monophasé et triphasé.

La sensibilité des débuts des transitoires des courbes représentant les grandeurs électriques (courants, tensions et puissances) par rapport au nombre de paire de pôles du RPR a aussi été mise en valeur. En effet, plus le nombre de paire de pôle est élevé, plus il a une influence sur les transitoires de courbes et moins les rotors effectuent de rotations.

Les principales recommandations relatives aux futurs travaux sont les suivantes :

- Refaire tous les essais de simulations avec les transformateurs élévateur et abaisseur respectivement couplés en Δ-Y_g et Y_g-Δ.
- Effectuer les mêmes simulations en temps discret.
- Réaliser des simulations dans lesquelles on inverse le sens du transit de puissances.
- Développer enfin, dans l'environnement Matlab/SPS, un modèle microscopique du transformateur déphaseur rotatif du RPR.

TABLE OF CONTENTS

LIST OF SIMULATION CASES

LIST OF TABLES

LIST OF FIGURES

LIST OF FIGURES (continue)

Figure No. **Page No.**

LIST OF FIGURES (continue)

Figure No. **Page No.**

LIST OF FIGURES (continue)

Figure No. **Page No.**

LIST OF FIGURES (continue)

Figure No. **Page No.**

LIST OF ABBREVIATIONS

A.O.	- Asymmetrical Operation
com	- compensation
contr	- control
E.A.	- Exploitation Asymétrique
E.S.	- Exploitation Symétrique
FACTS	- Flexible Alternating Current Transmission Systems
HV	- High Voltage
IREQ	- l'Institut de Recherche d'Hydro Québec
LV	- Low Voltage
PI	- Proportional / Integral
ref	- reference
rms/RMS	- Root-Mean-Square
RPFC	- Rotary Power Flow Controller
RPR	- Régulateur de Puissance Rotatif
RPST	- Rotary Phase-Shifting Transformer
rt	- rotary transformer
se	- series
sh	- shunt
S.O.	- Symmetrical Operation
SPS	- Simulation-Power-System
TDR	- Transformateur Déphaseur Rotatif
TFV	- Transformateur Fréquence Variable
UPFC	- Unified Power Flow Controller
VFT	- Variable Frequency Transformer

CHAPTER 1 INTRODUCTION

1.1 Review of power system operation

Consider a very simple power system, which is shown in Figure 1.1, through N parallel transmission lines from a surplus generation area that is represented by an equivalent generator ($\overline{V}_{source}$) and an impedance (Z_{source}) on the left (sending-end), to a deficit generation area which is represented by another equivalent generator ($\overline{V}_{load}$) and impedance (Z_{load}) on the right (receiving-end).

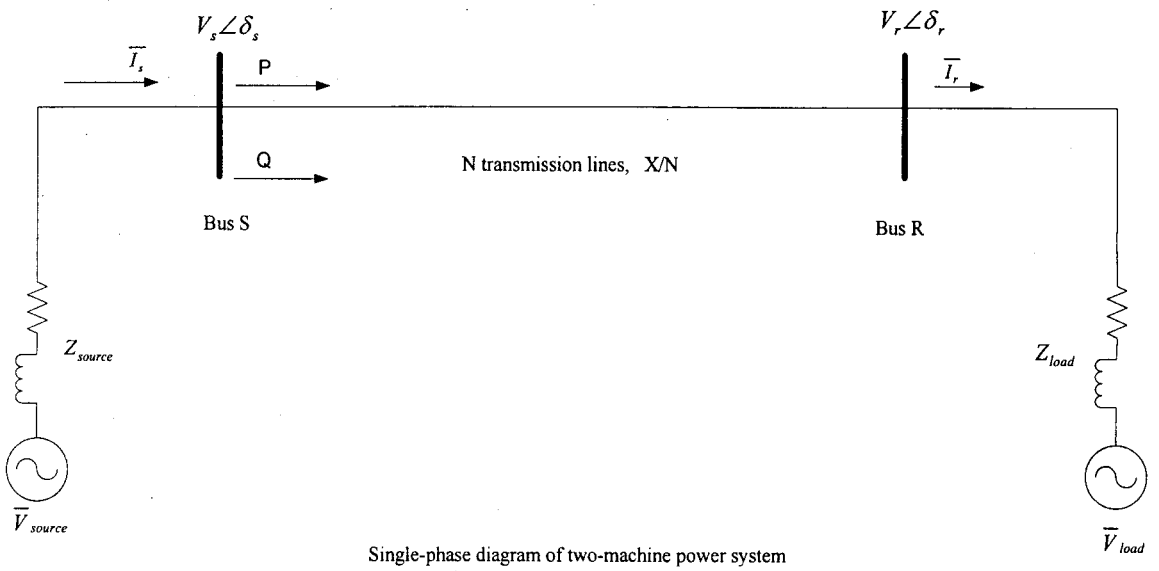

Figure 1.1 - Single-phase diagram of two-machine power system

Where,

N - number of transmission lines

X - reactance of each transmission line (neglect the resistance of the transmission line)

P - transmitted active power at Bus S through the transmission lines

Q - transmitted reactive power at Bus S through the transmission lines

From Figure 1.1, we have,

$$P = \frac{V_s \cdot V_r \cdot \sin(\delta_s - \delta_r)}{X/N} = N \cdot \frac{V_s \cdot V_r \cdot \sin\delta}{X} \tag{1-1}$$

$$Q = \frac{V_s (V_s - V_r \cdot \cos(\delta_s - \delta_r))}{X/N} = N \cdot \frac{V_s (V_s - V_r \cdot \cos\delta)}{X} \tag{1-2}$$

$\delta = \delta_s - \delta_r$ - angle difference between the voltages of the sending- and receiving-ends.

Refer to (1-1) and (1-2), P and Q can be controlled by:

(1) Varying V_s;
(2) Varying V_r;
(3) Varying δ;
(4) Varying X;
(5) Combinations of the above.

The simplest and most direct method to control P and Q is to regulate the output(s) of either of $\overline{V}_{source}$ and $\overline{V}_{load}$, or both of $\overline{V}_{source}$ and $\overline{V}_{load}$. But their regulating capacities are limited due to the machines' capacities. If we introduce certain compensations into the power system, P and Q can be controlled with flexibility, for example, if X is decreased to 0.9·X by inserting a series capacitor or δ is increased to 1.1 δ (<90°) by inserting a phase-shifter, the transmitted powers P and Q will be increased.

Thanks to FACTS (Flexible Alternating Current Transmission Systems) technology, a variety of compensation devices and controllers have been developed to meet the requirements for the power system operation and control. Conventional phase-shifting

transformers are catalogued into the series controllers for power flow control. The conventional phase-shifting transformers are classified into general phase-shifting transformers and rotary phase-shifting transformers. This Master dissertation will deal with the rotary phase-shifting transformers (RPSTs) that are the main components of an Rotary Power Flow Controller (RPFC).

1.2 Review of the application for an RPFC

The papers about the RPFC application were presented during 2000 to 2001 [2][3][4][5]. The application for an RPFC has been studied at the 500 kV Sunen substation by Chubu Electric Power Company (CEPCO, Japan). The RPFC model was designed and manufactured by GE Power Systems Energy Consulting for installation at the CEPCO's hybrid simulator, Power System Analyzer (PSA) in Nagoya, Japan. The dynamic performance of the RPFC model has been demonstrated successfully. The model is satisfactory for the PSA study of RPFC application in the CEPCO 500 kV circuit.

1.3 Master dissertation objectives

The objectives of this Master dissertation are:

(1) To develop an RPFC model in steady-state

(2) To implement the developed RPFC model and its control system of by using SPS (Simulation-Power-System developed by l'Institut de Recherche d'Hydro Québec--IREQ) and Matlab/Simulink

(3) To study the performance of a power system equipped with an RPFC in **symmetrical** and **asymmetrical** operations.

1.4 Methodology

The whole system is modeled and implemented by using SPS and Matlab/Simulink. Models for an RPFC and its control system are developed. Finally, simulations on a two-line power system equipped with the RPFC with different pole-pairs in **symmetrical** and **asymmetrical** operations are conducted.

1.5 Master dissertation outline

In Chapter 2, a concept of asymmetrical operation of a power system is presented.

In Chapter 3, the principle of the Rotary Power Flow Controller (RPFC) is presented, the equivalent circuits of the components of the RPFC are discussed, and the equivalent circuit of the RPFC is established.

In Chapter 4, the RPFC model is set up and implemented by SPS and Matlab/Simulink, and the control system of the RPFC is developed and implemented by SPS and Matlab/Simulink.

In Chapter 5, two simulations on a two-line power system equipped with the RPFC in **symmetrical** operation are conducted, in which the pole-pair numbers of the RPSTs are one (1) and six (6), respectively.

In Chapter 6, two simulations on a two-line power system equipped with the RPFC in **asymmetrical** operation are conducted, in which the pole-pair numbers of the RPSTs are one (1) and six (6), respectively.

In Chapter 7, the conclusions from this study and recommendations for future work are provided.

1.6 Master dissertation contributions

The RPFC model and control system of the RPFC are developed. The performance of the RPFC used in **asymmetrical** operation of power systems is studied. The study reveals that:

The RPFC can be used in **asymmetrical** operation of power systems to improve the capacity, security and economy of power supply.

CHAPTER 2 INTRODUCTION TO ASYMMETRICAL OPERATION OF A TRANSMISSION NETWORK

2.1 Introduction

The concept of asymmetrical operation of power systems was firstly presented to the CCECE in 1998 [23] and much research work has been done on this subject at École Polytechnique de Montréal since that time [20][21][22][26]. This chapter is only the review of this subject.

When the operation of a transmission network is symmetrical, the rule of permanent three-phase cut-off does not consider the nature of the contingency (i.e., single-phase fault, or line-line fault, or three--phase fault, etc.). Its capacity, security, reliability, economy and flexibility are then limited. It is clear that the effective power transmitted in one three-phase line is zero after a permanent three-phase cut-off due to a single-phase fault on this line.

From the point of view of operation, all the solutions to transmit the power without changing the integrity of the transmission network are welcome. For example, if power could be transmitted by a security way in a transmission line in spite of the loss of one phase of the line, the benefit would be obtained immediately in term of the relative capacity of the operation. That means, if each line that could no longer operate symmetrically as a single entity composed of three non-separate circuits could operate as three distinct entities that join together and supply the loads of absent (lost) phase(s), at least during urgent measures are taken, it would result in a considerable benefit as regards of transport capacity, flexibility and economy.

Usually, transmission networks operate in the balanced symmetrical mode and are presented by N parallel lines in operation forming an equivalent corridor. The previous research work has revealed that the number (≥ 2) of parallel lines in a corridor was sufficient so that the unbalances due to only one phase being opened in one line could be assumed negligible [20] [21]. Thus the compensation scheme proposed was only for the positive sequence current flowing in the lost phase of the corridor, taht means that it is possible to operate a three-phase line with one phase open on a permanent basis, without altering the integrity of the system. This is known as Asymmetrical Operation (A.O.) of transmission system. The unbalances due to A.O. are confined within the line itself by means of suitable compensations for the lost phase of the corridor at each end [21].

The concept of A.O. views the three-phase system as three independent single-phase circuits operating individually [26]. This means that one can work with single-phase schemes and adapt the results to the three phases. The technology of FACTS is useful and helpful to A.O. There are two kinds of possible implementation strategies for A.O--system strategy and localized strategy. In this Master dissertation, the system implementation strategy is considered for A.O.

2.2 Analysis of asymmetrical operation of a corridor with a few lines

Figure 2.1 represents a corridor with N transmission lines. The model of the transmission line is represented by 4-port parameters, i.e., A_0, B_0, C_0, and D_0. We have the general hypothesis as the following [20]:

(1) All the lines are not coupled;

(2) Each line can withstand the unbalance (i.e., the unbalanced voltage and current) resulting from the loss of one of the lines' own phases;

(3) Each line can withstand the unbalance resulting from the insertion of the series and shunt compensations in the faulted phase.

Based on Hypothesis (1), the phases of the corridor in Figure 2.1 are separated, as shown in Figure 2.2. Figure 2.3 represents the case that L out of N A-phases in Figure 2.2 are opened.

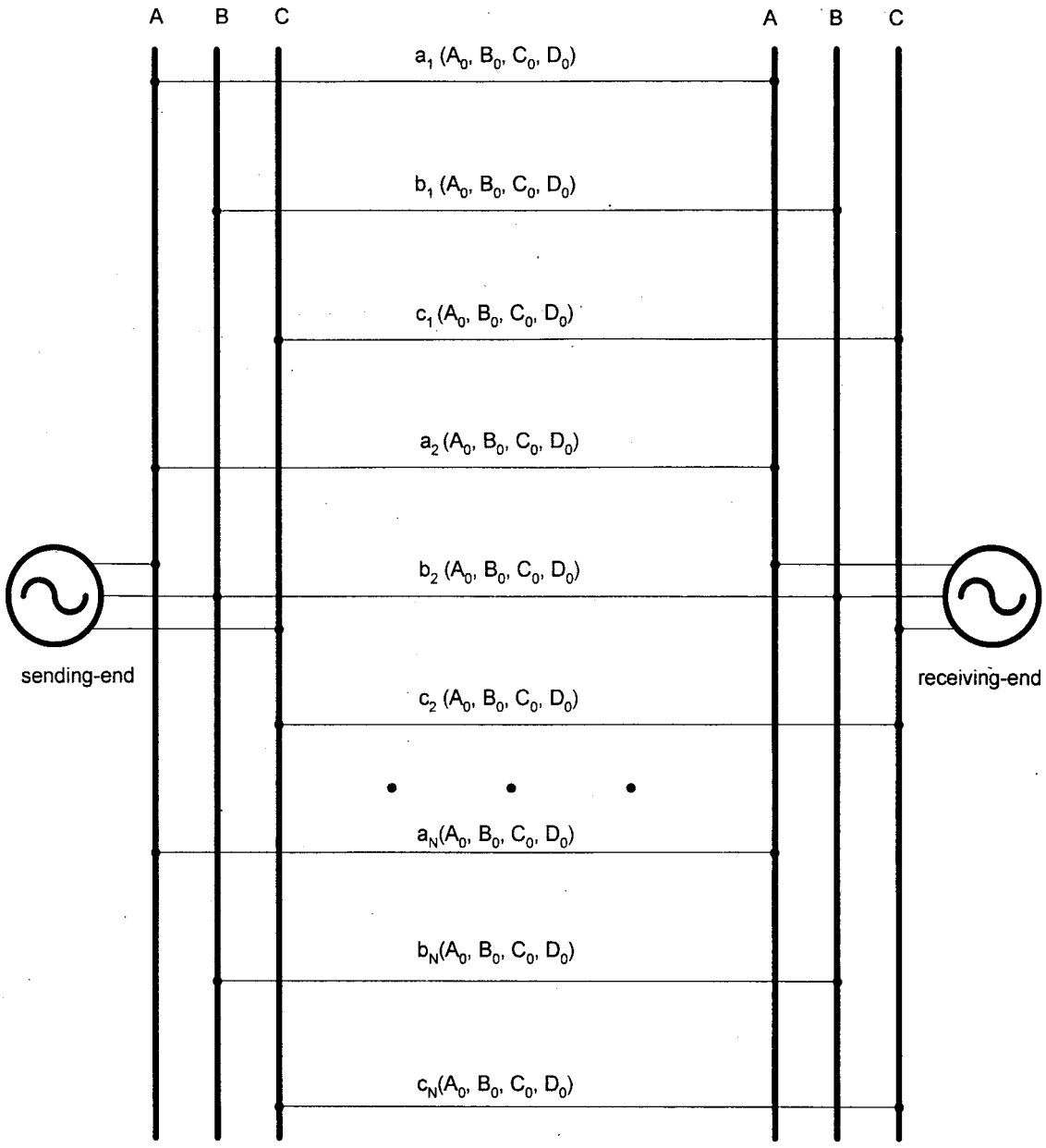

Simplified representation of a corridor with N transmission lines

Figure 2.1 - Simplified representation of a corridor with N transmission lines

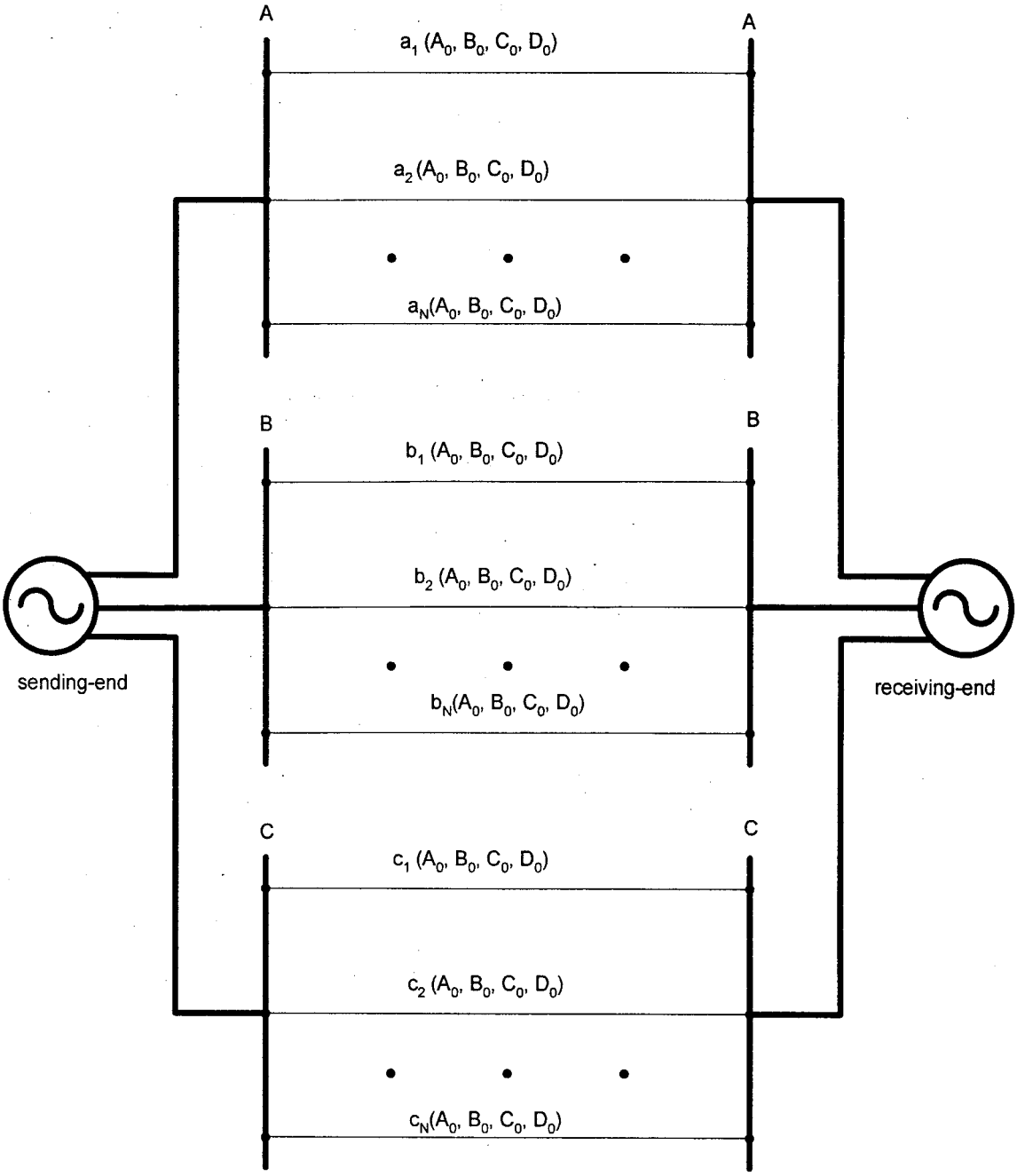

Separated-phases representation of a corridor with N transmission lines

Figure 2.2 - Separated-phase representation of a corridor with N transmission lines

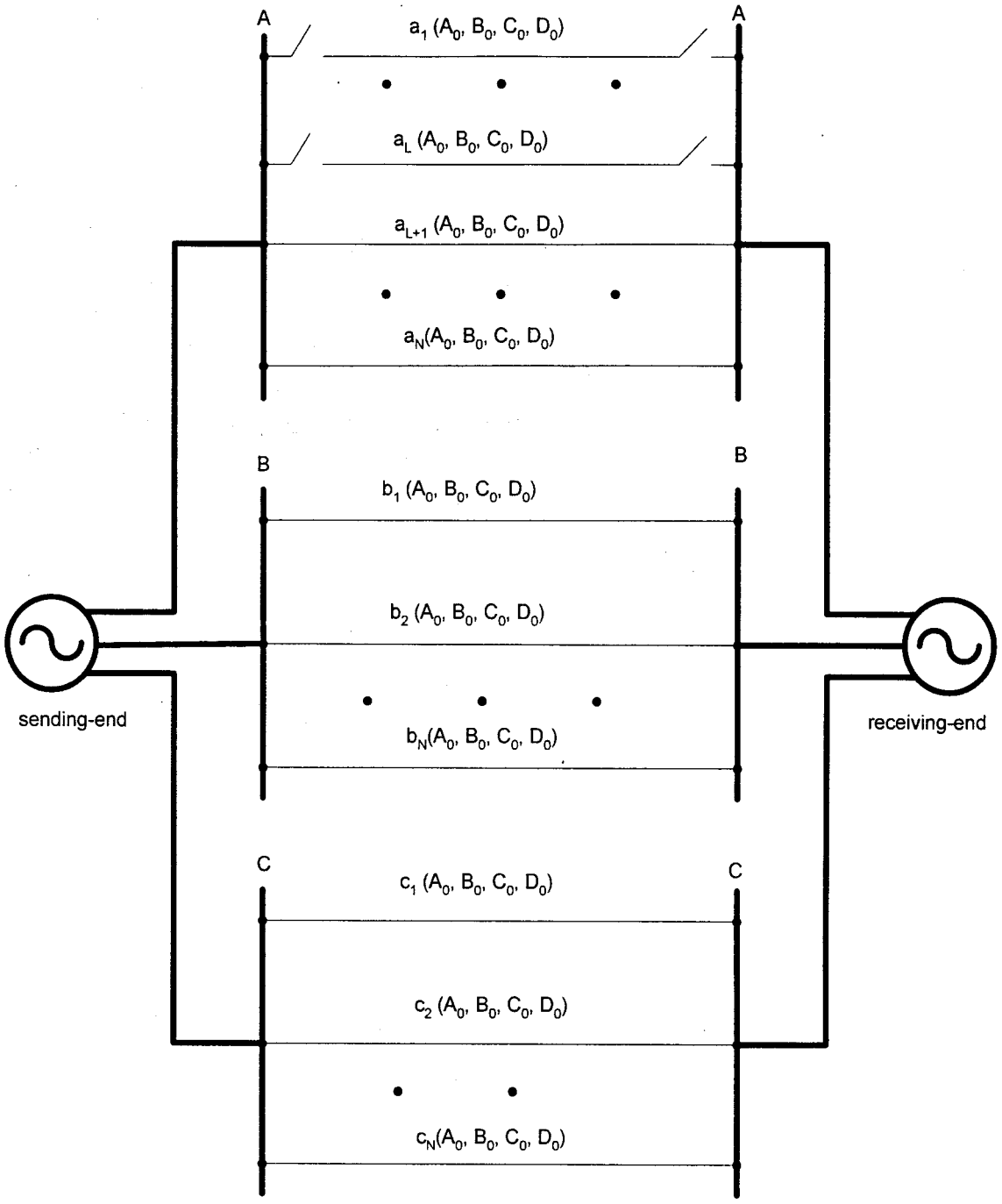

L out of N A-phases are opened in a corridor with N transmission lines (L <N)

Figure 2.3 - L out of N A-phases are opened in a corridor with N transmission lines (L <N)

It is clear that the total impedance of Phase-A in Figure 2.3 is greater than that in Figure 2.2, but the total impedances of Phase-B and Phase-C in Figure 2.3 are the same as those in Figure 2.2, respectively. So, the series and shunt compensations should be used for Phase-A in Figure 2.3 so as to preserve the same transmitted power in Figure 2.3 as that in Figure 2.2.

As mentioned before, the system implementation strategy is considered for A.O. in this Master dissertation; that means that the series and shunt compensations will be voltage and current sources, respectively. The voltage and current sources could be obtained from different ways, such as the converters based on power electronics. But, in this Master dissertation, we are interested only in the voltage source generated by classical machinery---transformers and induction machines which will be discussed in detail in Chapter 3. As for the current source, it is not specified how to obtain it due to the simplification for this project.

The positions of voltage and current sources could be either at the sending-end or at the receiving-end of Phase-A referring to Figure 2.3. Because the compensations are only connected to Phase-A, Figure 2.4 represents the pre-contingency diagram of Phase-A, and Figure 2.5 the post-contingency (i.e., loss of L A-phases ($L<N$)) with compensations referring to Figure 2.3. In Figure 2.4 and hereafter, the subscript A that could be used to represent Phase-A is omitted for convenience if it would not result in any confusion.

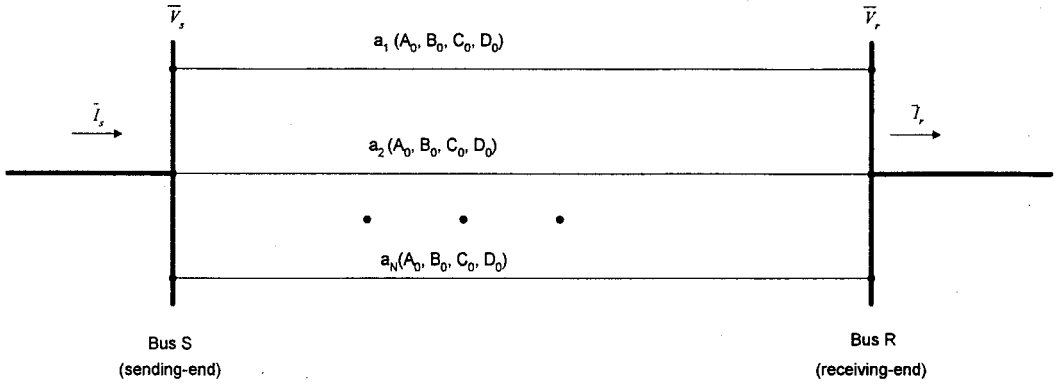

Phase-A diagram of Figure 2.2

Figure 2.4 - Phase-A diagram of Figure 2.2

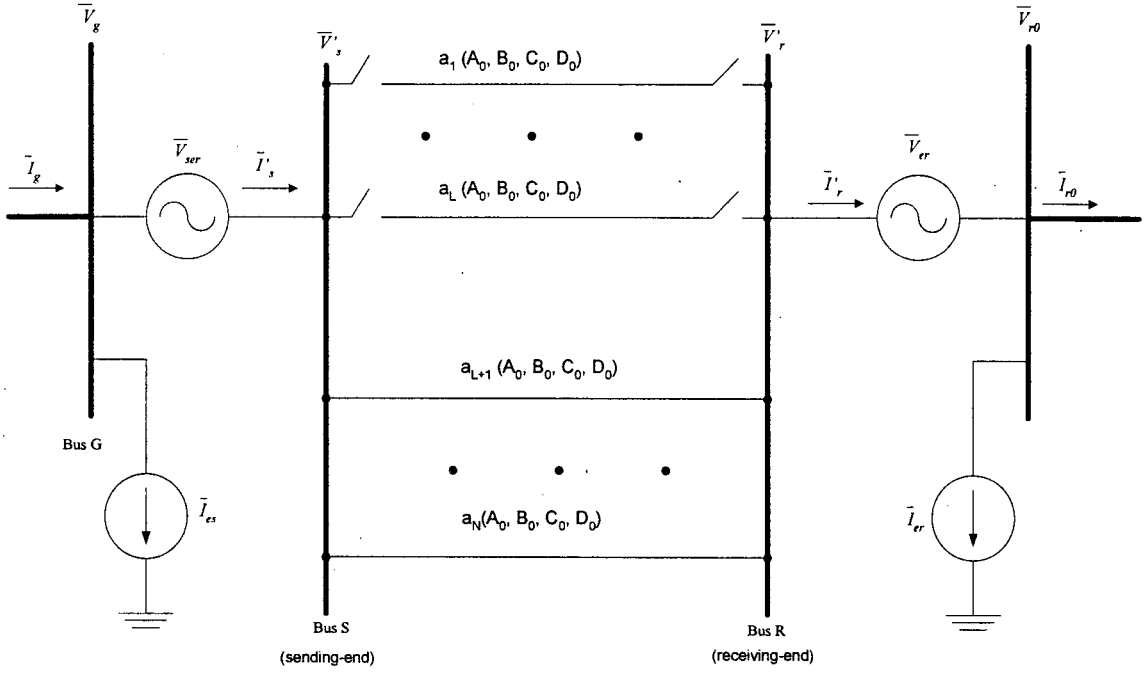

Representation of the compensations by voltage and current sources for Phase-A in Figure 2.3

Figure 2.5 - Representation of the compensations by voltage and current sources for Phase-A in Figure 2.3

Refer to Figure 2.5. It has been shown that two of the four sources are sufficient and necessary to assure the balance. The optimization would be dealt with if more than two sources are used [20].

If we use only two sources among the four, there are six possibilities for the positions of the two sources that are summarized in Table 2.1. In this Master dissertation, we chose the case (No.1 in Table 2.1) in which both voltage and current sources are at the sending-end (Figure 2.6).

Table 2.1 - Possible positions for two compensations

No.	Sending-end	Receiving-end
1	V_{ser}, I_{es}	N/A
2	N/A	V_{er}, I_{er}
3	V_{ser}	I_{er}
4	I_{es}	V_{er}
5	V_{ser}	V_{er}
6	I_{es}	I_{er}

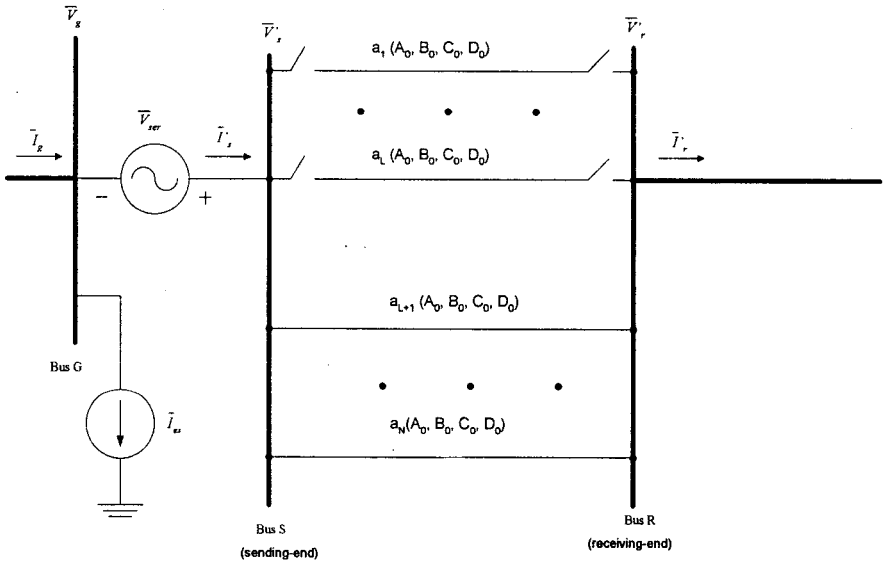

Both voltage and current sources are at the sending-end refer to Figure 2.5

Figure 2.6 - Both voltage and current sources are at the sending-end

In the pre-contingency state (Refer to Figure 2.4), we have,

$$\begin{bmatrix} \overline{V}_s \\ \overline{I}_s \end{bmatrix} = \begin{bmatrix} A_0 & B_0 / N \\ N \cdot C_0 & D_0 \end{bmatrix} \cdot \begin{bmatrix} \overline{V}_r \\ \overline{I}_r \end{bmatrix} \tag{2-1a}$$

Or equivalently,

$$\begin{bmatrix} \overline{I}_s \\ \overline{I}_r \end{bmatrix} = \begin{bmatrix} N \cdot \frac{D_0}{B_0} & -\frac{N}{B_0} \\ \frac{N}{B_0} & -N \cdot \frac{A_0}{B_0} \end{bmatrix} \cdot \begin{bmatrix} \overline{V}_s \\ \overline{V}_r \end{bmatrix} \tag{2-1b}$$

In the post-contingency state (Refer to Figure 2.4), we have,

$$\begin{bmatrix} \overline{V_s'} \\ \overline{I_s'} \end{bmatrix} = \begin{bmatrix} A_0 & B_0 /(N-L) \\ (N-L) \cdot C_0 & D_0 \end{bmatrix} \cdot \begin{bmatrix} \overline{V_r'} \\ \overline{I_r'} \end{bmatrix} \tag{2-2}$$

$$\overline{I_s'} = \overline{I}_g - \overline{I}_{es} \tag{2-3}$$

$$\overline{V_s'} = \overline{V}_g + \overline{V}_{ser} \tag{2-4}$$

Inserting (2-3) and (2-4) into (2-2) for the post-contingency condition, we obtain

$$\begin{bmatrix} \overline{V}_g + \overline{V}_{ser} \\ \overline{I}_g - \overline{I}_{es} \end{bmatrix} = \begin{bmatrix} A_0 & B_0 /(N-L) \\ (N-L) \cdot C_0 & D_0 \end{bmatrix} \cdot \begin{bmatrix} \overline{V_r'} \\ \overline{I_r'} \end{bmatrix} \tag{2-5}$$

In order to keep the power transmitted in Figure 2.6 the same as that in Figure 2.4, compare Equation (2-1) with (2-5). The following equations should be set up to represent similar loading conditions in the pre- and post-contingency conditions:

$$\bar{I}_s = \bar{I}_g \tag{2-6}$$

$$\bar{V}_s = \bar{V}_g \tag{2-7}$$

$$\bar{I}_r = \bar{I}_r' \tag{2-8}$$

$$\bar{V}_r = \bar{V}_r' \tag{2-9}$$

Inserting (2-6)~ (2-9) into (2-5) and taking (2-1a) and (2-1b) into consideration, we find that to maintain the voltages and the currents at the both sending-and receiving-ends, respectively, we must apply the following compensations,

$$\bar{V}_{ser} = \frac{L}{N-L}(\bar{V}_g - A_0 \cdot \bar{V}_r) \tag{2-10}$$

$$\bar{I}_{es} = L \cdot C_0 \cdot \bar{V}r \tag{2-11}$$

The needed compensation, i.e., voltage and current sources can be solved by (2-10) and (2-11), referring to Figure 2.4 and Figure 2.6.

2.3 Summary

In this chapter, we briefly reviewed the concept of A.O. of a transmission system, and derived the general formulas for finding the needed voltage and current compensations that were connected at the sending-end for A.O.

It is clear that all the discussion for A.O. in this chapter can be applied to another operation mode in which the three phases of a line are opened permanently and the those compensations are applied to the three independent phases that are symmetrical. We define this operation mode as Symmetrical Operation (S.O.) in this Master dissertation.

CHAPTER 3 EQUIVALENT CIRCUIT OF THE ROTARY POWER FLOW CONTROLLER (RPFC)

3.1 Introduction to the RPFC

The power transmitted between two electrical areas must always be controlled. In so doing, it is common to inject a voltage in series with a transmission path between the two electrical areas.

A conventional phase-shifting transformer has been utilized to inject a series voltage with the voltages in the two electrical areas being shifted in phase, but having the same amplitude.

Large power electronic inverters have been utilized to provide rapid, continuous control of a series voltage. Both the magnitude and angle of the series voltage is controllable, the net result is an effective phase shift and magnitude ratio between the voltages in the two electrical areas. These kinds of controllers provide means of regulating both real and reactive power flow between two electrical areas. Unfortunately, they are complex, have large physical size, are expensive, and generate harmonics.

The use of rotary phase-shifting transformers (RPSTs) to control power flow between two electrical areas was proposed by Mr. E.V. Larsen [12]. Later, the Rotary Power Flow Controller (RPFC) was also proposed by Mr. E.V. Larsen [13] to control the transmitted electric power (Figure 3.1). The RPFC consists of a series transformer, a shunt transformer, and two RPSTs.

A RPST is in fact a three-phase wound-rotor induction machine in the standstill operation mode. That means the RPST acts as a simple transformer that provides a three-phase output proportional in magnitude to the three-phase input, but shifted in phase by an amount proportional to the rotor's position compared to the stator's. The phase angle of the stator voltage with respect to that of the rotor voltage can be adjusted with a simple mechanical position control of the rotor. The control speed can be made much faster than that of the mechanical switches (load-tap changer) of a conventional phase-shifting transformer and sufficiently fast for power flow control. By using a RPST with high pole number, the mechanical motion needed for large electrical angle change is made small.

By using two RPSTs connected as shown in Figure 3.1, coordinated control of the rotor positions of the two RPSTs, whose output voltages ($\overline{U}_{s1}$ and $\overline{U}_{s2}$) are in series connection, yields a net series voltage ($\overline{V}_{ser}$) that can be continuously controlled in magnitude and phase so as to independently control both active and reactive power flows. The voltage $\overline{V}_{ser}$ is in fact a function of rotor positions of the two RPSTs (see Chapter 4).

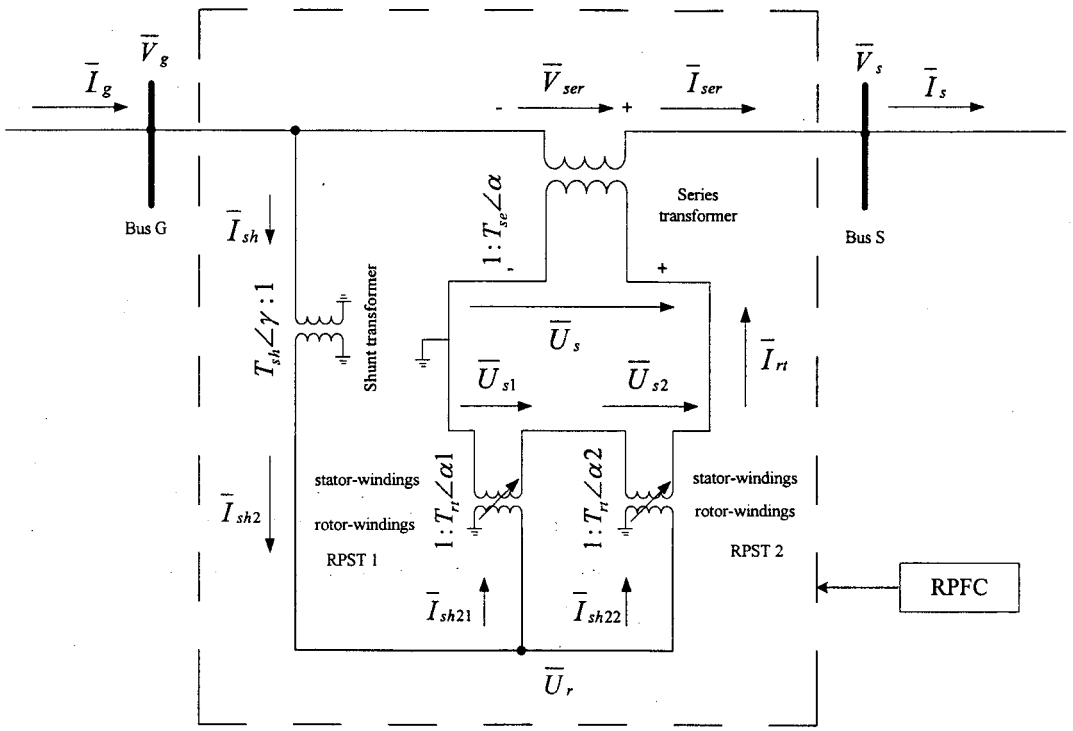

RPFC configuration

Figure 3.1- Single-phase diagram of RPFC configuration

Where,

T_{sh} - ratio of the shunt transformer

T_{se} - ratio of the series transformer

T_{rt} - ratio of RPST 1 and RPST 2, respectively, usually equal to 1

γ - phase-shifting angle of shunt transformer from HV-side to LV-side, It depends on the connection of the two-side windings of the shunt transformer. Usually, γ is 0°, or 30° or 90°.

α - phase-shifting angle of series transformer from LV-side to HV-side, It depends on the connection of the two-side windings of series transformer. Usually, α is 0° or 90°.

$\alpha1, \alpha2$ - rotor positions of the two RPSTs, respectively, lagging the stators of the RPSTs. $\alpha1$ and $\alpha2$ can vary in the range of 360 mechanical degrees, independently.

The ratios of the transformers are defined as the following:

$$Tsh = \frac{N_{sh\_LV}}{N_{sh\_HV}} \tag{3-1}$$

$$Tse = \frac{N_{se\_HV}}{N_{se\_LV}} \tag{3-2}$$

$$Trt = \frac{N_{stator}}{N_{rotor}} \tag{3-3}$$

Where,

N_{sh_LV} - low voltage side (non line side) turns of the shunt transformer

N_{sh_HV} - high voltage side (line side) turns of the shunt transformer

N_{se_HV} - high voltage side (line side) turns of the series transformer

N_{se_LV} - low voltage side (non line side) turns of the series transformer

N_{stator} - stator-winding turns of RPST 1 and RPST 2, respectively

N_{rotor} - rotor-winding turns of RPST 1 and RPST 2, respectively

Refer to Figure 3.1,

$$\overline{V}_s = \overline{V}_g + \overline{V}_{ser} \tag{3-4}$$

$$\overline{I}_g = \overline{I}_{ser} + \overline{I}_{sh} \tag{3-5}$$

$$\overline{I}_s = \overline{I}_{ser} \tag{3-6}$$

Figure 3.2 shows the general relationship among $\overline{V}_g$, $\overline{V}_s$ and $\overline{V}_{ser}$.

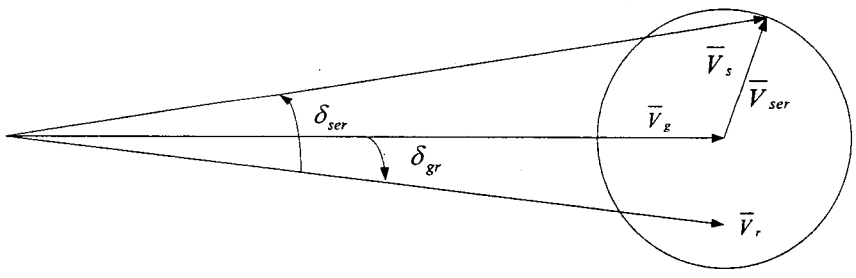

Figure 3.2 - Schematic diagram of voltage phasors of the RPFC

3.2 Equivalent circuit of the shunt transformer

Figure 3.3 represents the equivalent circuit of the shunt transformer in Figure 3.1.

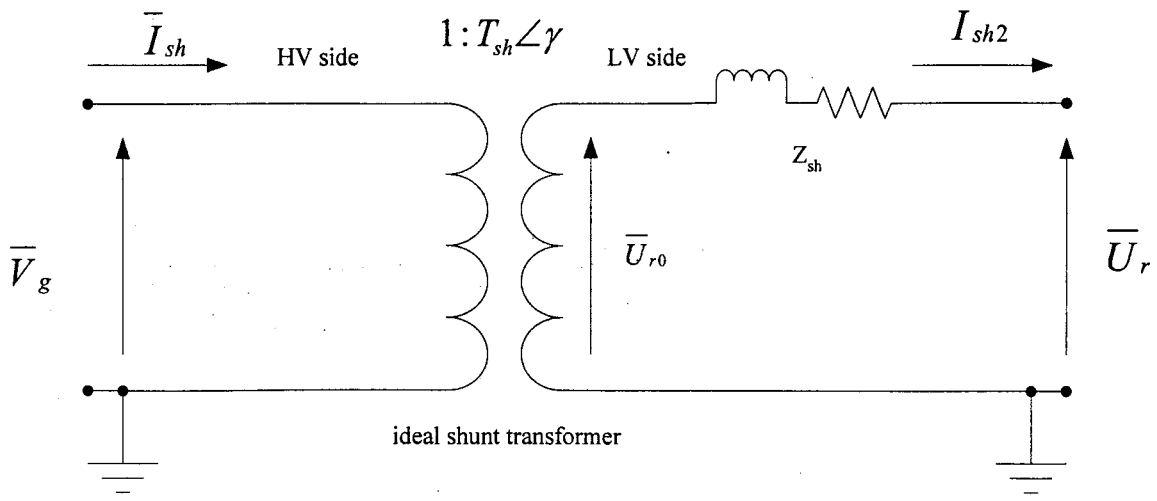

Figure 3.3 - Equivalent circuit of the shunt transformer

From Figure 3.3, we can establish the following equations,

$$\bar{U}_{r0} = T_{sh} \cdot e^{j\gamma} \cdot \bar{V}_g \tag{3-7}$$

$$\bar{I}_{sh2} = \frac{e^{j\gamma}}{T_{sh}} \bar{I}_{sh} \tag{3-8}$$

$$\bar{U}_r = \bar{U}_{r0} - \bar{I}_{sh2} \cdot Z_{sh} = T_{sh} \cdot e^{j\gamma} \cdot \bar{V}_g - \bar{I}_{sh2} \cdot Z_{sh} \tag{3-9}$$

Z_{sh} - total impedance of the shunt transformer with respect to LV-side (i.e., non line-side).

3.3 Equivalent circuit of the Rotary Phase-Shifting Transformer (RPST)

As mentioned in section 3.1, a RPST is actually a wound-rotor induction machine in the standstill operation mode. Figure 3.4 shows a scheme of an induction machine.

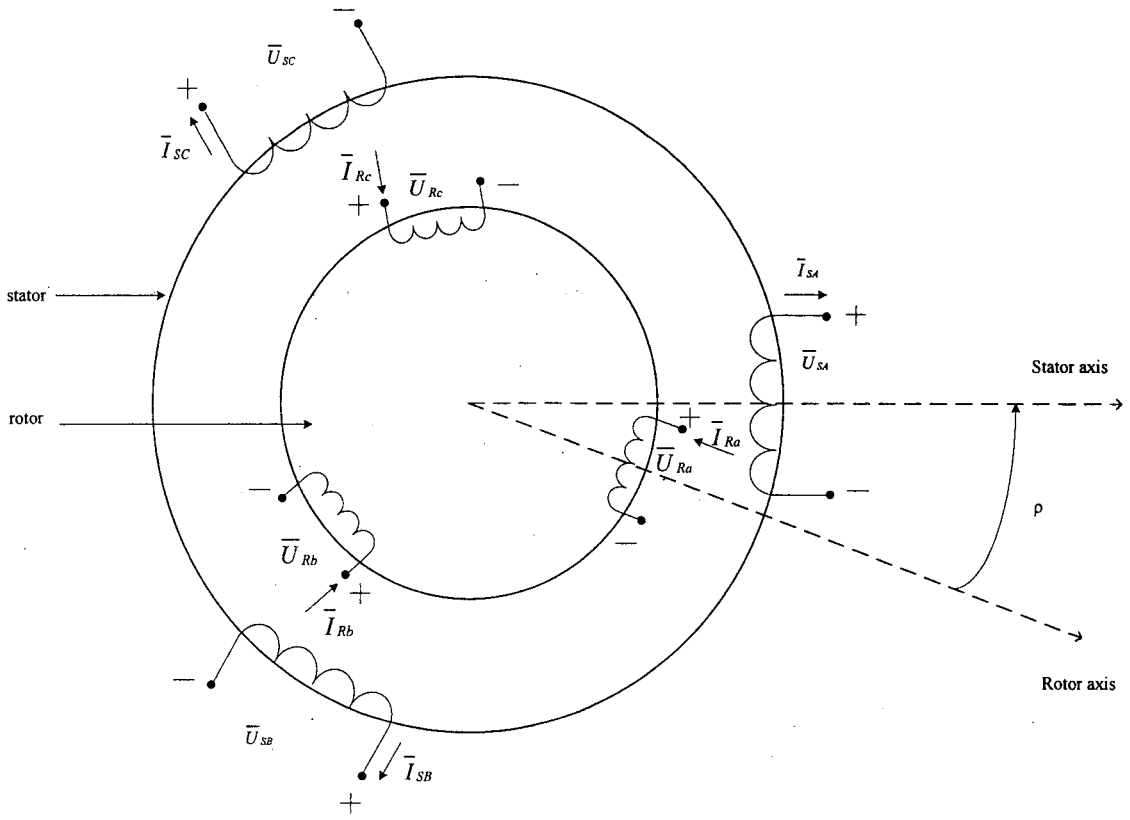

Figure 3.4 - Scheme of an induction machine

Where,

$\overline{U}_{SA}$, $\overline{U}_{SB}$, $\overline{U}_{SC}$ - three-phase output voltages of the stator-windings

$\overline{I}_{SA}$, $\overline{I}_{SB}$, $\overline{I}_{SC}$ - three-phase currents in the stator-windings

$\overline{U}_{Ra}$, $\overline{U}_{Rb}$, $\overline{U}_{Rc}$ - three-phase voltages applied to the rotor-windings

$\overline{I}_{Ra}$, $\overline{I}_{Ra}$, $\overline{I}_{Ra}$ - three-phase currents in the rotor-windings

From Figure 3.4, we have:

$$\overline{U}_{SA} = \overline{E}_{SA} - \overline{I}_{SA} \cdot Z_{SA} \tag{3-10}$$

$$\overline{U}_{Ra} = \overline{E}_{Ra} - \overline{I}_{Ra} \cdot Z_{Ra} \tag{3-11}$$

Where,

$\overline{E}_{SA}$ - induced voltage in Phase-A stator-winding

Z_{SA} - impedance of Phase-A stator-winding

$\overline{E}_{Ra}$ - induced voltage in Phase-A rotor-winding

Z_{Ra} - impedance of Phase-A rotor-winding

If the induction machine in Figure 3.4 is in the standstill operation mode (i.e., the slip is 1), we have:

$$\overline{E}_{SA} = T_{st} \cdot \overline{E}_{Ra} \cdot e^{j(p \cdot \rho)} \tag{3-12}$$

$$\overline{I}_{SA} = \frac{e^{j(p \cdot \beta)}}{T_{st}} \overline{I}_{Ra} \cdot e^{-j(p \cdot \rho)} \tag{3-13}$$

Where,

p - number of pole-pair of the rotor

ρ - angle between the stator- and rotor- winding axes

T_{st} - turn-ratio of the stator-winding over the rotor- winding

Equations (3-12) and (3-13) show that there is a phase-shifting angle (i.e., $p \cdot \beta$) between the induced voltages and currents in the stator- and rotor-windings, respectively. It is clear that the phase-shifting angle can be adjusted with a simple mechanical position control of the rotor. With larger pole numbers of the induction machines, less mechanical motion is needed to achieve a given electrical phase-shifting angle.

Based on (3-12) and (3-13), we get the equivalent circuits of RPST 1 and RPST 2 in Figure 3.1, which are shown in Figure 3.5.

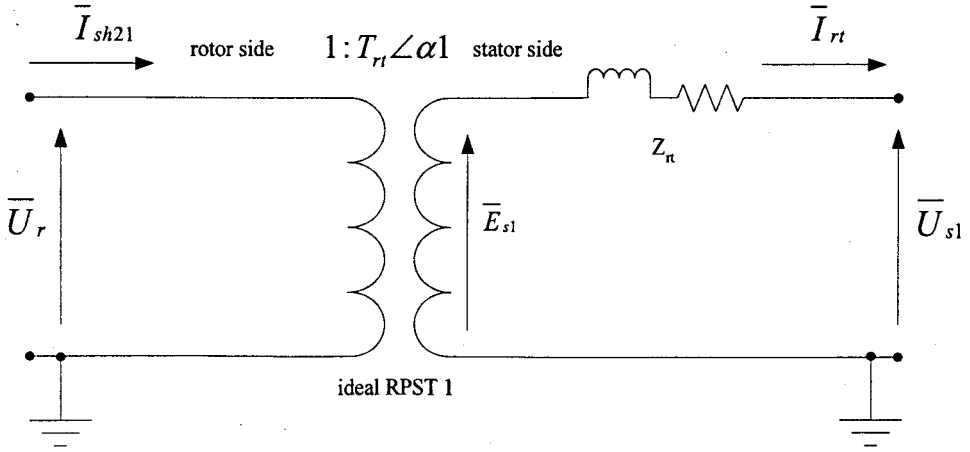

Equivalent circuit of RPST 1

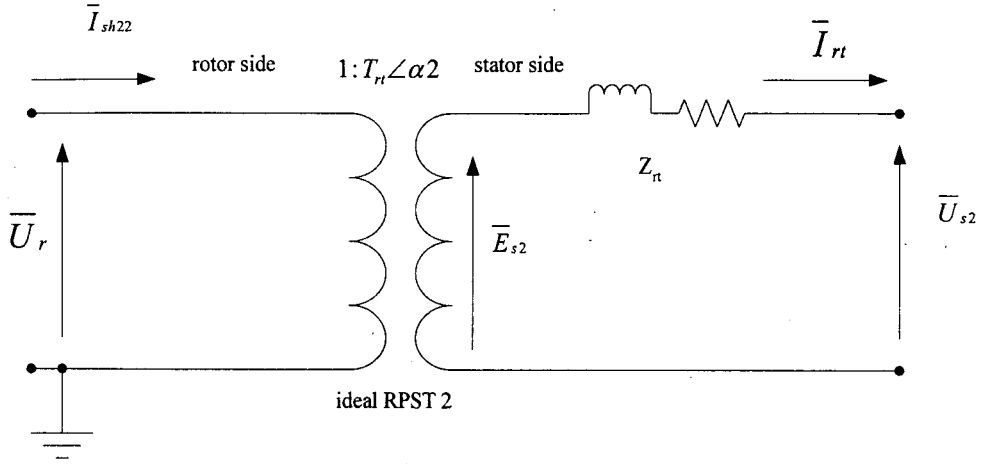

Equivalent circuit of RPST 2

a) - Single-phase equivalent circuit of RPST 1

b) - Single-phase equivalent circuit of RPST 2

Figure 3.5 - Single-phase equivalent circuits of RPST 1 and RPST 2

From Figure 3.5, we can establish the following equations,

$$\overline{E}_{s1} = T_{rt} \cdot e^{j\alpha 1} \cdot \overline{U}_r \tag{3-14}$$

$$\overline{E}_{s2} = T_{rt} \cdot e^{j\alpha 2} \cdot \overline{U}_r \tag{3-15}$$

$$\overline{I}_{sh21} = T_{rt} \cdot \overline{I}_{rt} \cdot e^{-j\alpha 1} \tag{3-16}$$

$$\overline{I}_{sh22} = T_{rt} \cdot \overline{I}_{rt} \cdot e^{-j\alpha 2} \tag{3-17}$$

Z_{rt} - total impedance of RPST 1 and RPST 2 with respect to stator sides of RPST 1 and RPST 2, respectively. The subscript rt represents Rotary Transformer

I_{rt} - output current of RPST 1 and RPST 2, respectively i.e., current in the stator-winding of RPST 1 and PST 2, respectively

I_{sh21} - current in the rotor-winding of RPST 1, part of the current in the secondary winding of the shunt transformer

I_{sh21} - current in the rotor-winding of RPST 2, part of the current in the secondary winding of the shunt transformer

From Figure 3.5, (3-14) and (3-15), we have,

$$\overline{U}_{s1} = \overline{E}_{s1} - \overline{I}_{rt} \cdot Z_{rt} = T_{rt} \cdot e^{j\alpha 1} \cdot \overline{U}_r - \overline{I}_{rt} \cdot Z_{rt} \tag{3-18}$$

$$\overline{U}_{s2} = \overline{E}_{s2} - \overline{I}_{rt} \cdot Z_{rt} = T_{rt} \cdot e^{j\alpha 2} \cdot \overline{U}_r - \overline{I}_{rt} \cdot Z_{rt} \tag{3-19}$$

Referring to Figure 3.5, we get the equivalent circuit of the two series-connected RPSTs in Figure 3.1, which is shown in Figure 3.6.

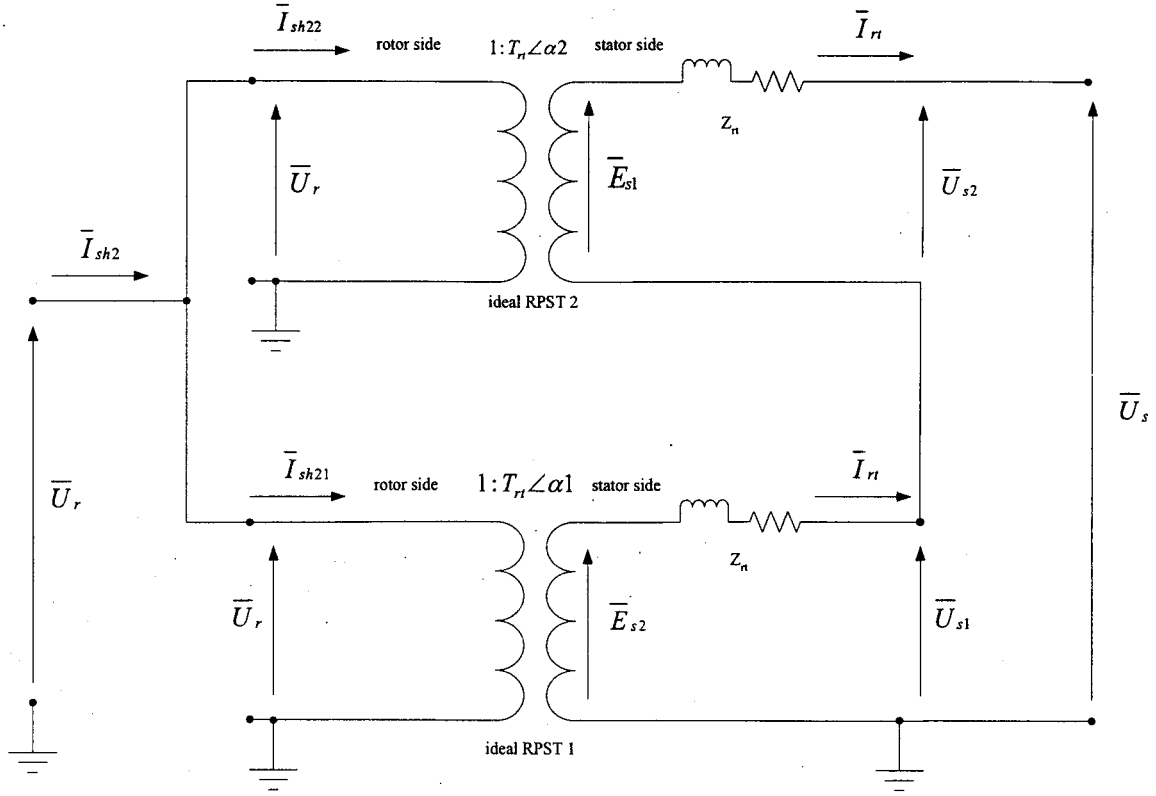

Equivalent circuit of combination of RPST 1 and RPST 2

Figure 3.6 - Equivalent circuit 1 of the two-series connected RPSTs

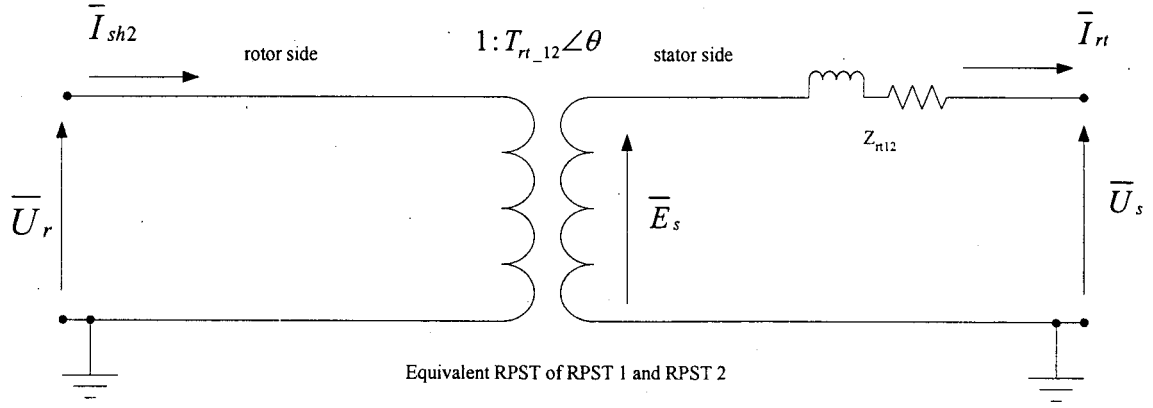

Equivalent RPST of RPST 1 and RPST 2

Equivalent circuit of equivalent RPST of RPST 1 and RPST 2

Figure 3.7 - Equivalent circuit 2 of the two-series connected RPSTs

From Figure 3.6 and equations (3-16) ~ (3-19),

$$\begin{aligned}\overline{U}_s &= \overline{U}_{s1} + \overline{U}_{s2} = T_{rt} \cdot \overline{U}_r \cdot (e^{j\alpha 1} + e^{j\alpha 2}) - 2 \cdot \overline{I}_{rt} \cdot Z_{rt} \\ &= 2 \cdot |\cos\delta| e^{j\theta} \cdot T_{rt} \cdot \overline{U}_r - 2 \cdot Z_{rt} \cdot \overline{I}_{rt}\end{aligned} \tag{3-20}$$

See the Appendix for the derivation of the sum of vectors $e^{j\alpha 1}$ and $e^{j\alpha 2}$.

$$\overline{I}_{sh2} = \overline{I}_{sh21} + \overline{I}_{sh22} = T_{rt} \cdot \overline{I}_{rt}(e^{-j\alpha 1} + e^{-j\alpha 2}) = 2 \cdot |\cos\delta| e^{-j\theta} \cdot T_{rt} \cdot \overline{I}_{rt} \tag{3-21}$$

Where,

$$\delta = \frac{\alpha 2 - \alpha 1}{2} \tag{3-22}$$

$$\theta = \frac{\alpha 2 + \alpha 1}{2} \tag{3-23}$$

From (3-20) ~ (3-21), we get the equivalent circuit of the two-series connected RPSTs in Figure 3.6, which is shown in Figure 3.7 where,

$$T_{rt\_12} = 2|\cos\delta| \cdot T_{rt} \tag{3-24}$$

From Figure 3.7, we can establish the following equations,

$$\overline{E}_s = T_{rt\_12} \cdot e^{j\theta} \cdot \overline{U}_r = 2 \cdot |\cos\delta| e^{j\theta} \cdot T_{rt} \cdot \overline{U}_r \tag{3-25}$$

$$\overline{I}_{rt} = \frac{e^{j\theta}}{T_{rt\_12}} \overline{I}_{sh2} = \frac{e^{j\theta}}{2|\cos\delta| \cdot T_{rt}} \overline{I}_{sh2} \tag{3-26}$$

$$Z_{rt\_12} = 2 \cdot Z_{rt} \tag{3-27}$$

Z_{rt_12} - total equivalent impedance of RPST 1 and RPST 2 with respect to stator side.

Figure 3.7 and (3-22)~(3-27) show that the two-series connected RPSTs can be represented by an equivalent RPST whose turn-ratio (T_{rt_12}) of stator-winding over rotor-winding and phase-shifting angle (θ) are functions of rotor positions of the two-series connected RPSTs.

3.4 Equivalent circuit of the series transformer

Figure 3.8 represents the equivalent circuit of the series transformer in Figure 3.1.

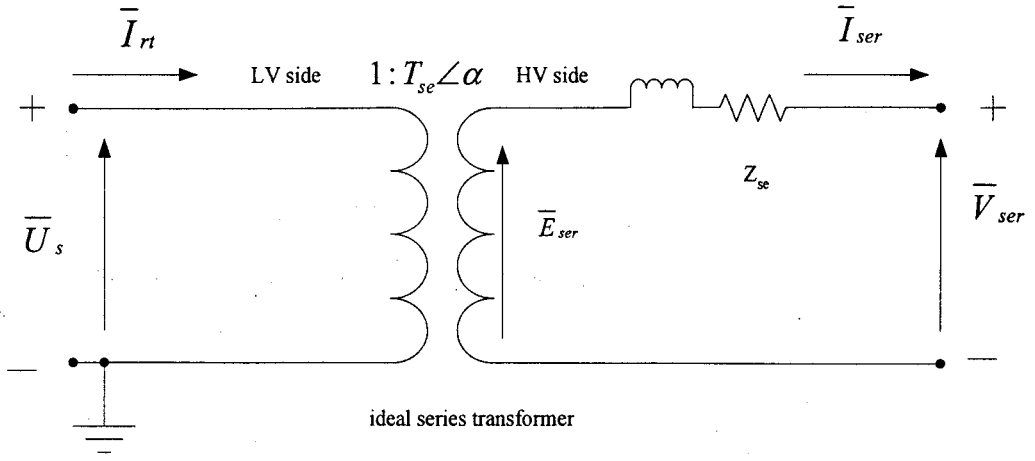

Figure 3.8 Equivalent circuit of the series transformer

From Figure 3.8, we can establish the following equations,

$$\bar{E}_{ser} = T_{se} \cdot e^{j\alpha} \cdot \bar{U}_s \tag{3-28}$$

$$\bar{I}_{ser} = \frac{e^{j\alpha}}{T_{se}} \bar{I}_{rt} \tag{3-29}$$

$$\bar{V}_{ser} = \bar{E}_{ser} - \bar{I}_{ser} \cdot Z_{se} = T_{se} \cdot e^{j\alpha} \cdot \bar{U}_s - \bar{I}_{ser} \cdot Z_{se} \tag{3-30}$$

Z_{se} - total impedance of series transformer with respect to HV-side (i.e., line-side).

3.5 Equivalent circuit of the RPFC

As an RPFC consists of a shunt and a series transformers, and two RPSTs, its equivalent circuit will include these components.

Inserting (3-20) into (3-30), we have

$$\begin{aligned}\overline{V}_{ser} &= 2\cdot T_{se}\cdot e^{j\alpha}(T_{rt}|\cos\delta|e^{j\theta}\cdot\overline{U}_r-\overline{I}_{rt}\cdot Z_{rt})-\overline{I}_{ser}\cdot Z_{se}\\ &= 2|\cos\delta|T_{se}\cdot T_{rt}\cdot e^{j(\alpha+\theta)}\cdot\overline{U}_r-2\cdot T_{se}\cdot e^{j\alpha}\cdot\overline{I}_{rt}\cdot Z_{rt}-\overline{I}_{ser}\cdot Z_{se}\end{aligned} \tag{3-31}$$

Inserting (3-9) into (3-31), we have

$$\overline{V}_{ser} = 2|\cos\delta|T_{se}\cdot T_{rt}\cdot e^{j(\alpha+\theta)}(T_{sh}\cdot e^{j\gamma}\cdot\overline{V}_g-\overline{I}_{sh2}\cdot Z_{sh})-2\cdot T_{se}\cdot e^{j\alpha}\cdot\overline{I}_{rt}\cdot Z_{rt}-\overline{I}_{ser}\cdot Z_{se}$$

$$\begin{aligned}&= 2|\cos\delta|T_{sh}\cdot T_{se}\cdot T_{rt}\cdot e^{j(\gamma+\alpha+\theta)}\cdot\overline{V}_g\\ &\quad -2|\cos\delta|T_{se}\cdot T_{rt}\cdot e^{j(\alpha+\theta)}\cdot\overline{I}_{sh2}\cdot Z_{sh}-2\cdot T_{se}\cdot e^{j\alpha}\cdot\overline{I}_{rt}\cdot Z_{rt}-\overline{I}_{ser}\cdot Z_{se}\end{aligned} \tag{3-32}$$

With (3-5), (3-8), (3-26) and (29), we have,

$$\overline{I}_{ser} = \frac{1}{1+2|\cos\delta|T_{sh}\cdot T_{rt}\cdot T_{se}\cdot e^{-j(\gamma+\alpha+\theta)}}\overline{I}_g \tag{3-33}$$

$$\overline{I}_{sh} = 2|\cos\delta|T_{sh}\cdot T_{rt}\cdot T_{se}\cdot e^{-j(\theta+\gamma+\alpha)}\cdot\overline{I}_{ser} \tag{3-34}$$

$$\overline{I}_{sh2} = 2\cdot T_{rt}\cdot T_{se}\cdot|\cos\delta|e^{-j(\theta+\alpha)}\cdot\overline{I}_{ser} \tag{3-35}$$

Inserting (3-29) and (3-35) into (3-32), we have

$$\begin{aligned}\overline{V}_{ser} &= 2\left|\cos\delta\right|T_{sh}\cdot T_{rt}\cdot T_{se}\cdot e^{j(\theta+\gamma+\alpha)}\overline{V}_g \\ &\quad -\overline{I}_{ser}(Z_{se}+4\cdot T_{rt}^2\cdot T_{se}^2\cdot\cos^2\delta\cdot Z_{sh}+2\cdot T_{se}^2\cdot Z_{rt})\end{aligned} \tag{3-36}$$

For convenience, we define,

$$T = 2\cdot T_{sh}\cdot T_{rt}\cdot T_{se} \tag{3-37}$$

$$\varphi = \theta+\gamma+\alpha = \frac{\alpha 2+\alpha 1}{2}+\gamma+\alpha \tag{3-38}$$

$$Z_{rpfc} = Z_{se}+4\cdot T_{rt}^2\cdot T_{se}^2\cdot\cos^2\delta\cdot Z_{sh}+2\cdot T_{se}^2\cdot Z_{rt} \tag{3-39}$$

Inserting (3-37) ~ (3-39) into (3-36) and (3-33), respectively, we have

$$\overline{V}_{ser} = T\left|\cos\delta\right|e^{j\varphi}\cdot\overline{V}_g-\overline{I}_{ser}\cdot Z_{rpfc} \tag{3-40}$$

$$\overline{I}_{ser} = \frac{1}{1+T\left|\cos\delta\right|e^{-j\varphi}}\overline{I}_g = \frac{1}{T_{eq}}\angle\beta_0\cdot\overline{I}_g \tag{3-41}$$

Inserting 40 into (3-4), we have

$$\begin{aligned}\overline{V}_s &= (1+T\left|\cos\delta\right|\cdot e^{j\varphi})\overline{V}_g-\overline{I}_{ser}\cdot Z_{rpfc} \\ &= T_{eq}\angle\beta_0\cdot\overline{V}_g-\overline{I}_{ser}\cdot Z_{rpfc}\end{aligned} \tag{3-42}$$

From (3-41) and (3-42), we get the equivalent circuit (Figure 3.9) of RPFC in Figure 3.1.

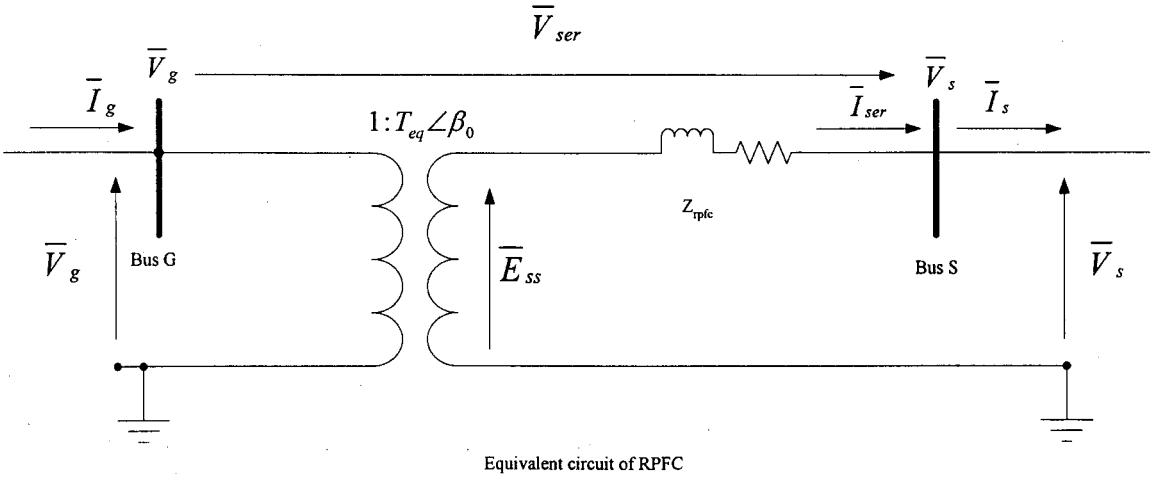

a) Representation of the equivalent circuit of the RPFC

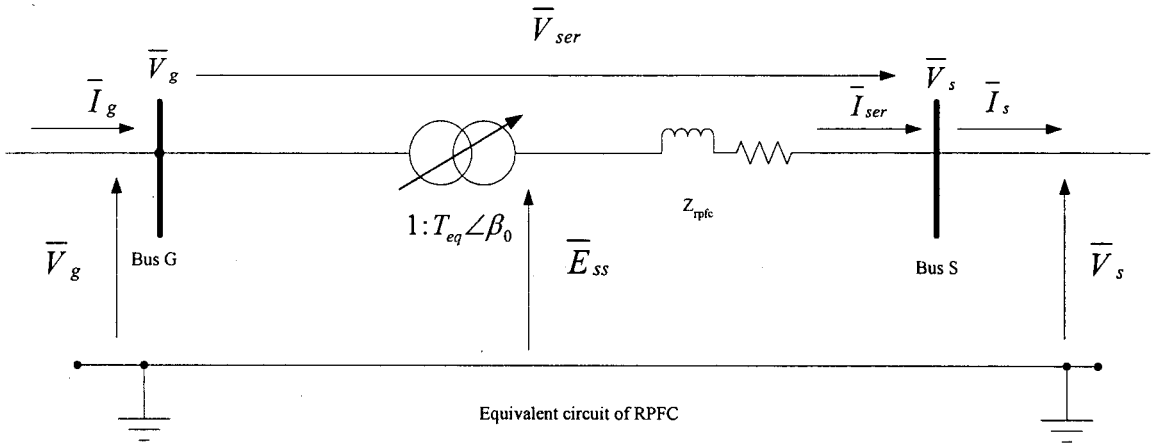

b) Representation of the equivalent circuit of the RPFC

Figure 3.9 - Representations of the equivalent circuits of the RPFC

From Figure 3.9, (3-41) and (3-42), we can establish the following equations:

$$\overline{E}_{ss} = T_{eq} \cdot e^{j\beta_0} \cdot \overline{V}_g \tag{3-43}$$

$$\overline{I}_{ser} = \frac{e^{j\beta_0}}{T_{eq}} \overline{I}_g \tag{3-44}$$

$$\begin{aligned} T_{eq} &= \left|1 + T \cdot \left|\cos\delta\right| \cdot e^{j\varphi}\right| \\ &= \sqrt{1 + T^2 \cdot \cos^2\delta + 2 \cdot T \cdot \left|\cos\delta\right| \cos\varphi} \end{aligned} \tag{3-45}$$

$$\begin{aligned} \beta_0 &= \angle(1 + T \cdot \left|\cos\delta\right| \cdot e^{j\varphi}) \\ &= \cos^{-1} \frac{1 + T\left|\cos\delta\right| \cos\varphi}{\sqrt{1 + T^2 \cdot \cos^2\delta + 2 \cdot T \cdot \left|\cos\delta\right| \cos\varphi}} \end{aligned} \tag{3-46}$$

Figure 3.9 shows that the equivalent circuit of the RPFC can be represented by an induction machine in the standstill operation mode, which has a turn-ratio T_{eq} of stator-winding over rotor-winding, a phase-shifting angle β_0, and an impedance Z_{rpfc}. Further, T_{eq}, β_0, and Z_{rpfc} are functions of the rotor positions of the two RPSTs ((3-22), (3-23), (3-45), (3-46) and (3-39)).

In (3-39), Z_{rpfc} consists of two parts, one is independent of δ, i.e., $Z_{se} + 2 \cdot T_{se}^2 \cdot Z_{rt}$, and another one is dependent of δ, i.e., $4 \cdot T_{rt}^2 \cdot T_{se}^2 \cdot \cos^2\delta \cdot Z_{sh}$. We define:

$$Z_{rpfc\_c} = Z_{se} + 2 \cdot T_{se}^2 \cdot Z_{rt} \tag{3-47}$$

$$Z_{rpfc\_v} = 4 \cdot T_{rt}^2 \cdot T_{se}^2 \cdot \cos^2\delta \cdot Z_{sh} \tag{3-48}$$

3.6 Voltage phasor diagram of the RPFC

Inserting (3-9) into (3-18) ~ (3-20), we have

$$\begin{aligned}\overline{U}_{s1} &= T_{rt}\cdot e^{j\alpha 1}\cdot\overline{U}_{r0} - T_{rt}\cdot e^{j\alpha 1}\cdot\overline{I}_{sh2}\cdot Z_{sh} - \overline{I}_{rt}\cdot Z_{rt} \\ &= \overline{U}_{s10} - T_{rt}\cdot e^{j\alpha 1}\cdot\overline{I}_{sh2}\cdot Z_{sh} - \overline{I}_{rt}\cdot Z_{rt}\end{aligned} \tag{3-49}$$

$$\begin{aligned}\overline{U}_{s2} &= T_{rt}\cdot e^{j\alpha 2}\cdot\overline{U}_{r0} - T_{rt}\cdot e^{j\alpha 2}\cdot\overline{I}_{sh2}\cdot Z_{sh} - \overline{I}_{rt}\cdot Z_{rt} \\ &= \overline{U}_{s20} - T_{rt}\cdot e^{j\alpha 2}\cdot\overline{I}_{sh2}\cdot Z_{sh} - \overline{I}_{rt}\cdot Z_{rt}\end{aligned} \tag{3-50}$$

$$\begin{aligned}\overline{U}_{s} &= \overline{U}_{s1} + \overline{U}_{s2} = T_{rt}(e^{j\alpha 1} + e^{j\alpha 2})\overline{U}_{r0} - T_{rt}(e^{j\alpha 1} + e^{j\alpha 2})\overline{I}_{sh2}\cdot Z_{sh} - 2\cdot\overline{I}_{rt}\cdot Z_{rt} \\ &= 2\left|\cos\delta\right|e^{j\theta}\cdot T_{rt}\cdot\overline{U}_{r0} - 2\left|\cos\delta\right|e^{j\theta}\cdot T_{rt}\cdot\overline{I}_{sh2}\cdot Z_{sh} - 2\cdot\overline{I}_{rt}\cdot Z_{rt} \\ &= \overline{U}_{s0} - 2\left|\cos\delta\right|e^{j\theta}\cdot T_{rt}\cdot\overline{I}_{sh2}\cdot Z_{sh} - 2\cdot\overline{I}_{rt}\cdot Z_{rt}\end{aligned} \tag{3-51}$$

Where,

$$\delta = \frac{\alpha 2 - \alpha 1}{2} \tag{3-22}$$

$$\theta = \frac{\alpha 2 + \alpha 1}{2} \tag{3-23}$$

$$\overline{U}_{s10} = T_{rt}\cdot e^{j\alpha 1}\cdot\overline{U}_{r0} \tag{3-52}$$

$$\overline{U}_{s20} = T_{rt}\cdot e^{j\alpha 2}\cdot\overline{U}_{r0} \tag{3-53}$$

$$\overline{U}_{s0} = \overline{U}_{s10} + \overline{U}_{s20} = 2\left|\cos\delta\right|e^{j\theta}\cdot T_{rt}\cdot\overline{U}_{r0} \tag{3-54}$$

Inserting (3-51) into (3-30), we have

$$\begin{aligned}\overline{V}_{ser} &= T_{se}\cdot e^{j\alpha}(\overline{U}_{s0} - 2|\cos\delta|e^{j\theta}\cdot T_{rt}\cdot \overline{I}_{sh2}\cdot Z_{sh} - 2\cdot \overline{I}_{rt}\cdot Z_{rt}) - \overline{I}_{ser}\cdot Z_{se} \\ &= T_{se}\cdot e^{j\alpha}\cdot \overline{U}_{s0} - 2\cdot T_{se}\cdot e^{j\alpha}(|\cos\delta|e^{j\theta}\cdot T_{rt}\cdot \overline{I}_{sh2}\cdot Z_{sh} + \overline{I}_{rt}\cdot Z_{rt}) - \overline{I}_{ser}\cdot Z_{se} \\ &= \overline{V}_{ser0} - 2\cdot T_{se}\cdot e^{j\alpha}(|\cos\delta|e^{j\theta}\cdot T_{rt}\cdot \overline{I}_{sh2}\cdot Z_{sh} + \overline{I}_{rt}\cdot Z_{rt}) - \overline{I}_{ser}\cdot Z_{se} \end{aligned} \quad (3\text{-}55)$$

Where,

$$\overline{V}_{ser0} = T_{se}\cdot e^{j\alpha}\cdot \overline{U}_{s0} \quad (3\text{-}56)$$

Inserting(3-55) into (3-4), we have

$$\begin{aligned}\overline{V}_s &= \overline{V}_g + \overline{V}_{ser0} - 2\cdot T_{se}\cdot e^{j\alpha}(|\cos\delta|e^{j\theta}\cdot T_{rt}\cdot \overline{I}_{sh2}\cdot Z_{sh} + \overline{I}_{rt}\cdot Z_{rt}) - \overline{I}_{ser}\cdot Z_{se} \\ &= \overline{V}_{s0} - 2\cdot T_{se}\cdot e^{j\alpha}(|\cos\delta|e^{j\theta}\cdot T_{rt}\cdot \overline{I}_{sh2}\cdot Z_{sh} + \overline{I}_{rt}\cdot Z_{rt}) - \overline{I}_{ser}\cdot Z_{se} \end{aligned} \quad (3\text{-}57)$$

Where,

$$\overline{V}_{s0} = \overline{V}_g + \overline{V}_{ser0} \quad (3\text{-}58)$$

Based on (3-4), (3-7), (3-52)~(5-54), (3-56) and (3-58) that are repeated as the following, we get the voltage phasor diagram (Figure 3.10) of the RPFC in Figure 3.1.

$$\overline{V}_s = \overline{V}_g + \overline{V}_{ser} \quad (3\text{-}4)$$

$$\overline{U}_{r0} = T_{sh}\cdot e^{j\gamma}\cdot \overline{V}_g \quad (3\text{-}7)$$

$$\overline{U}_{s10} = T_{rt}\cdot e^{j\alpha 1}\cdot \overline{U}_{r0} \quad (3\text{-}52)$$

$$\overline{U}_{s20} = T_{rt}\cdot e^{j\alpha 2}\cdot \overline{U}_{r0} \quad (3\text{-}53)$$

$$\overline{U}_{s0} = \overline{U}_{s10} + \overline{U}_{s20} = 2|\cos\delta|e^{j\theta}\cdot T_{rt}\cdot \overline{U}_{r0} \quad (3\text{-}54)$$

$$\overline{V}_{ser0} = T_{se}\cdot e^{j\alpha}\cdot \overline{U}_{s0} \quad (3\text{-}56)$$

$$\overline{V}_{s0} = \overline{V}_g + \overline{V}_{ser0} \quad (3\text{-}58)$$

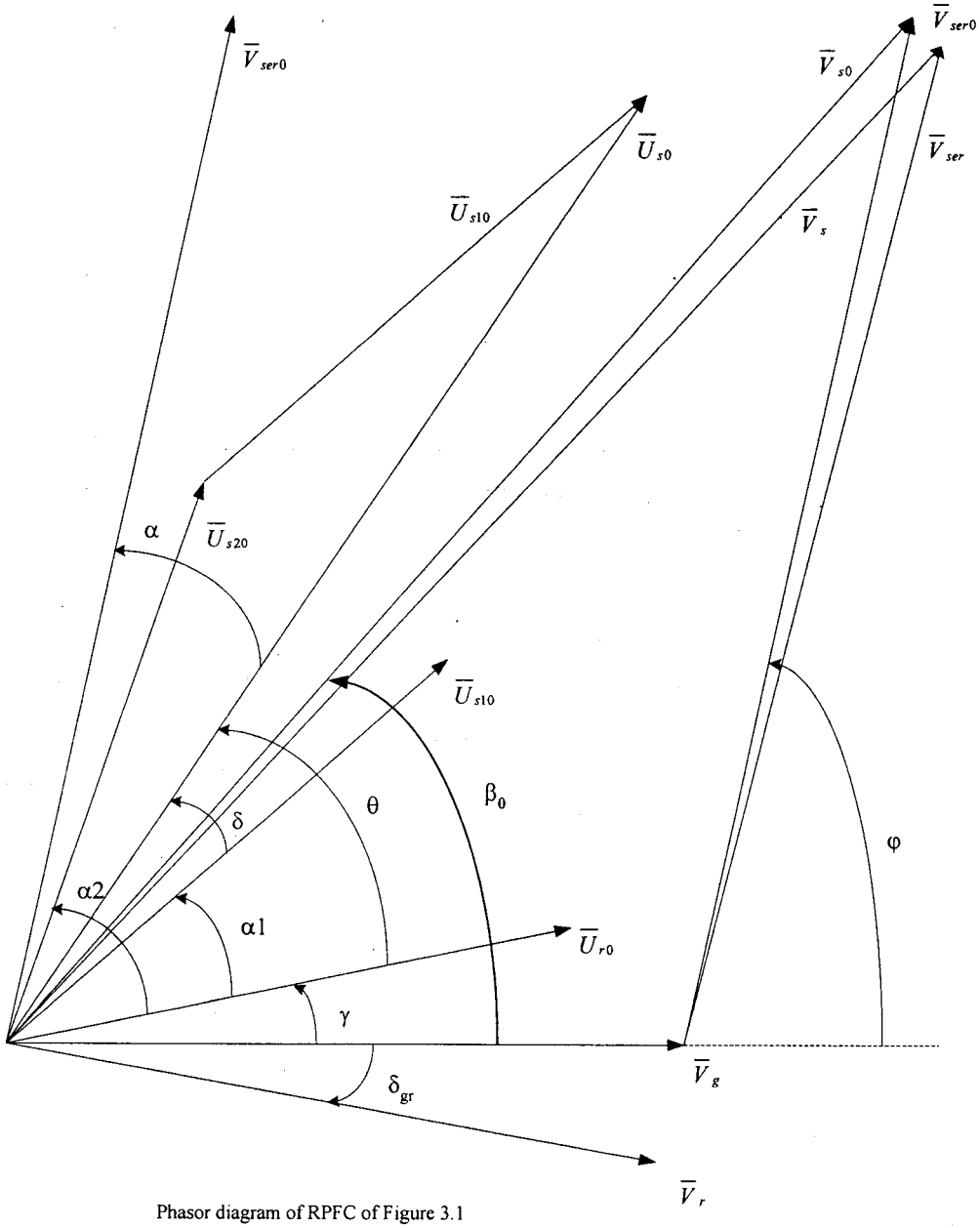

Phasor diagram of RPFC of Figure 3.1

Figure 3.10 - Voltage phasor diagram of the RPFC

Where, the subscript zero (0) represents the case when the RPFC is ideal (lossless), i.e., all the components of PRFC are lossless.

3.7 Summary

In this chapter, based on the equivalent circuits and equations of each component of the RPFC, the equivalent circuit of the RPFC has been developed. Its equivalent can be represented by an induction machine in the standstill operation mode, whose turn-ratio of stator-winding over rotor-winding, T_{eq}, angle between stator- and rotor-windings' axes, β_0, and impedance Z_{rpfc}, are functions of the rotor positions of the two-series connected RPSTs of the RPFC.

Note: All the equations derived above assume that the pole-pair number of each induction machine is 1. If each RPST has p pairs of poles, $\alpha 1$ and $\alpha 2$ in all the equations will be replaced by $p \cdot \alpha 1$ and $p \cdot \alpha 2$, respectively, because

$$\alpha_{ele} = p \cdot \alpha_{mec}$$

where,

α_{ele} - electrical angle in degree or radian

α_{mec} - mechanical angle in degree or radian

That means that an RPST with high pole number can produce large electrical phase-shifting with less rotor rotation.

CHAPTER 4 MODELING OF THE RPFC

4. 1 Model of the RPFC

Refer to Figure 3.1. The RPFC is connected to the power system through the series transformer's HV-side winding (series branch) and the shunt transformer's HV-side winding (shunt branch) which are connected to the power system in series and in parallel, respectively. Thus, the modeling of the RPFC is the modeling of the series and the shunt branches of the RPFC.

For convenience, (3-7), (3-34), (3-38), (3-40), (3-54) and (3-56) are repeated,

$$\overline{U}_{r0} = T_{sh} \cdot e^{j\gamma} \cdot \overline{V}_g \tag{3-7}$$

$$\overline{I}_{sh} = 2\left|\cos\delta\right| T_{sh} \cdot T_{rt} \cdot T_{se} \cdot e^{-j(\theta+\gamma+\alpha)} \cdot \overline{I}_{ser} \tag{3-34}$$

$$T = 2 \cdot T_{sh} \cdot T_{rt} \cdot T_{se} \tag{3-37}$$

$$\varphi = \theta + \gamma + \alpha = \frac{\alpha 2 + \alpha 1}{2} + \gamma + \alpha \tag{3-38}$$

$$\overline{V}_{ser} = T\left|\cos\delta\right| e^{j\varphi} \cdot \overline{V}_g - \overline{I}_{ser} \cdot Z_{rpfc} \tag{3-40}$$

$$\overline{U}_{s0} = \overline{U}_{s10} + \overline{U}_{s20} = 2\left|\cos\delta\right| e^{j\theta} \cdot T_{rt} \cdot \overline{U}_{r0} \tag{3-54}$$

$$\overline{V}_{ser0} = T_{se} \cdot e^{j\alpha} \cdot \overline{U}_{s0} \tag{3-56}$$

With (3-7), (3-37), (3-38), (3-54) and (3-56),

$$\overline{V}_{ser0} = T\left|\cos\delta\right| \cdot e^{j\varphi} \cdot \overline{V}_g \tag{4-1}$$

Insert (3-37)~ (3-38) into (3-34),

$$\overline{I}_{sh} = \left|\cos\delta\right| T \cdot e^{-j\varphi} \cdot \overline{I}_{ser} \tag{4-2}$$

Inserting (4-1) into (3-40), we have

$$\overline{V}_{ser} = \overline{V}_{ser0} - \overline{I}_{ser} \cdot Z_{rpfc} \tag{4-3}$$

Refer to Figure 3.1, and (4-2) and (4-3), the series and the shunt branches of the RPFC could be modeled by a voltage source ($\overline{V}_{ser0}$) with its own internal impedance (Z_{rpfc}) and an inductive current source ($\overline{I}_{sh}$), respectively. The voltage source operates like a series compensation, and the inductive current source operates like a shunt inductive load that will absorb the reactive power from the power system. So, there should be an extra shunt compensation, such as $\overline{I}_{sh\_com}$ that could at least compensate the shunt branch of the RPFC, $\overline{I}_{sh}$. The model of the RPFC is shown in Figure 4.1.

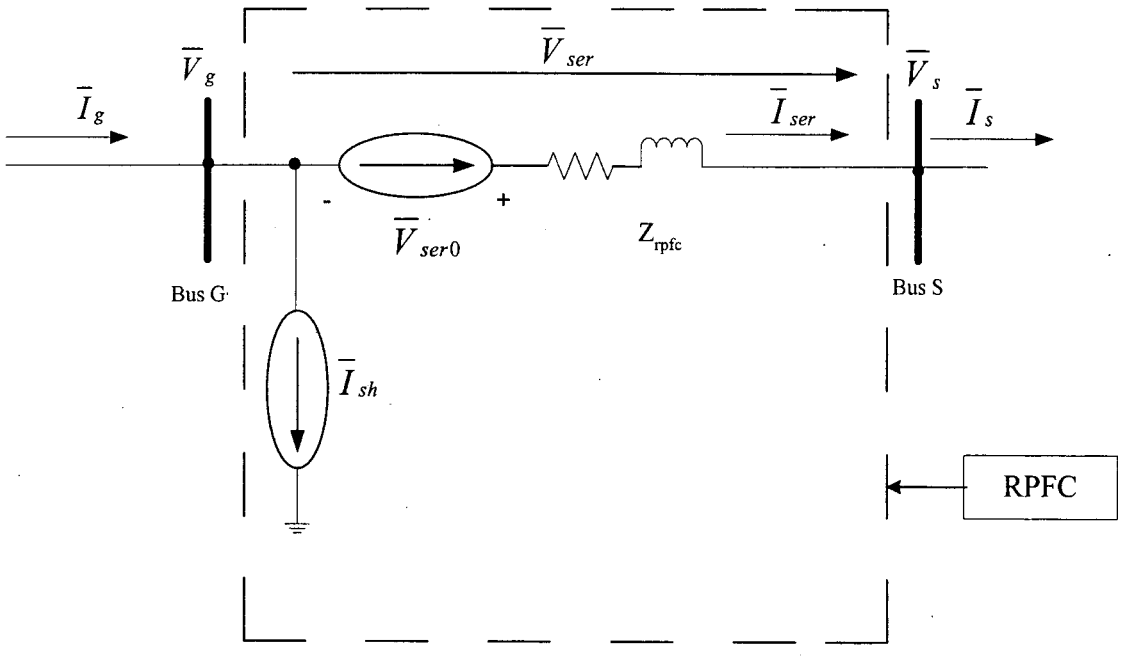

Figure 4.1- RPFC model

4.2 Operation of the RPFC

Figure 4.2 represents a power system equipped with an RPFC and a shunt compensation.

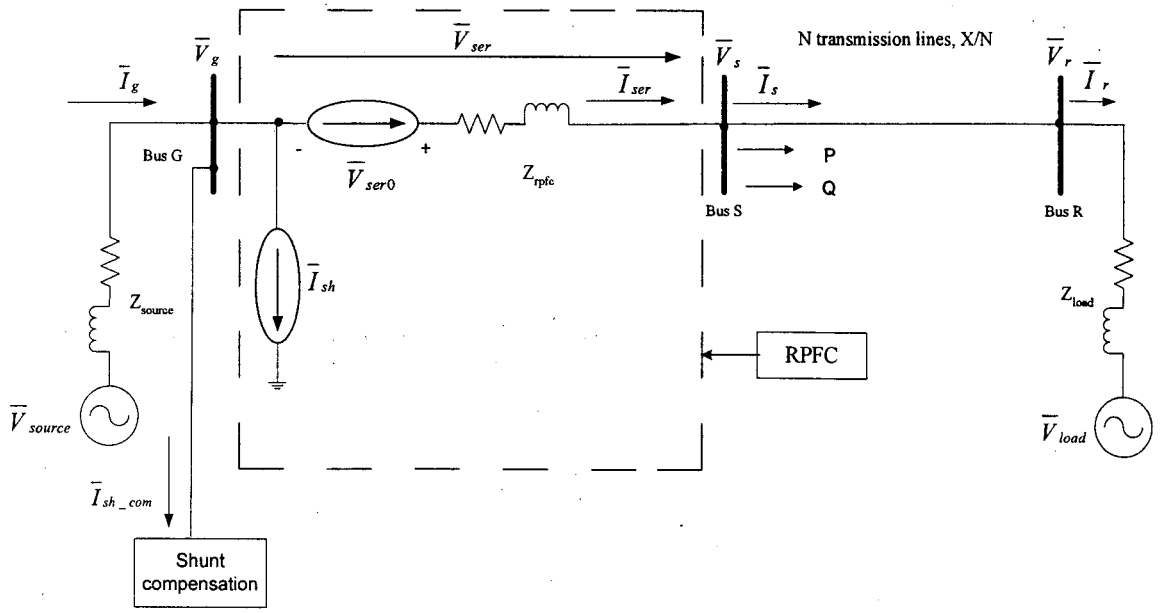

Figure 4.2 - Power system equipped with an RPFC and a shunt compensation

Where,

N - number of transmission lines

X - reactance of each transmission line (neglect the resistance)

P - transmitted active power at Bus S through the transmission lines

Q - transmitted reactive power at Bus S through the transmission lines

$$\overline{V}_{ser0} = T\left|\cos\delta\right| \cdot e^{j\varphi} \cdot \overline{V}_g \tag{4-1}$$

$$\overline{I}_{sh} = \left|\cos\delta\right| T \cdot e^{-j\varphi} \cdot \overline{I}_{ser} \tag{4-2}$$

From Figure 4.2 and (3-40), we have

$$\begin{aligned}\overline{V}_s &= \overline{V}_g + \overline{V}_{ser} \\ &= \overline{V}_g + T\left|\cos\delta\right| \cdot e^{j\varphi} \cdot \overline{V}_g - \overline{I}_{ser} \cdot Z_{rpfc} \\ &= (1 + T\left|\cos\delta\right| \cdot e^{j\varphi}) \cdot \overline{V}_g - \overline{I}_{ser} \cdot Z_{rpfc} = T_{eq} \cdot e^{j\beta_0} \cdot \overline{V}_g - \overline{I}_{ser} \cdot Z_{rpfc}\end{aligned} \tag{4-4}$$

Where,

$$T_{eq} = \sqrt{\left(1 + T^2 \cdot \cos^2\delta + 2 \cdot T \cdot \left|\cos\delta\right| \cdot \cos\varphi\right)} \tag{3-45}$$

$$\beta_0 = \cos^{-1} \frac{1 + T\left|\cos\delta\right| \cos\varphi}{\sqrt{\left(1 + T^2 \cdot \cos^2\delta + 2 \cdot T \cdot \left|\cos\delta\right| \cdot \cos\varphi\right)}} \tag{3-46}$$

Suppose $Z_{rpfc} = 0$, i.e., the RPFC is lossless, then (4-4) becomes,

$$\overline{V}_{s0} = T_{eq} \cdot e^{j\beta_0} \cdot \overline{V}_g = T_{eq} \cdot V_g \cdot e^{j(\delta_g + \beta_0)} = T_{eq} \cdot V_g \cdot e^{j\delta_{s0}} \tag{4-5}$$

Where,

δ_g - phase angle of $\overline{V}_g$

δ_{s0} - phase angle of $\overline{V}_{s0}$

$\delta_{s0} = \delta_g + \beta_0$

The powers transmitted through the transmission lines are:

$$P_0 = \frac{V_{s0} \cdot V_r \cdot \sin(\delta_{s0} - \delta_r)}{X/N} = N \cdot \frac{T_{eq} \cdot V_g \cdot V_r \cdot \sin(\delta_g - \delta_r + \beta_0)}{X} \tag{4-6}$$

$$Q_0 = \frac{V_{s0}(V_{s0} - V_r \cdot \cos(\delta_{s0} - \delta_r))}{X/N}$$

$$= N \cdot \frac{Teq \cdot V_g (Teq \cdot V_g - V_r \cdot \cos(\delta_g - \delta_r + \beta_0))}{X} \tag{4-7}$$

Compare Figure 4.2 with Figure 1.1, (1-1) and (1-2) with (4-6) and (4-7), respectively. If $\overline{V}_g$ and $\overline{V}_r$ in Figure 4.2 are equal to $\overline{V}_s$ and $\overline{V}_r$ in Figure 1.1, respectively, the transmitted powers (P_0 and Q_0) through the transmission lines in Figure 4.2 are different from those (P and Q) in Figure 1.1. That means the RPFC can control the load flow of the power system.

Refer to (3-22), (3-23), (3-38), (3-45), (3-46), (4-6) and (4-7). P_0 and Q_0 are in fact the functions of rotor positions of the two RPSTs. So, the RPFC can control the load flow of the power system through regulating the rotor positions.

Refer to (3-40). It is possible that a real $\overline{V}_{ser}$ could not approach the given $\overline{V}_{ser}$, known as $\overline{V}_{ser\_ref}$, as close as possible no matter how we regulate α1 and α2 because of the improper combination of the ratios of the series and shunt transformers (The ratio of each RPST is supposed to be 1.). That means that the RPFC could not function as desired due to these ratios. For example, if the given V_{ser} = 5 kV, T_{sh} = 0.025, T_{se} = 4, T_{rt} = 1, V_{g0} = 230 kV, then, V_{ser0_max} = 4.6 kV (< 5 kV) from (4-1). So, it is very important to choose the ratios of the two transformers (series and shunt) for the particular application.

4.3 Control of the RPFC

Based on the discussion in section 4.2, the control of the RPFC is in fact the matter of control of α1 and α2 according to the system operation requirements, such as the transmitted powers (active and/or reactive), the injected series voltage like $\overline{V}_{ser}$ and/or the shunt compensation like $\overline{I}_{sh\_com}$ in Figure 4.2, etc. In this Master dissertation, the control of α1 and α2 based on the desired $\overline{V}_{ser}$, known as $\overline{V}_{ser\_ref}$ that could be calculated based on some initial conditions as mentioned in Chapter 2, is presented. The control system of the RPFC is a regulator that will be described as the following.

For convenience, (3-22), (3-38) and (4-1) are repeated,

$$\delta = \frac{\alpha 2 - \alpha 1}{2} \tag{3-22}$$

$$\varphi = \theta + \gamma + \alpha = \frac{\alpha 2 + \alpha 1}{2} + \gamma + \alpha \tag{3-38}$$

$$\overline{V}_{ser0} = T\left|\cos\delta\right| \cdot \overline{V}_g \cdot e^{j\varphi} \tag{4-1}$$

From (3-22) and (3-38), we have

$$\alpha 1 = \varphi - \delta - (\alpha + \gamma) \tag{4-8}$$

$$\alpha 2 = \varphi + \delta - (\alpha + \gamma) \tag{4-9}$$

Refer to Figure 4.2. From the point of view of operation, it is impossible to measure $\overline{V}_{ser0}$ directly due to the losses even though $\overline{V}_{ser0}$ could be solved. The performance of $\overline{V}_{ser0}$ is indirectly represented by $\overline{V}_{ser}$ that can be measured directly.

The idea of the RPFC regulator is to get the reference $\overline{V}_{ser0\_ref}$ through controllers based on the difference between the references $\overline{V}_{ser\_ref}$ and measured $\overline{V}_{ser}$, and then δ_ref and φ_refby (4-1) and α1_ref and α2_ref by (4-8) and (4-9) that produce the actual α1 and α2 through the closed-loop control system. It is obvious that the so-called $\overline{V}_{ser\_ref}$, δ_ref φ_ref, α1_ref and α2_ref are variable parameters.

The phasor equation (4-1) can be broken into two non-phasor equations. One deals with the amplitudes of the phasors, another one deals with the angles of the phasors, as shown in (4-10) and (4-11),

$$V_{ser0} = T\left|\cos\delta\right| \cdot V_g \tag{4-10}$$

$$\angle\overline{V}_{ser0} = \varphi + \angle\overline{V}_g \tag{4-11}$$

From (4-10) and (4-11), we notice that, the angle and amplitude of $\overline{V}_{ser0}$ are proportional to φ and $\left|\cos\delta\right|$, respectively, if $\overline{V}_g$ is a constant.

The model of the RPFC regulator is implemented based on (4-8) and (4-11), as shown in Figure 4.3.

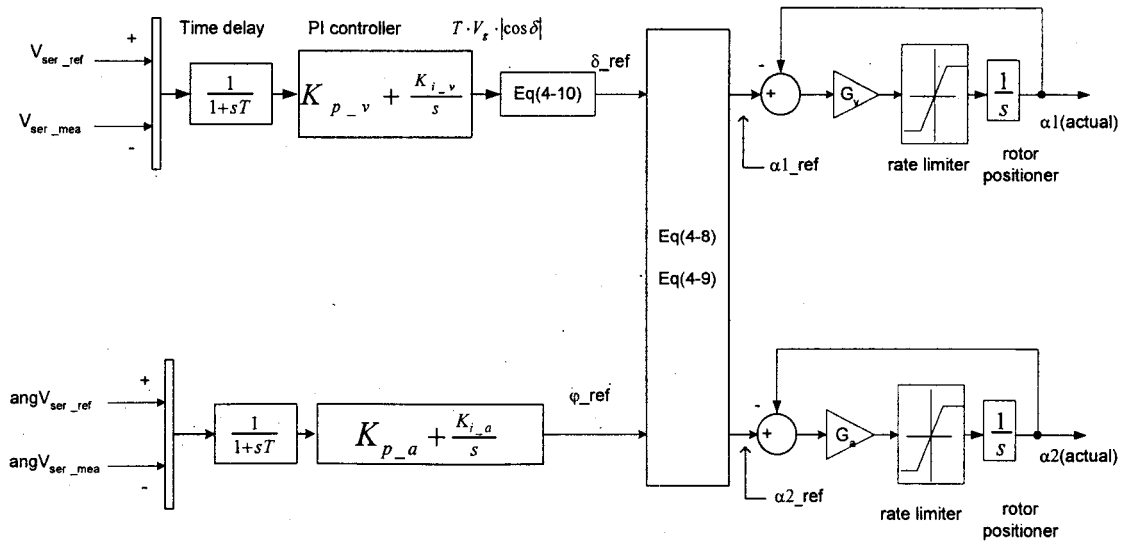

RPFC regulator model

Figure 4.3 - RPFC regulator model

Where,

V_{ser_ref} - the amplitude of reference $\overline{V}_{ser\_ref}$

V_{ser_mea} - the amplitude of measured $\overline{V}_{ser}$ (i.e., real $\overline{V}_{ser}$) ;

$angV_{ser\_ref}$ - the angle of reference $\overline{V}_{ser\_ref}$

$angV_{ser\_mea}$ - the angle of measured $\overline{V}_{ser}$ (i.e., real $\overline{V}_{ser}$)

K_{p_v} , K_{p_a} - proportional factors of PI controllers

K_{i_v} , K_{i_a} - integral factors of PI controllers

G_v , G_a - gains of amplifiers

In the RPFC regulator model, two independent error signals, i.e., (V_{ser_ref} - V_{ser_mea}) and ($angV_{ser\_ref}$ - $angV_{ser\_mea}$), are applied to two individual proportional/integral (PI) controllers to determine the ideal δ_ref and φ_ref, and then the desired rotor position signals α1 and α2 through (4-10) and (4-11). The two rotor positioners move the two RPSTs' rotors to the desired positions, subject to a limit on the rate of change.

The formula, (4-8)~(4-11), which are used to determine the desired rotor positions, are based on the ideal RPFC without considering the reactance drop of the series and shunt transformers and the two RPSTs. Therefore, the measured $\overline{V}_{ser}$, which is produced by α1 (actual) and α2 (actual) through the closed-loop control system based on the ideal RPFC, will not match $\overline{V}_{ser\_ref}$. However, this does not matter since the individual regulator will attempt to drive its own error signal to zero through its own PI controller.

It should be noted that the control system of the RPFC is a two-input-two-output system. The parameters, K_{p_v} and K_{p_a}, K_{i_v} and K_{i_a}, G_v and G_a, could not be the same, respectively. The control system of the RPFC could work properly based on the proper coordination between those parameters. But finding those suitable parameters is time-consuming and complicated, and there definitely exist the optimal parameters because δ_ref is controlled by K_{p_v} and K_{i_v} in one one-input-one-output system, φ_ref is controlled by K_{p_a} and K_{i_a} in another one one-input-one-output system; but, α1_ref and α2_ref are determined by δ_ref and φ_ref. It is similar to G_v and G_a for the final outputs (i.e., α1(actual) and α2(actual)) of the control system of the RPFC.

In this Master dissertation, the parameters, which are used in the simulations in the following chapters, are based on [4], and as the following,

$$K_{p\_v} = 0.1,\ K_{i\_v} = 1.75,\ G_v = 35$$
$$K_{p\_a} = 0.1,\ K_{i\_a} = 0.7,\quad G_a = 20$$
$$\text{rate limiter} = 150 \text{ deg / s}$$

4.4 Implementation of the RPFC Model by SPS and Matlab/Simulink

Inserting (3-47) and (3-48) into (4-1), we have,

$$\overline{V}_{ser} = \overline{V}_{ser0} - \overline{I}_{ser} \cdot Z_{rpfc} = \overline{V}_{ser0} - \overline{I}_{ser} \cdot Z_{rpfc\_c} - \overline{I}_{ser} \cdot Z_{rpfc\_v} \tag{4-12}$$

Define:

$$T_{ser} = T\left|\cos\delta\right| \tag{4-13}$$

$$\overline{V}_{Z_{rpfc\_v}} = \overline{I}_{ser} \cdot Z_{rpfc\_v} \tag{4-14}$$

Inserting (4-13) and (4-14) into (4-1), (4-2) and (4-12), respectively, we have,

$$\overline{V}_{ser0} = T_{ser} \cdot e^{j\varphi} \cdot \overline{V}_g \tag{4-15}$$

$$\overline{I}_{sh} = T_{ser} \cdot e^{-j\varphi} \cdot \overline{I}_{ser} \tag{4-16}$$

$$\overline{V}_{ser} = \overline{V}_{ser0} - \overline{I}_{ser} \cdot Z_{rpfc\_c} - \overline{V}_{Z_{rpfc\_v}} \tag{4-17}$$

With (4-15) ~ (4-17), the RPFC model in Figure 4.1 is implemented by SPS and Matlab/Simulink, as shown in Figure 4.4.

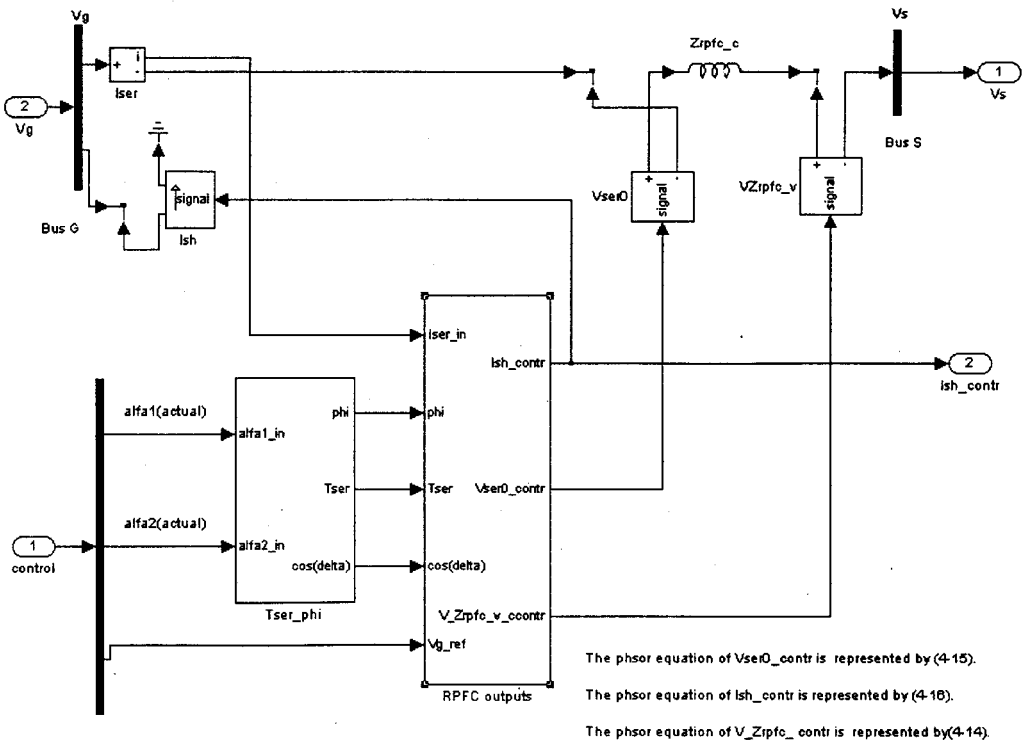

Figure 4.4 - RPFC model implemented by SPS and Matlab/Simulink

Where,

a. Signals α1(actual) and α2(actual) come from Figure 4.3;
b. In Block Tser_phi, the outputs are calculated through (3-22), (3-38), and (4-13);
c. In Block RPFC outputs, the outputs are calculated through (4-14), (4-15), (4-16);
d. The phasor equation of $V\_Z_{rpfc\_contr}$ is represented by (4-14);
e. The phasor equation of V_{ser0_contr} is represented by (4-15);
f. The phasor equation of I_{sh_contr} is represented by (4-16).

4.5 Summary

- The RPFC has been modeled by a voltage source in series with the transmission system and an inductive current source in parallel with the system (Figure 4.1).
- The improper coordination between T_{sh} and T_{se} could result in the RPFC not reaching its expected performance.
- The control system for the RPFC is a two-inputs-two-outputs system (Figure 4.3). The coordination among the parameters of the control system is very important for the successful RPFC operation.
- The RPFC can be simulated in SPS and Matlab/Simulink (Figure 4.4).

CHAPTER 5 SIMULATIONS OF A POWER SYSTEM EQUIPPED WITH AN RPFC IN SYMMETRICAL OPERATION

5.1 Power system being simulated and its components

In this chapter, two simulations, in which an RPFC and a three-phase shunt compensation are applied to a two-line power system in symmetrical operation, are carried out in the Matlab/Simulink environment. In the two simulations, the pole-pair numbers of each RPST are one (1) and six (6), respectively. So, we will observe not only the operation of the RPFC as a whole, but also the operation of the pole-pair numbers of RPST from the two simulations.

Here, the term "symmetrical operation" refers to the operation mode in which the RPFC and the three-phase shunt compensation are applied to the three phases of the 2-line power system after the three phases of one of the two lines are opened.

5.1.1 Power system being simulated

The power system to be simulated is a two-machine, two-line system. Figure 5.1 and Figure 5.2 represent the pre- and post-contingency power systems to be simulated, respectively. In the systems, there are:

- Two synchronous machines, $\overline{V}_{source}$ and $\overline{V}_{load}$, with their own internal impedances, Z_{source} and Z_{load}, which represent the source and load respectively;
- Two transmission lines in parallel, Line 1 and Line 2, one step-up transformer and one step-down transformer;
- One RPFC that includes one shunt transformer, one series transformer, and two RPSTs each of which has 1 pole-pair.
- One three-phase shunt compensation.

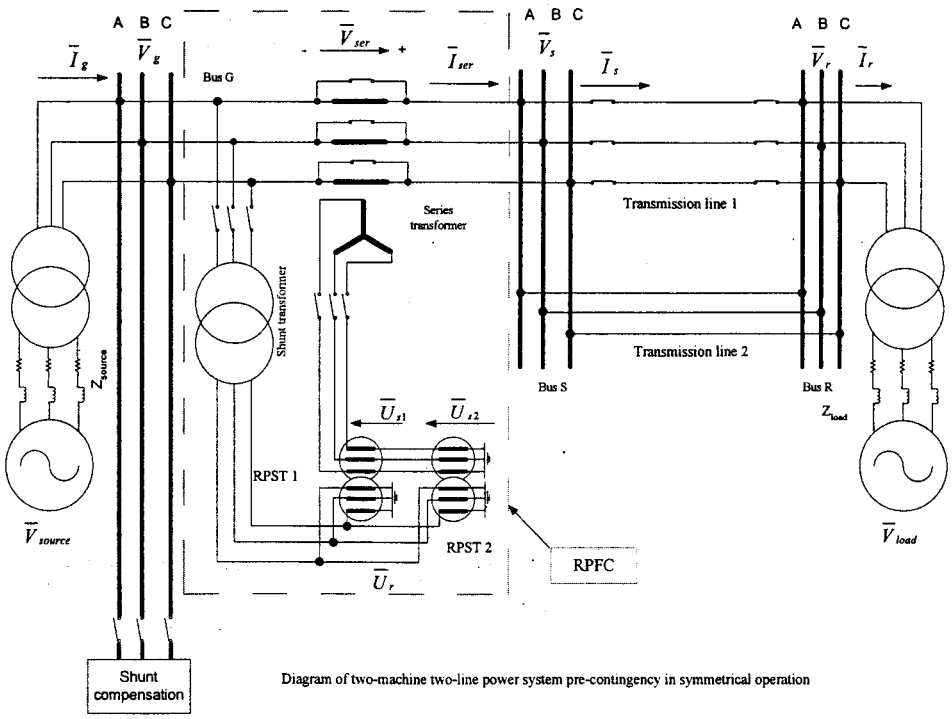

Figure 5.1 - Diagram of a two-machine two-line power system pre-contingency

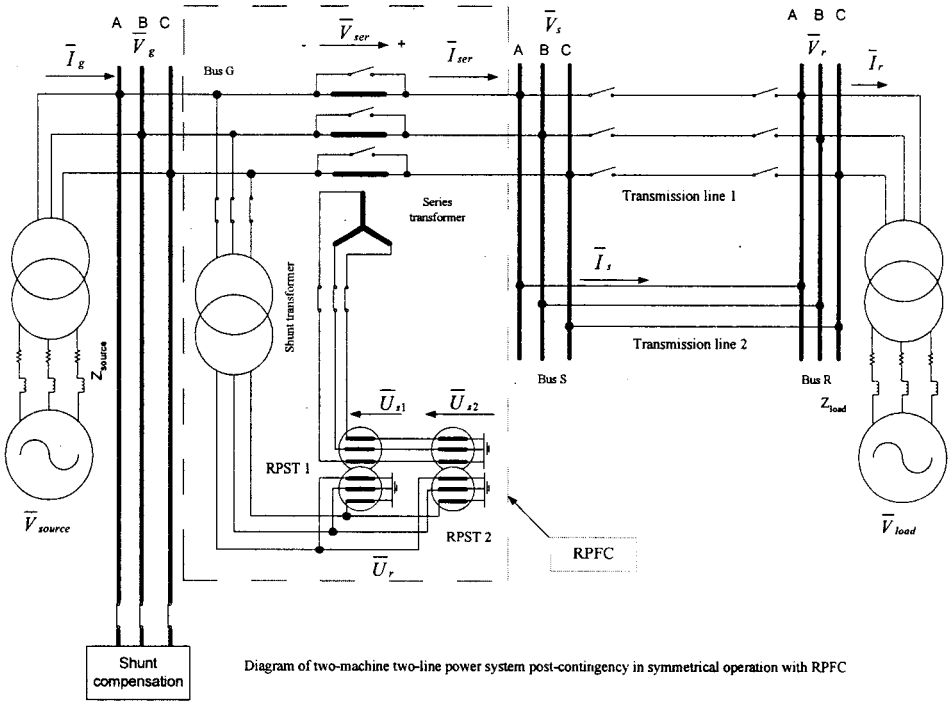

Figure 5.2 - Diagram of a two-machine two-line power system post-contingency in symmetrical operation with the RPFC and a three-phase shunt compensation

The pre-contingency power system (Figure 5.1) refers to two lines (Line 1 and Line 2) in service; and the post-contingency power system (Figure 5.2) refers to Line 2 in service with the RPFC and a three-phase shunt compensation after the three phases of Line 1 are opened permanently.

5.1.2 Parameters of the electrical equipment in the power system

a) Transmission line [20]

Table 5.1 presents the parameters of each transmission line.

Table 5.1 - Parameters of the transmission line

Electrical Equipment	Parameters
Line	• Nominal voltage = 400 kV • Length = 150 km • Parameters per kilometer: $r_L = 0.02\ \Omega$ / km , $x_L = 0.3\ \Omega$ / km, $b_L = 6.0\ \mu S$ / km.

Based on Table 5.1,

- The lumped parameters of each transmission line are:

  $R_L = 3\ \Omega$, $X_L = 45\ \Omega$, $B_L = 0.0009$ S

- The 4-port parameters of the π-type transmission line are:

  $A_0 = D_0 = 0.919 \angle 0.34$,

  $B_0 = 45.10 \angle 86.19\ \Omega$,

  $C_0 = 8.91 \times 10^{-4} \angle 90.04$ S

b) - Source, Load and step-up and step-down transformers [20]

Table 5.2 presents the parameters of the electrical equipment.

Table 5.2 - Parameters of Source, Load, and Transformers

Electrical Equipment	Parameters
Source	• Balanced and three-phase sinusoidal source at 60 Hz • Nominal voltage = 14.0 kV • Capacity = 1500 MVA • Internal resistance R_{source} = 0.013 Ω • Internal inductance L_{source} = 0.347 mH
Load	• Balanced and three-phase sinusoidal source at 60 Hz • Nominal voltage = 69.0 kV • Capacity = 1400 MVA • Internal resistance R_{load} = 0.34 Ω • Internal inductance L_{load} = 9.02 mH
Step-up transformer	• Nominal voltage = 13.8 / 459 kV • Capacity = 1500 MVA, three-phase • Leakage reactance in percentage X_{t_source} = 8.5% • Resistance in percentage R_{t_source} = 0.05% * • Connection of the transformer: Yg/ Yg.
Step-down transformer	• Nominal voltage = 459 / 69 kV • Capacity = 1500 MVA, three-phase • Leakage reactance in percentage X_{t_load} = 8.5% • Resistance in percentage R_{t_load} = 0.05%* • Connection of the transformer: Yg/ Yg

*For the convenience of simulations, acceptable minimum values are used.

c) The Rotary Power Flow Controller (RPFC) [4]

Table 5.3 presents the parameters of components of the RPFC.

Table 5.3 - Parameters of electrical equipment of the RPFC

Electrical Equipment	Parameters
Series transformer	• Nominal voltage = 125 / 50 kV • Capacity = 500 MVA, three-phase • Leakage reactance Xse(p.u.) = 0.1 • Connection of the transformer: Y /Yg
Shunt transformer	• Nominal voltage = 400 / 25 kV • Capacity = 500 MVA, three-phase • Leakage reactance X_{sh}(p.u.) = 0.1 • Connection of the transformer: Yg / Yg
RPST (RPST 1 and RPST 2)	• Nominal voltage = 25 / 25 kV • Capacity = 250 MVA, three-phase • Leakage reactance Xrt (p.u.)= 0.2

Referring to Table 5.3, (3-1) ~(3-3), and (3-37), we obtain

- The real value of the leakage reactance of the series transformer seen from the 125 kV side is $X_{se} = 3.125\ \Omega$; $T_{se} = 125 / 50 = 2.5$.
- The real value of the leakage reactance of the shunt transformer seen from the 25 kV side is $X_{sh} = 0.125\ \Omega$; $T_{sh} = 25 / 400 = 0.0625$.
- The real value of the leakage reactance of the RPST seen from the 25 kV side is $X_{rt} = 0.5\ \Omega$; $T_{rt} = 25 / 25 = 1$.
- T=0.3125 (Equation (3-37))

5.2 Equivalent circuit of the post-contingency power system

Because the post-contingency power system is in symmetrical operation, its three-phase circuit (Figure 5.2) can be represented by a single-phase circuit (Figure 5.3a, where, N = 2, L = 1).

Reviewing Chapter 4, we can get the equivalent circuit (Figure 5.3b) of Figure 5.3a. Of course, Figure 5.3b is the single-phase equivalent circuit of Figure 5.2. From Figure 5.3b, we have the following equations with respect to Bus S and Bus R:

$$\begin{bmatrix} \overline{V}_g + \overline{V}_{ser} \\ \overline{I}_g - \overline{I}_{sh\_com} - \overline{I}_{sh} \end{bmatrix} = \begin{bmatrix} A_0 & B_0/(N-L) \\ (N-L)\cdot C_0 & D_0 \end{bmatrix} \cdot \begin{bmatrix} \overline{V}_r \\ \overline{I}_r \end{bmatrix} \tag{5-1}$$

Review Chapter 2. $\overline{V}_g$, $\overline{I}_g$, $\overline{V}_r$ and $\overline{I}_r$ in (5-1) should be the load flows when N (N = 2) lines are in service referring to Figure 5.1.

From (5-1), we have

$$\overline{V}_{ser} = \frac{L}{N-L}(\overline{V}_g - A_0 \cdot \overline{V}_r) \tag{5-2}$$

$$\overline{I}_{sh\_com} - \overline{I}_{sh} = L \cdot C_0 \cdot \overline{V}r \tag{5-3}$$

From (5-2), the desired $\overline{V}_{ser}$, called the reference series compensation, $\overline{V}_{ser\_ref}$, can be solved. But, from (5-3), the desired $\overline{I}_{sh\_com}$, called the reference $\overline{I}_{sh\_com\_ref}$, cannot be solved because of the existence of $\overline{I}_{sh}$--the shunt branch of the equivalent circuit of the RPFC, which varies with α1 and α2 that also control the real series compensation $\overline{V}_{ser}$ based on $\overline{V}_{ser\_ref}$. This is the characteristic of the RPFC operation from the point of view of operation and control.

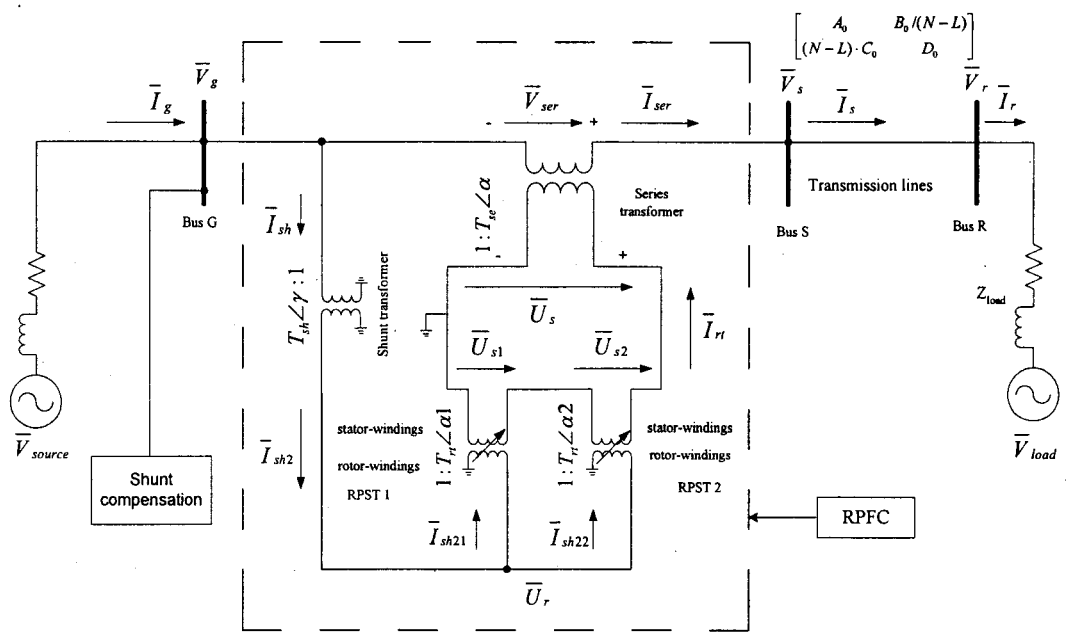

Single-phase diagram of power system equipped with RPFC and a shunt compensation

Figure 5.3a - Single-phase circuit of Figure 5.2

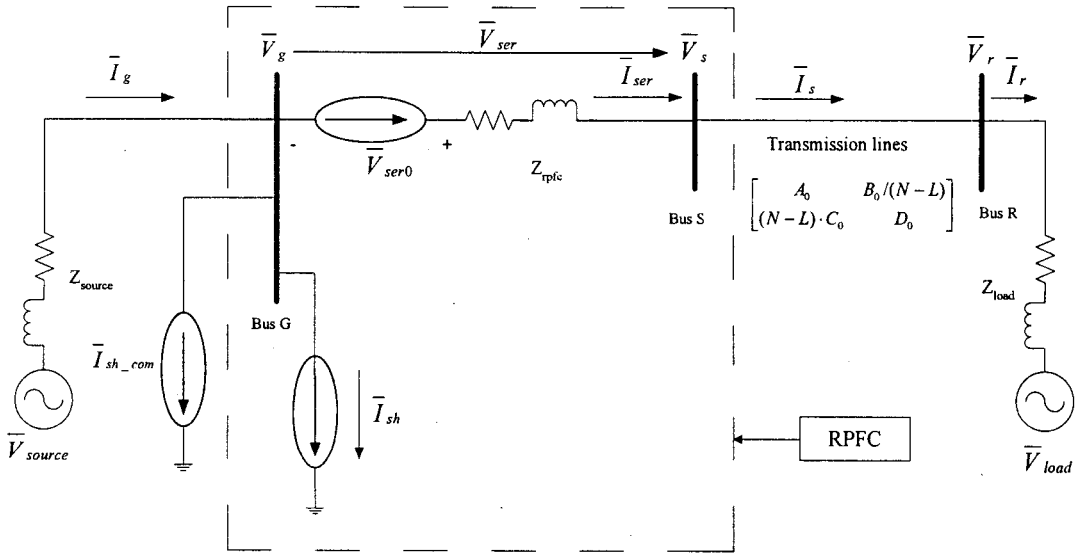

Single-phase equivalent circuit of Figure 4.2

Figure 5.3b - Single-phase equivalent circuit of Figure 5.2

Comparing Figure 2.6 with Figure 5.3b, and (2-11) with (5-3), we have,

$$\overline{I}_{es} = \overline{I}_{sh\_com} - \overline{I}_{sh}$$

That means that the net shunt compensation is a constant that can be solved by equation (5-3). A so-called reference of net shunt compensation could be defined as $\overline{I}_{es\_ref}$ from the point of view of shunt compensation.

Based on the above, we define:

$$\overline{V}_{ser\_ref} = \frac{L}{N-L}(\overline{V}_g - A_0 \cdot \overline{V}_r) \tag{5-4}$$

$$\overline{I}_{es\_ref} = L \cdot C_0 \cdot \overline{V}r \tag{5-5}$$

- ***Calculations for the relevant reference values***

Refer to Figure 5.1.The pre-contingency load flows of Phase-A at Bus G and Bus R are shown in Table 5.4. (in the forms of phasor).

Table 5.4 Phase-A load flow of the pre-contingency system simulated

At Source	At Bus G		At Bus R		At Load
$\overline{V}_{source}$ (kV/deg)	$\overline{V}_g$ (kV/deg)	$\overline{I}_g$ (A/deg)	$\overline{V}_r$ (kV/deg)	$\overline{I}_r$ (A/deg)	$\overline{V}_{load}$ (kV/deg)
$1.493 \cdot 14\angle 53.47$	$230.8\angle 0.$	$2034\angle 4.11$	$230.1\angle -11.34$	$2006\angle -7.6$	$1.49 \cdot 69\angle -66.8$

Based on Table 5.4, $\overline{V}_{ser\_ref}$ and $\overline{I}_{es\_ref}$ can be calculated by (5-4) and (5-5),

$$\overline{V}_{ser\_ref} = 44.9\angle 78.52 \quad \text{kV}$$

$$\overline{I}_{es\_ref} = 205.0\angle 78.70 \quad \text{A}$$

And, the current through each of the two lines is $\bar{I}_{line\_pre\_fault} = 1014.9\angle -1.75$ A.

Where, $\bar{I}_{line\_pre\_fault} = 0.5(\bar{I}_g - \bar{I}_{2\_line\_capacitor}) = 0.5(\bar{I}_g - 2 \cdot 0.5 B_L \cdot \bar{V}_g)$.

5.3 Simulation cases

5.3.1 Description of the simulation process

The simulation model (Figure 5.4) is represented by SPS and Matlab/Simulink. The simulation process in Figure 5.4 is described in Table 5.5.

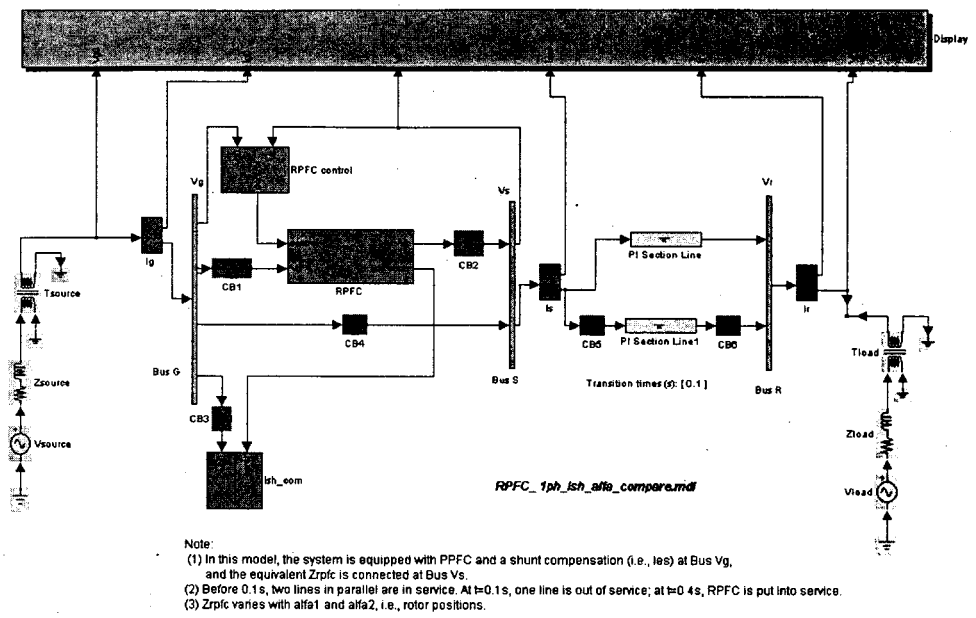

Figure 5.4 Simulation model in symmetrical operation represented by SPS and Matlab/Simulink

Table 5.5 Description of the simulation process

Time(s)	Circuit-breakers in open state	Circuit-breakers in closed state	Operation of transmission lines
0.0	CB1, CB2, CB3	CB4, CB5, CB6	2 lines
0.1	CB1, CB2, CB3, CB5, CB6	CB4	1 line without RPFC
0.4	CB4, CB5, CB6	CB1, CB2, CB3	1 line with RPFC

In Table 5.5, each circuit-breaker would keep its own initial state until there is a switching operation on it at the prescribed instant.

5.3.2 Simulation Case 1 - Symmetrical operation with two one-pole-pair RPSTs

5.3.2.1 Results of Simulation Case 1

- In our study, the insertion of the RPFC and the three-phase shunt compensation after a contingency preserves the pre-contingency load flows at Bus G and Bus R, so we are interested in the voltages, currents and powers at the two buses during the simulation;
- From the point of view of compensations, we are interested in the shunt compensation I_{sh_com} and series compensation $\overline{V}_{ser}$.
- From the point of view of control of the RPFC (see Figure 4.3), we are interested in δ_ref, φ_ref, $\alpha 1$ and $\alpha 2$.

Figure 5.5 to Figure 5.16 show the curves of Simulation Case 1.

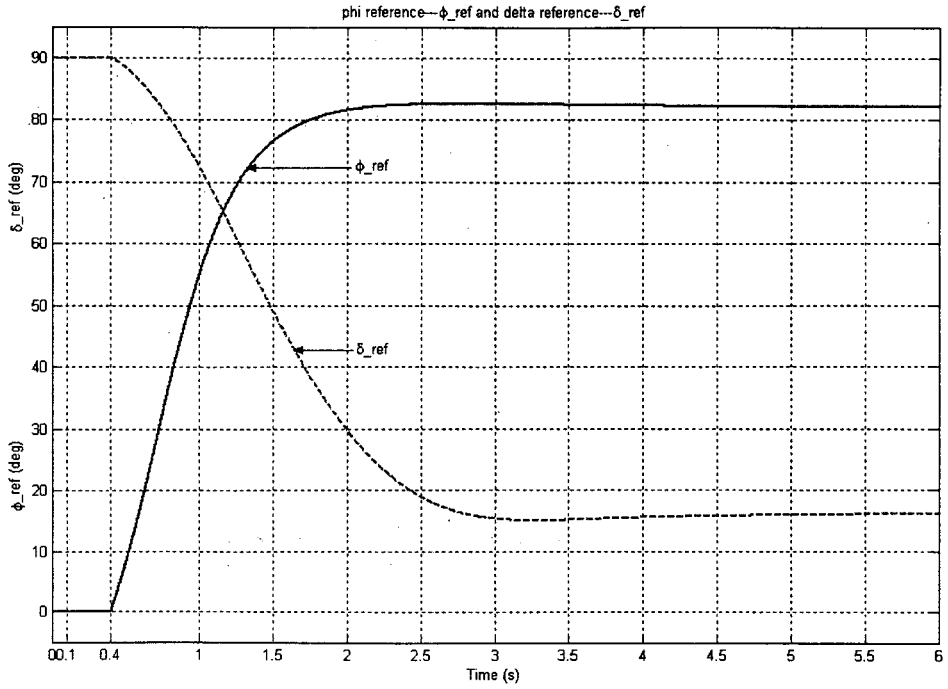

Figure 5.5 - Curves of φ_ref and δ_ref in Simulation Case 1

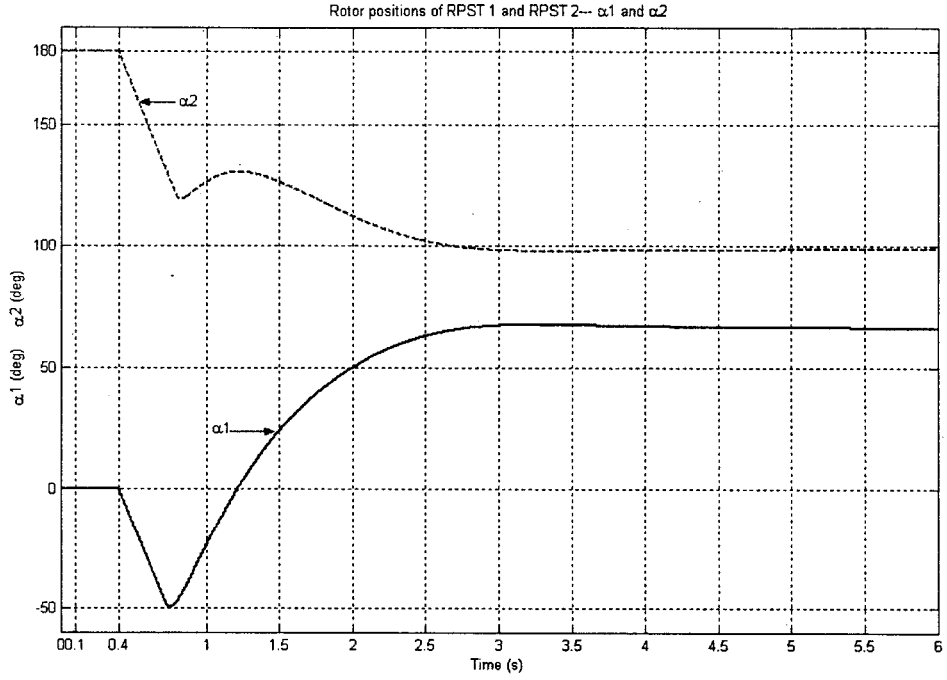

Figure 5.6 - Rotor positions of RPST 1 and RPST 2--α1 and α2 in Simulation Case 1

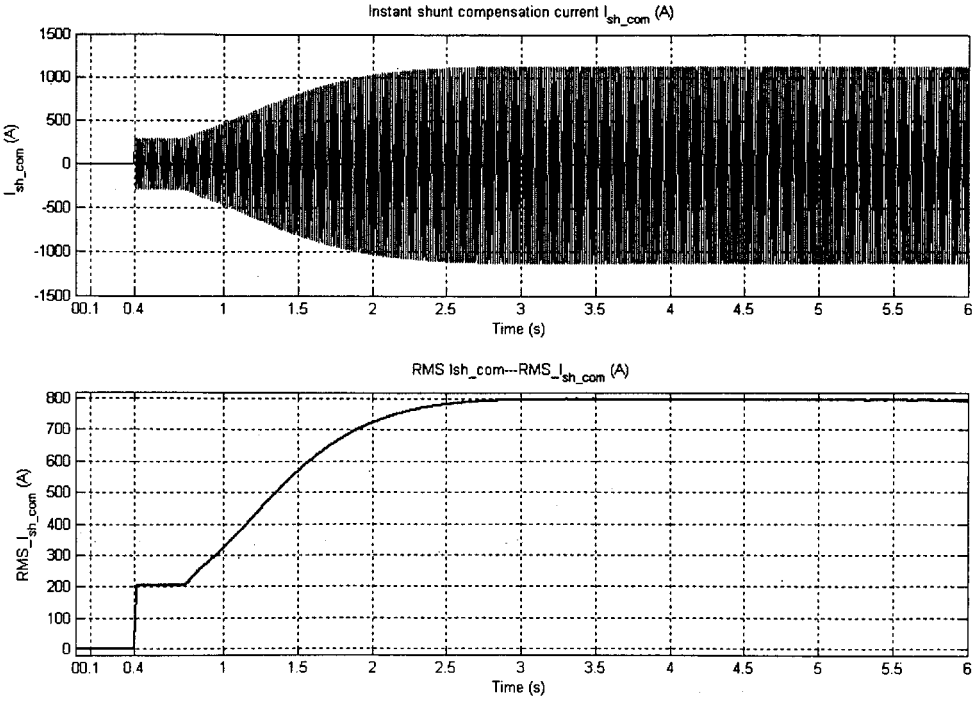

Figure - 5.7 Shunt compensation current $I_{sh\ com}$ in Simulation Case 1

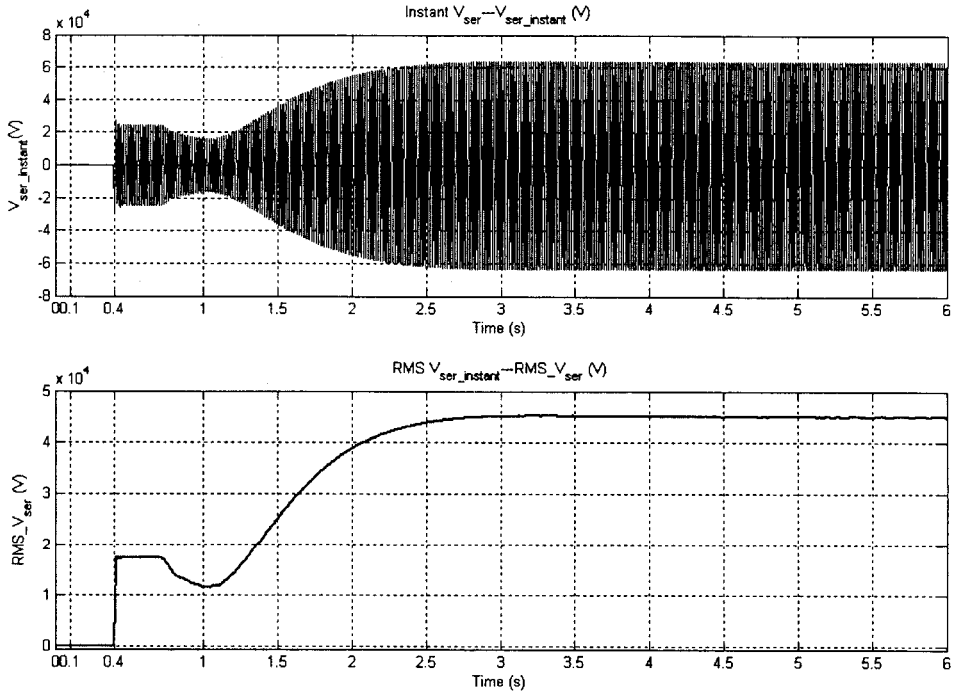

Figure 5.8 - Inserted series voltage V_{ser} in Simulation Case 1

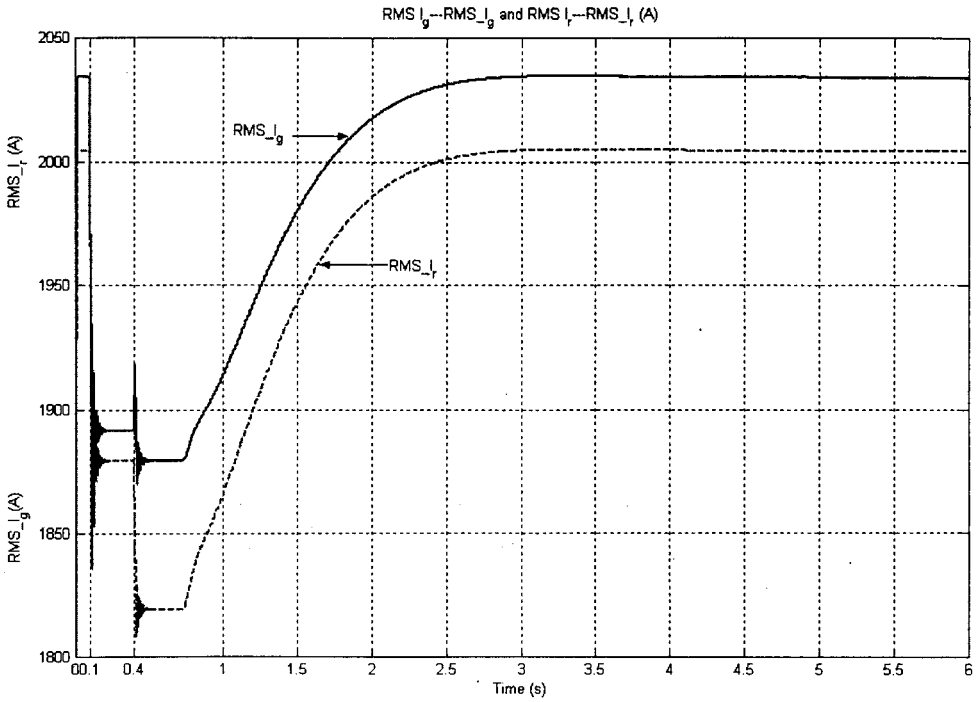

Figure 5.9 - The rms currents at Bus G and Bus R in Simulation Case 1

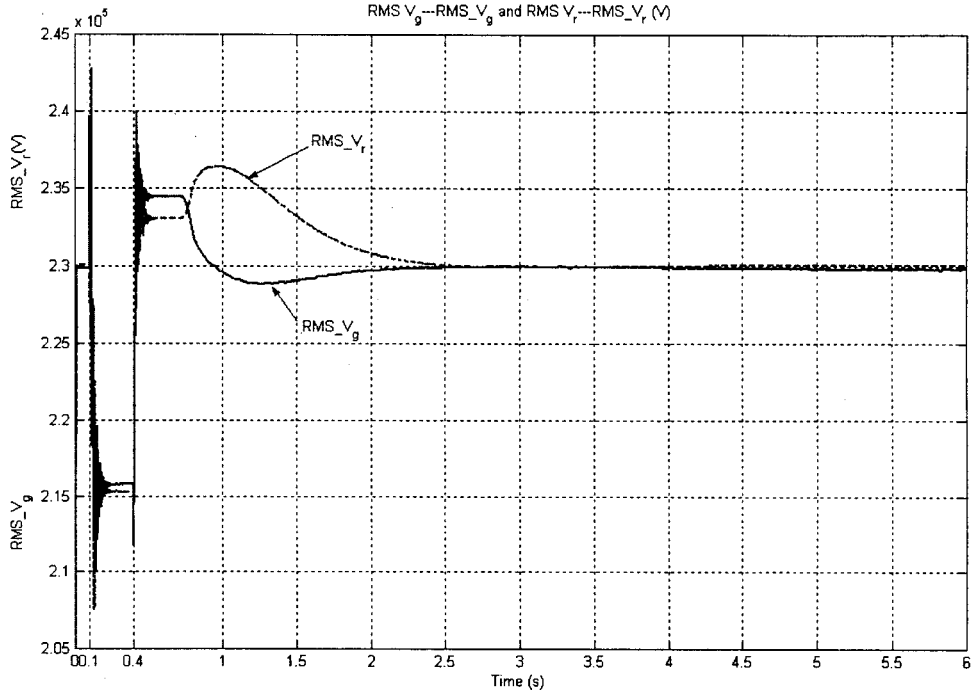

Figure 5.10 - The rms voltages at Bus G and Bus R in Simulation Case 1

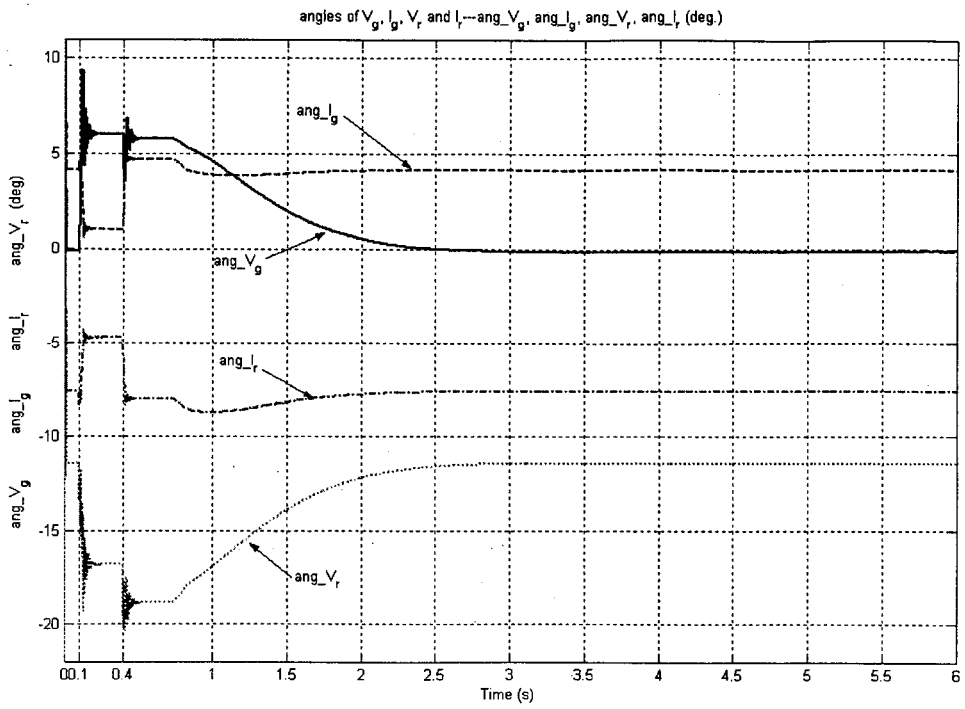

Figure 5.11 - Angles of voltages and currents at Bus G and Bus R in Simulation Case 1

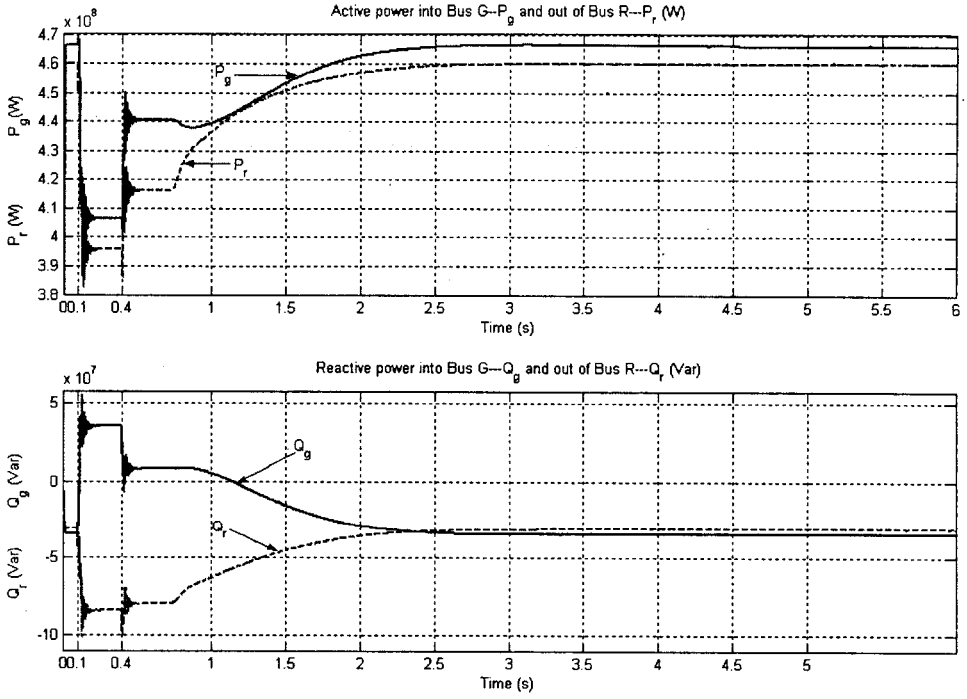

Figure 5.12 - Active and reactive powers at Bus G and Bus R in Simulation Case 1

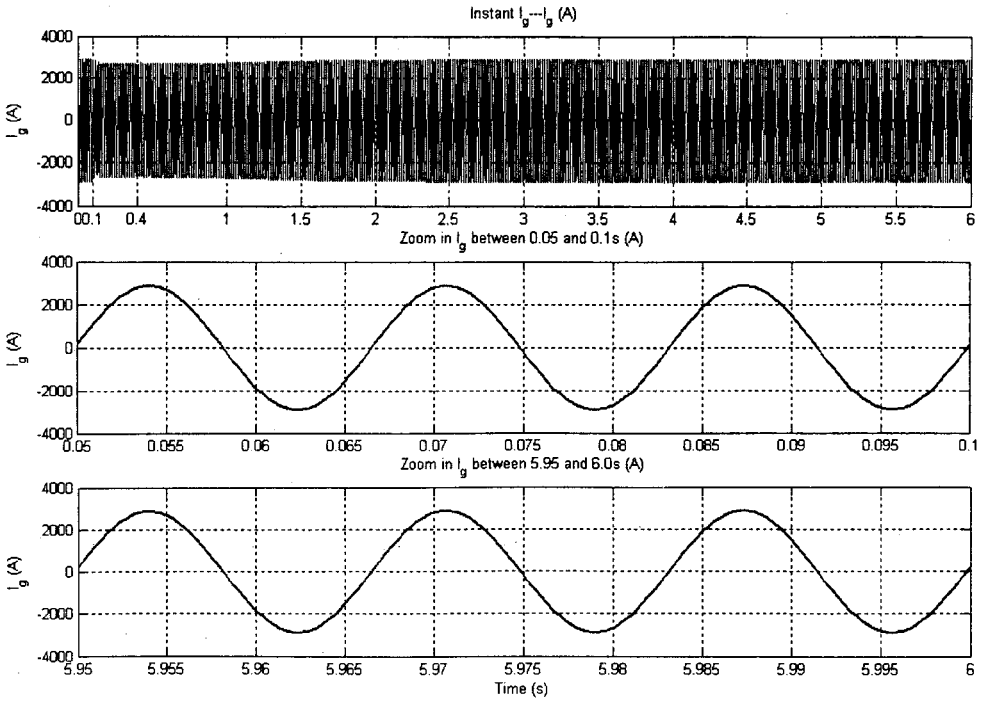

Figure 5.13 - Instantaneous current at Bus G in Simulation Case 1

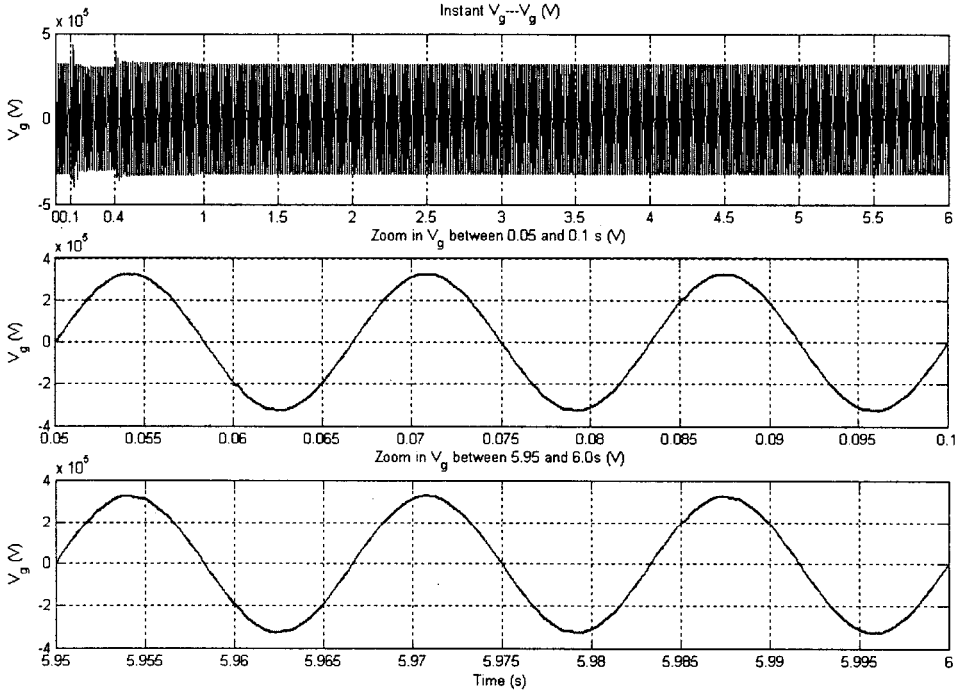

Figure 5.14 - Instantaneous voltage at Bus G in Simulation Case 1

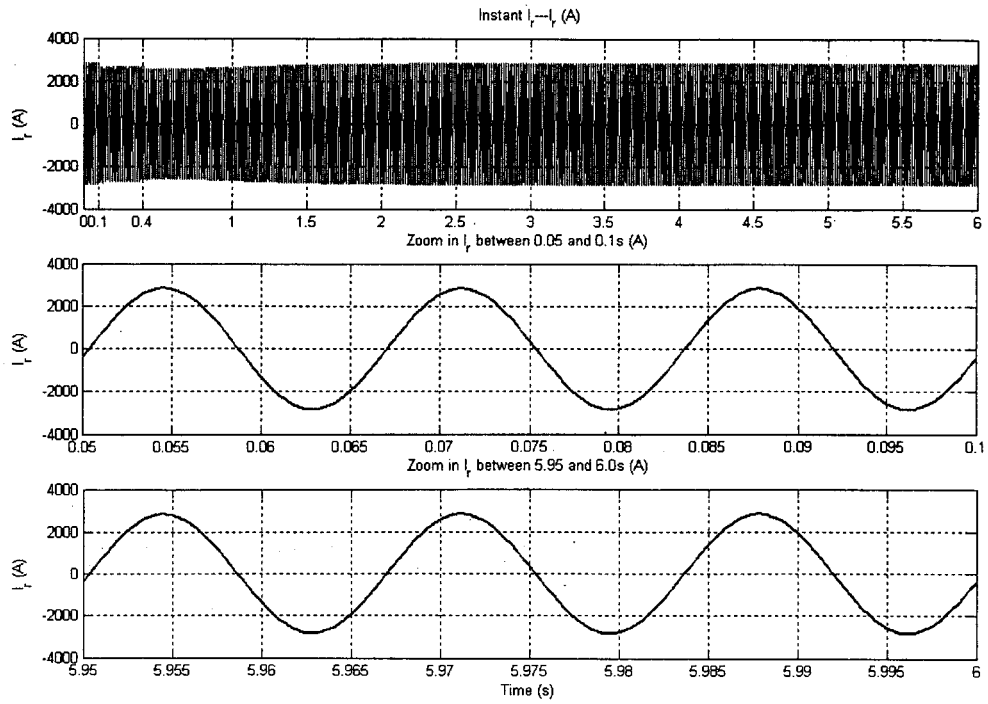

Figure 5.15 - Instantaneous current at Bus R in Simulation Case 1

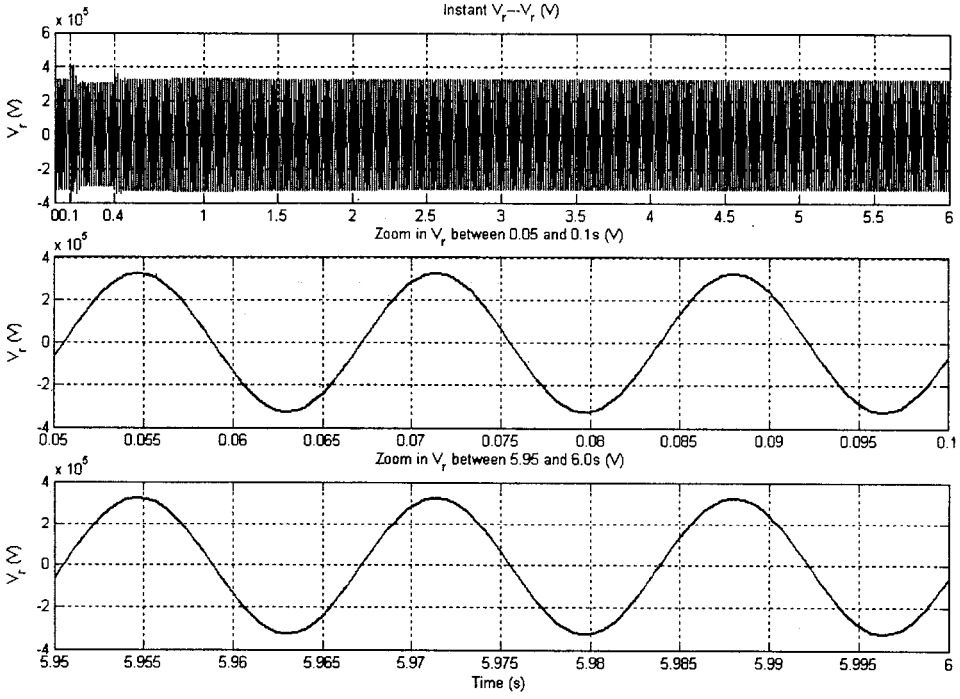

Figure 5.16 - Instantaneous at Bus R in Simulation Case 1

5.3.2.2 Analysis of results of Simulation Case 1

(1) Refer to Figure 5.5. The steady-state references (t = 6.0 s) of φ_ref and δ_ref for the control of the RPFC are:

$$\varphi\_ref = 82.29 \text{ deg.} \quad (5\text{-}6)$$

$$\delta\_ref = 16.30 \text{ deg.} \quad (5\text{-}7)$$

(2) Refer to Figure 5.6. The steady-state values (t = 6.0 s) of rotor positions of the two RPSTs are:

$$\alpha 1 = 65.99 \text{ deg.} \quad (5\text{-}8)$$

$$\alpha 2 = 98.58 \text{ deg.} \quad (5\text{-}9)$$

- Inserting (5-8) and (5-9) into (3-22) and (3-38), we get,

$$\delta = \frac{\alpha 2 - \alpha 1}{2} = 16.30 \text{ (deg.)} \quad (5\text{-}10)$$

$$\varphi = \theta + \gamma + \alpha = \frac{\alpha 2 + \alpha 1}{2} + \gamma + \alpha = 82.29 \text{ (deg.)} \quad (5\text{-}11)$$

It shows that the steady-state φ and δ are almost the same as the steady-state φ_ref and δ_ref, respectively.

Note: In our project, γ and α are zeros.

- Inserting (3-37), (5-10) and (5-11) into, (3-45) and (3-46), we get,

$$T_{eq} = 1.0819 \quad (5\text{-}12)$$

$$\beta_0 = 15.95 \text{ (deg)} \quad (5\text{-}13)$$

(3) Refer to c) in Section 5.1.2 and (5-10). The two parts of the equivalent impedance of the RPFC can be calculated by (3-47) and (3-48),

$$Z_{rpfc\_c} = Z_{se} + 2 \cdot T_{se}^2 \cdot Z_{rt} = j9.375 \quad (\Omega) \tag{5-14}$$

$$Z_{rpfc\_v} = 4 \cdot T_{rt}^2 \cdot T_{se}^2 \cdot \cos^2 \delta \cdot Z_{sh} = j2.879 \quad (\Omega) \tag{5-15}$$

Then, $$Z_{rpfc} = Z_{rpfc\_c} + Z_{rpfc\_v} = j12.245 \quad (\Omega) \tag{5-16}$$

(4) Refer to Figure 5.7 and Figure 5.8. The steady-state shunt compensation current (t = 6.0 s), $\overline{I}_{sh\_com}$, and the injected series voltage, $\overline{V}_{ser}$, are:

$$\overline{I}_{sh\_com} = 794.2\angle 91.52 \text{ (A)} \tag{5-17}$$

$$\overline{V}_{ser} = 44.92\angle 78.57 \text{ (kV)} \tag{5-18}$$

It shows that $\overline{V}_{ser}$ is close to $\overline{V}_{ser\_ref}$ that is $44.9\angle 78.52$ kV.

Refer to Figure 5.3b, Table 5.6, and (5-18). The steady-state value $\overline{V}_s$ (t = 6.0 s) is:

$$\overline{V}_s = \overline{V}g + \overline{V}ser = 242.67\angle 10.38 \text{ (kV)} \tag{5-19}$$

(5) Inserting T=0.3125 (see c) in section 5.1.2), $\overline{V}_g = 229.8 \times 10^3 \angle -0.08$ (Table 5.6), (5-10), (5-11), (5-16) and (5-18) into (3-40), we obtain

$$\overline{I}_{ser} = \frac{T \cdot |\cos\delta| \cdot \overline{V}_g \cdot e^{j\varphi} - \overline{V}_{ser}}{Z_{rpfc}} = 1980.2\angle -1.055 \text{ (A)} \tag{5-20}$$

Then, the current through the sound line is $\bar{I}_{line\_post\_fault} = 2004.7\angle -4.12$ A.
Where,

$$\bar{I}_{line\_post\_fault} = \bar{I}_{ser} - \bar{I}_{line\_capacitor} = \bar{I}_{ser} - 0.5B_L \cdot \bar{V}_s \qquad (5\text{-}21)$$

It shows that $\bar{I}_{line\_post\_fault}$ is increased, compared with the current through one of the two pre-fault transmission lines ($\bar{I}_{line\_pre\_fault} = 1014.9\angle -1.75$, see section 5.2).

And, the power through the sound line (i.e., out of Bus S) is

$$S_{BUS\_S} = \bar{V}s \cdot (\bar{I}_{ser})^* = 471 + j95.26 \quad \text{(MW, MVar)} \qquad (5\text{-}22)$$

Thus, the three-phase active power transmitted through the sound transmission line (3*471 MW) is greater than that through the two pre-fault transmission lines (3*466 MW)

(6) Refer to Figure 5.3b, Table 5.6, (5-17) and (5-20). The steady-state value $\bar{I}_{sh}$ (t = 6.0 s) is:

$$\bar{I}_{sh} = \bar{I}_g - \bar{I}_{sh\_com} - \bar{I}_{ser} = 615.28\angle -83.5 \text{ (A)} \qquad (5\text{-}23)$$

Then, the three-phase power into the two RPSTs is

$$S_{RPSTs} = 2 \cdot 3 \cdot \bar{V}r \cdot (\bar{I}_{sh2})^* = 6(\bar{V}g \cdot (\bar{I}_{sh})^* \cdot e^{j2\gamma} - \left|\frac{\bar{I}_{sh} \cdot e^{j\gamma}}{T_{sh}}\right|^2 \cdot Z_{sh})$$

$$= 97.21 + j770.1 \quad \text{(MW, MVar)}$$

$$= 776.0\angle 82.8 \quad \text{(MVA)} \qquad (5\text{-}24)$$

Comparing (24) with the total capacity of the two RPSTs in Table 5.3, we find the two machines are overloaded. Similarly, the shunt and the series transformers are also overloaded.

(7) Referring to Table 5.6 and the above results, we have

- $\overline{V}_{ser}$ leads $\overline{I}_{ser}$ by 79.63deg. (78.57-(1.06))
- $\overline{V}_s$ leads $\overline{V}_g$ by 10.46 deg. (10.38-(-0.08))
- $\overline{V}_s$ leads $\overline{V}_r$ by 21.83 deg. (10.38-(-11.45))
- $\overline{V}_s$ leads $\overline{I}_{ser}$ by 11.44deg. (10.38-(-1.06))
- $|\overline{V}_s|$ is greater than $|\overline{V}_g|$

(8) Figure 5.9 to Figure 5.12 are the curves of RMS values and angles of $\overline{V}_g$, $\overline{V}_r$, $\overline{I}_g$ and $\overline{I}_r$, and the curves of P_g, P_r, Q_g and Q_r at Bus G and Bus R. Based on these curves, the load flows at Bus G and Bus R at three instants are summarized in Table 5.6.

In Figure 5.12,

- During 0 ~ 0.4 s, the differences between P_g and P_r, Q_g and Q_r are the losses of the two transmission lines, respectively;
- During 0.4 ~ 1.0 s, the differences between P_g and P_r, Q_g and Q_r are the losses of the one transmission line without the service of the RPFC and the three-phase shunt compensation, respectively;
- During 1.0 ~ 6.0 s, the differences between P_g and P_r, Q_g and Q_r are the sum of the losses of the one transmission line and the power supplied by the RPFC and the three-phase shunt compensation, respectively.

(9) Refer to Table 5.6 and Figure 5.13 through Figure 5.16. For the symmetrical operation, the RPFC and the three-phase shunt compensation can preserve the pre-contingency load flows as expected.

Table 5.6 Phase-A load flow at Bus G and Bus R in Simulation Case 1

t (s)	At Bus G				At Bus R			
	$\overline{V}_g$ (kV / deg.)	$\overline{I}_g$ (A / deg.)	P_g (MW)	Q_g (MVar)	$\overline{V}_r$ (kV / deg.)	$\overline{I}_r$ (A / deg.)	P_r (MW)	Q_r (MVar)
0.09	$229.8\angle -0.1$	$2034\angle 4.15$	466.0	-34.5	$230.\angle -11.44$	$2004\angle -7.57$	459.9	-31.0
0.39	$215.7\angle 6.03$	$1892\angle 1.05$	406.0	35.5	$215.3\angle -16.77$	$1880\angle -4.75$	396.0	-84.5
6.0	$229.8\angle -0.08$	$2034\angle 4.12$	466.2	-33.2	$230.\angle -11.45$	$2004\angle -7.58$	460.1	-31.2

5.3.3 Simulation Case 2 - Symmetrical operation with two six-pole-pair RPSTs

The main purpose of this simulation is to observe how the pole-pair number affects the transient process of the power system and performance of the RPFC itself, comparing to Simulation Case1 in which the pole-pair number of the RPST is one.

5.3.3.1 Results of Simulation Case 2

The operational parameters are the same as those in Simulation Case1 of section 5.3.2.1.

Figure 5.17 to Figure 5.28 show the curves of Simulation Case 2.

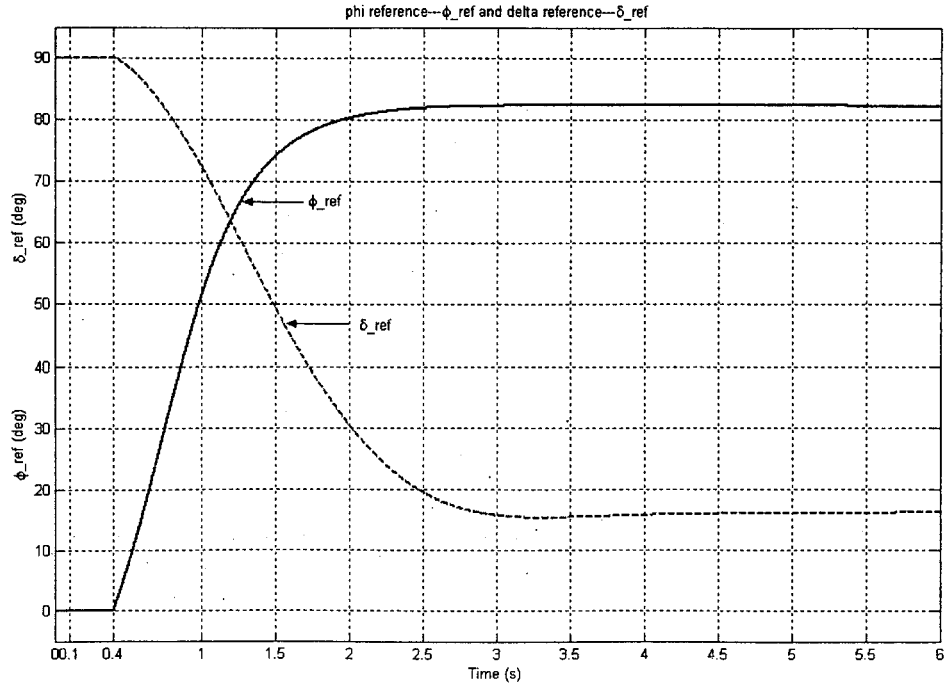

Figure 5.17 - Curves of φ_ref and δ_ref in Simulation Case 2

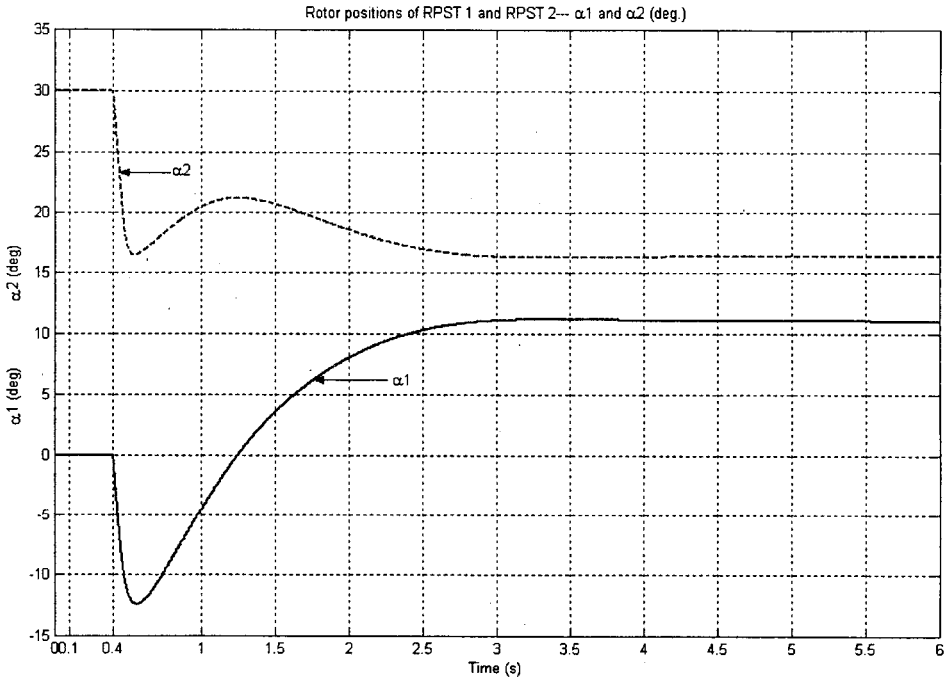

Figure 5.18 - Rotor positions of RPST 1 and RPST 2--α1 and α2 in Simulation Case 2

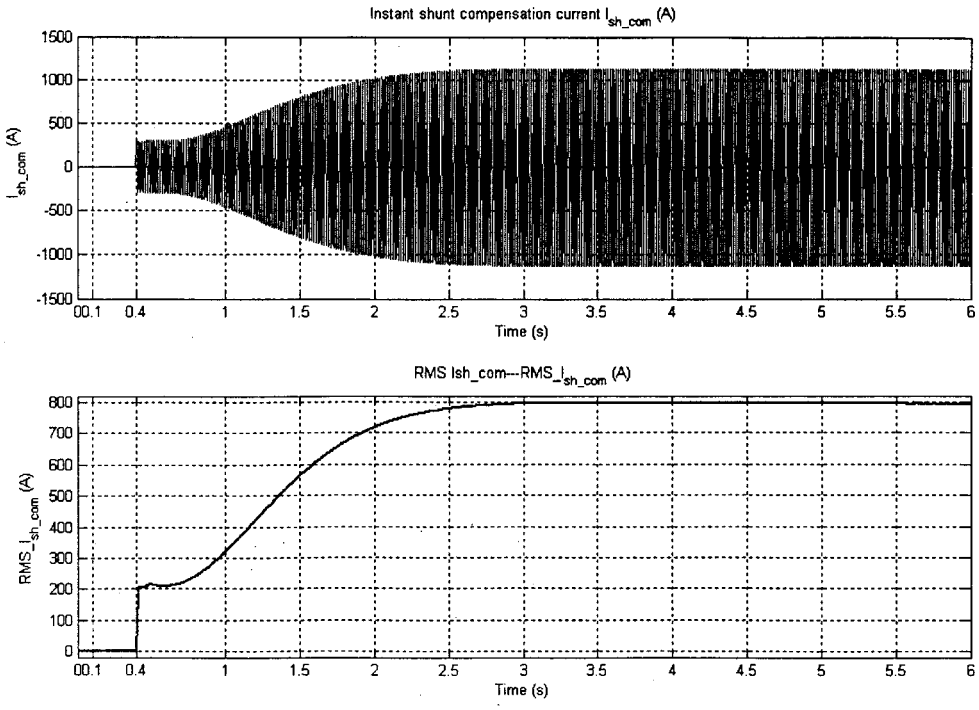

Figure 5.19 - Shunt compensation current I_{sh_com} in Simulation Case 2

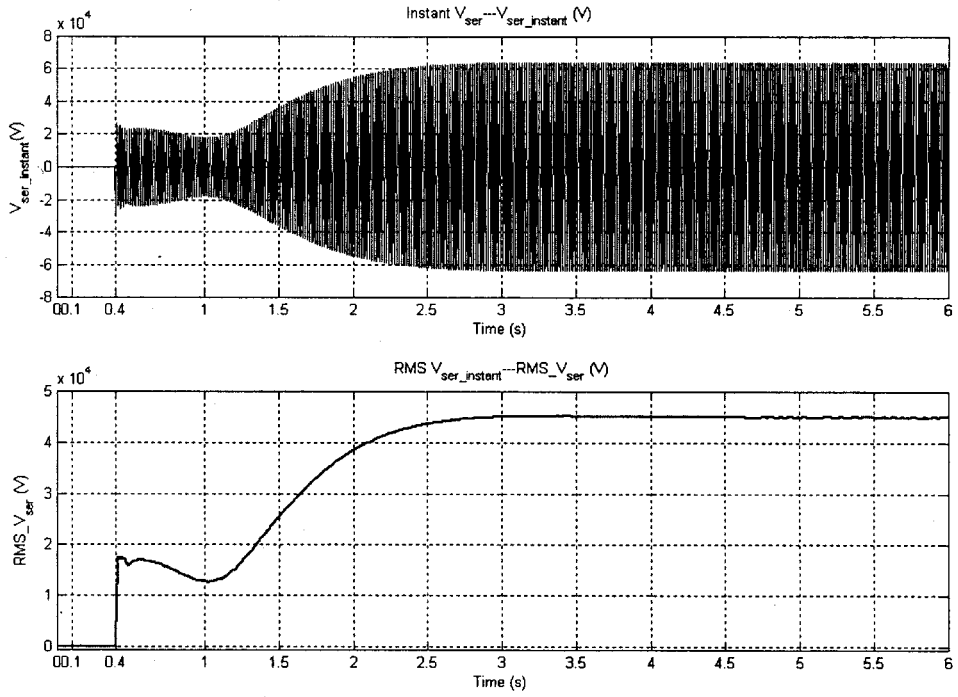

Figure 5.20 - Inserted series voltage V_{ser} in Simulation Case 2

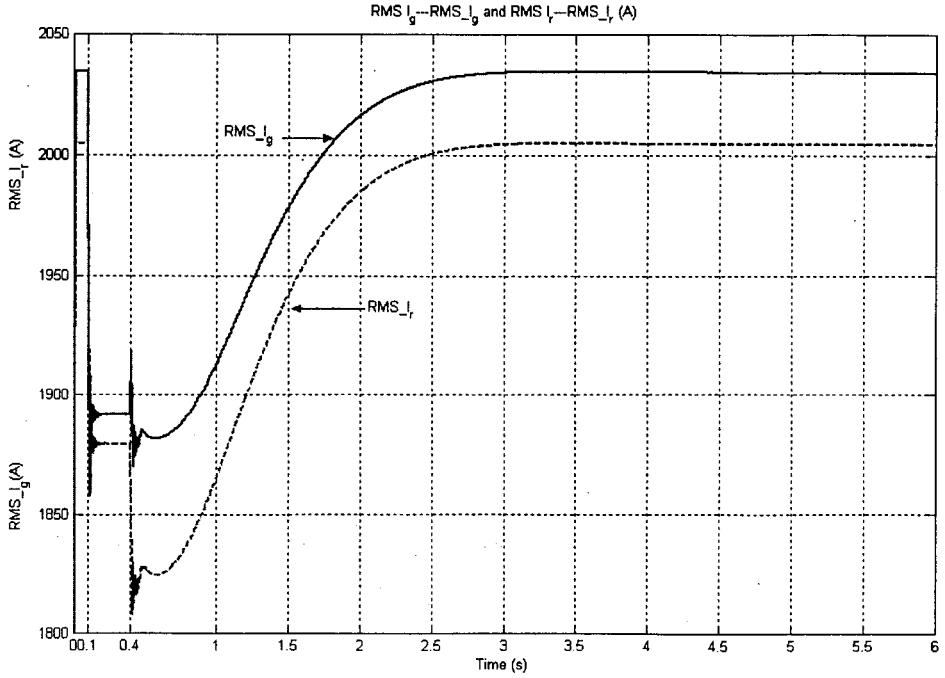

Figure 5.21 - The rms currents at Bus G and Bus R in Simulation Case 2

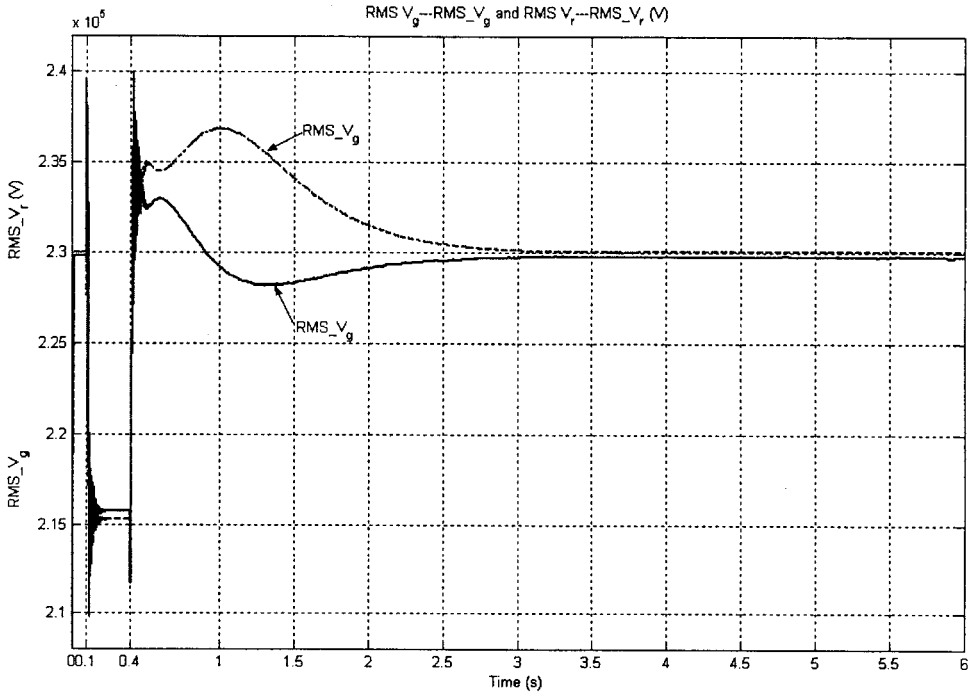

Figure 5.22 – The rms voltages at Bus G and Bus R in Simulation Case 2

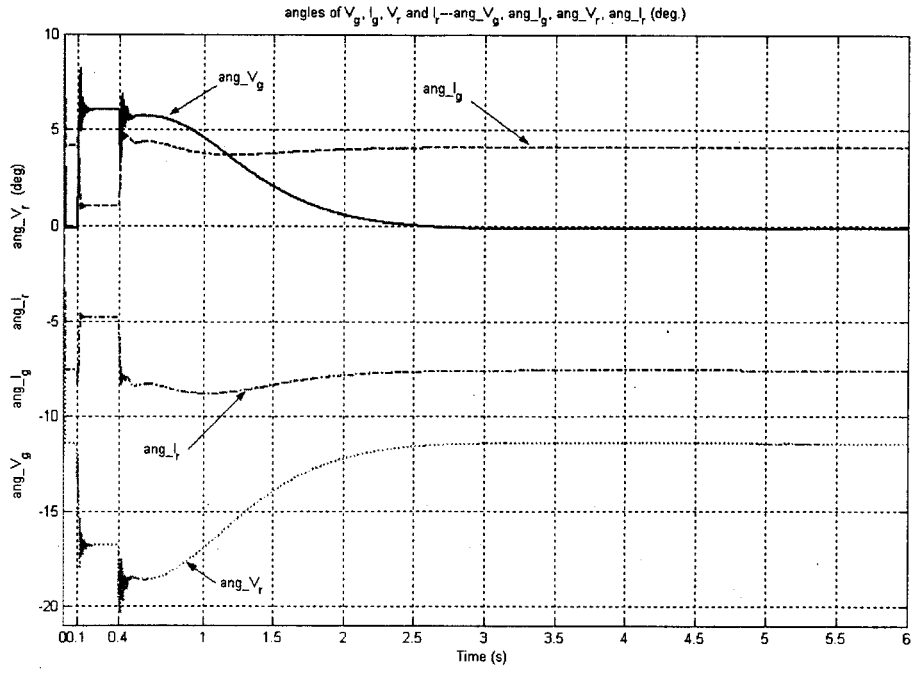

Figure 5.23 - Angles of voltages and currents at Bus G and Bus R in Simulation Case 2

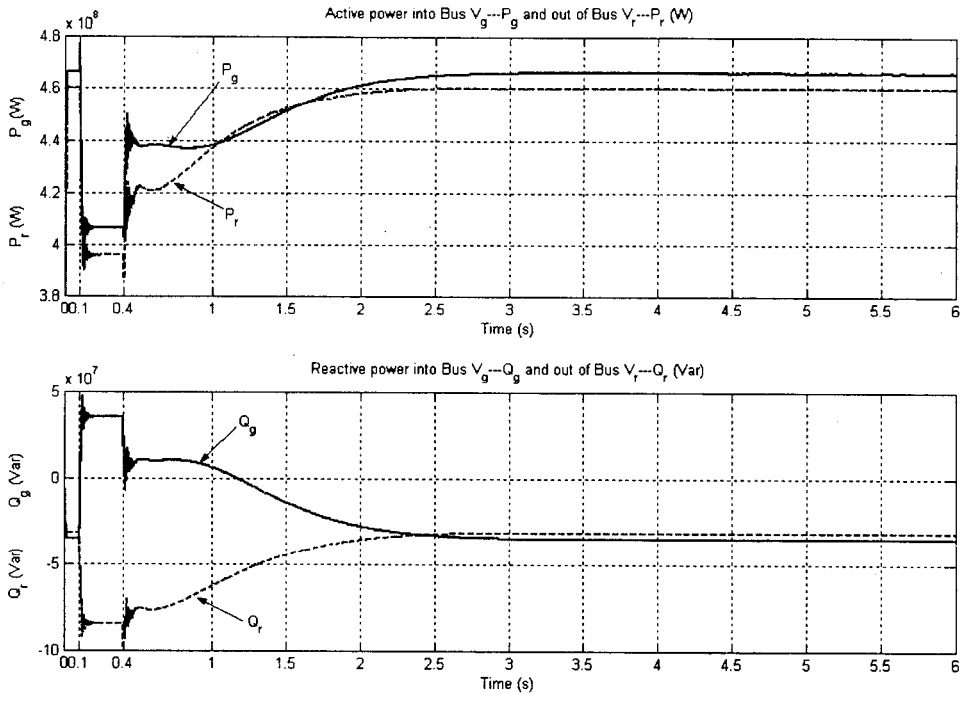

Figure 5.24 - Active and reactive powers at Bus G and Bus R in Simulation Case 2

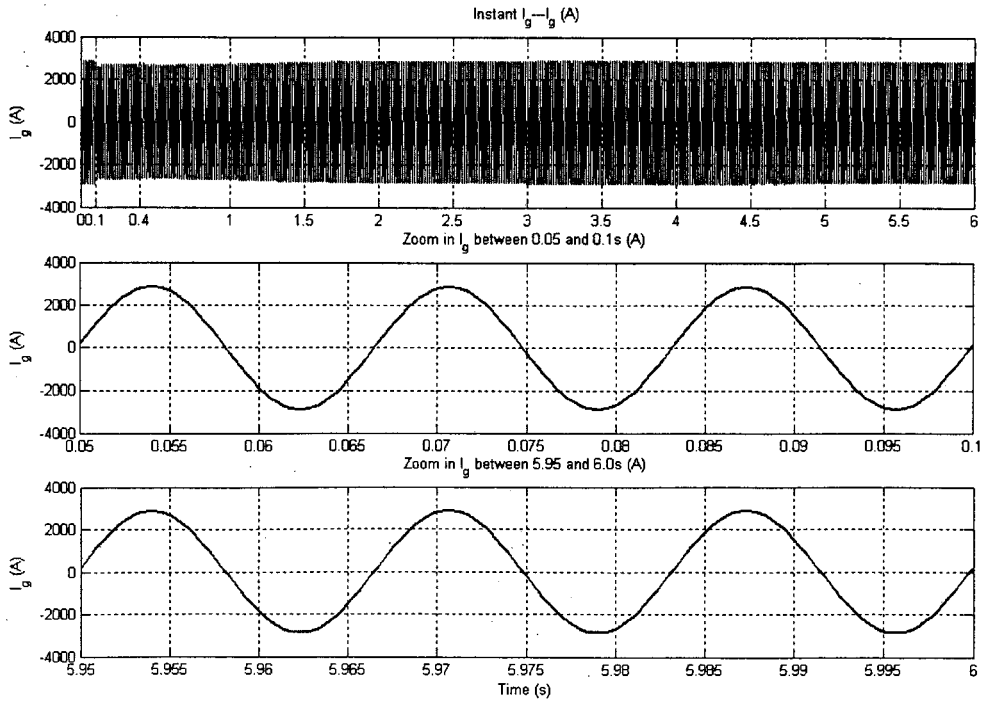

Figure 5.25 - Instantaneous current at Bus G in Simulation Case 2

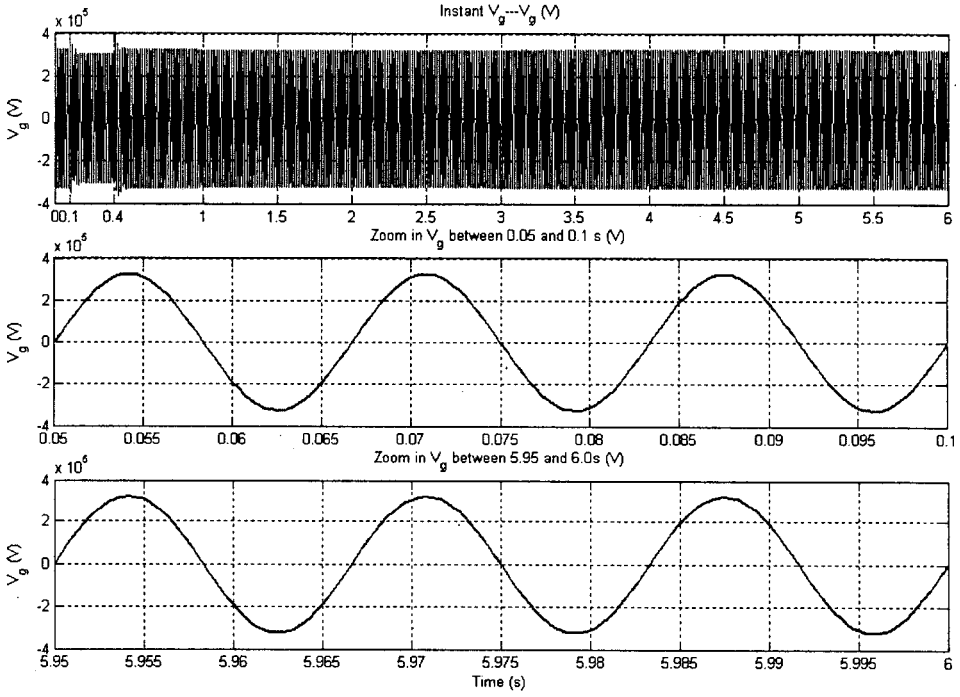

Figure 5.26 - Instantaneous voltage at Bus G in Simulation Case 2

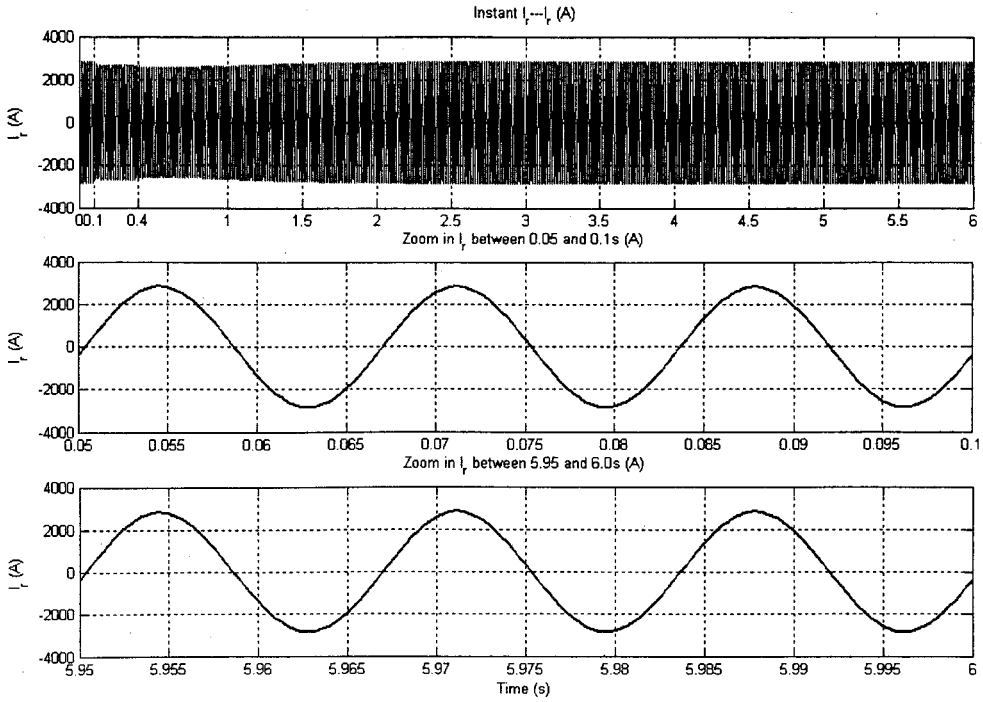

Figure 5.27 - Instantaneous current at Bus R in Simulation Case 2

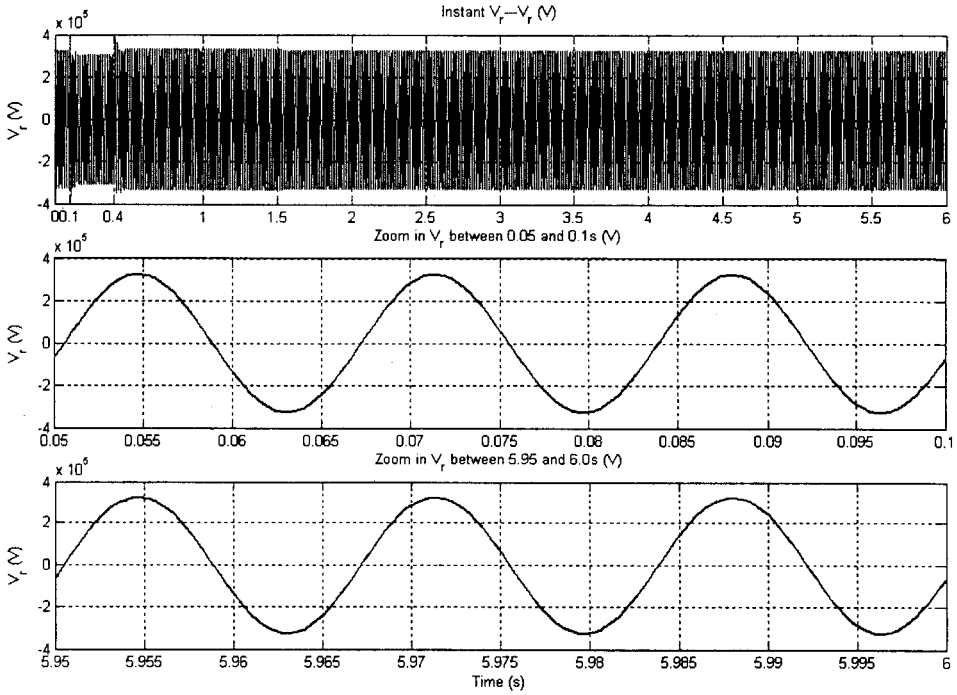

Figure 5.28 - Instantaneous voltage at Bus R in Simulation Case 2

5.3.3.2 Analysis of results of Simulation Case 2

(1) Refer to Figure 5.17. The steady-state references (t = 6.0 s) of φ_ref and δ_ref for the control of the RPFC are:

$$\varphi\_ref = 82.25 \text{ deg.} \quad (5\text{-}25)$$

$$\delta\_ref = 16.29 \text{ deg.} \quad (5\text{-}26)$$

(2) Refer to Figure 5.18, the steady-state values (t = 6.0 s) of rotor positions of the two RPSTs are:

$$\alpha 1 = 11.00 \text{ deg.} \quad (5\text{-}27)$$

$$\alpha 2 = 16.42 \text{ deg.} \quad (5\text{-}28)$$

Note: the pole-pair number is 6.

- Reviewing the **Note** in Section 3.7, we multiply (5-27) and (5-28) by 6, then insert them into (3-22) and (3-38), we get,

$$\delta = \frac{\alpha 2 - \alpha 1}{2} = 16.26 \text{ (deg.)} \quad (5\text{-}29)$$

$$\varphi = \theta + \gamma + \alpha = \frac{\alpha 2 + \alpha 1}{2} + \gamma + \alpha = 82.26 \text{ (deg.)} \quad (5\text{-}30)$$

It shows that the steady-state φ and δ are close to the steady-state φ_ref and δ_ref, respectively.

Note: In our project, γ and α are zeros.

- Inserting (3-37), (5-29) and (5-30) into, (3-45) and (3-46), we get,

$$T_{eq} = 1.0820 \quad (5\text{-}31)$$

$$\beta_0 = 15.95 \text{ (deg)} \quad (5\text{-}32)$$

(3) Refer to c) in Section 5.1.2 and (5-29). The two parts of the equivalent impedance of RPFC can be calculated by (3-47) and (3-48),

$$Z_{rpfc\_c} = Z_{se} + 2 \cdot T_{se}^2 \cdot Z_{rt} = j9.375 \quad (\Omega)$$

$$Z_{rpfc\_v} = 4 \cdot T_{rt}^2 \cdot T_{se}^2 \cdot \cos^2 \delta \cdot Z_{sh} = j2.88 \quad (\Omega)$$

$$\text{Then, } Z_{rpfc} = Z_{rpfc\_c} + Z_{rpfc\_v} = j12.255 \quad (\Omega) \qquad (5\text{-}33)$$

(4) Refer to Figure 5.19 and Figure 5.20. The steady-state shunt compensation current (t = 6.0 s), $\overline{I}_{sh\_com}$, and the injected series voltage, $\overline{V}_{ser}$, are:

$$\overline{I}_{sh\_com} = 794.1\angle 91.48 \text{ A} \qquad (5\text{-}34)$$

$$\overline{V}_{ser} = 45.02\angle 78.61 \text{ kV} \qquad (5\text{-}35)$$

It shows that $\overline{V}_{ser}$ is close to $\overline{V}_{ser\_ref}$ that is $44.9\angle 78.52$ kV.

Refer to Figure 5.3b, Table 5.7, and (5-35). The steady-state value $\overline{V}_s$ (t = 6.0 s) is:

$$\overline{V}_s = \overline{V}g + \overline{V}ser = 242.68\angle 10.40 \quad \text{(kV)} \qquad (5\text{-}36)$$

(5) Inserting T=0.3125 (see c) in section 5.1.2), $\overline{V}_g = 229.8 \times 10^3 \angle -0.08$ (see Table 5.7), (5-29), (5-30), (5-33) and (5-35) into (3-40), we obtain

$$\overline{I}_{ser} = \frac{T \cdot |\cos\delta| \cdot \overline{V}_g \cdot e^{j\varphi} - \overline{V}_{ser}}{Z_{rpfc}} = 1972.3\angle -1.16 \quad \text{(A)} \qquad (5\text{-}37)$$

Then, the current through the sound line is $\overline{I}_{line\_post\_fault} = 1997.1\angle -4.23$ A.

Where, $\overline{I}_{line\_post\_fault} = \overline{I}_{ser} - \overline{I}_{line\_capacitor} = \overline{I}_{ser} - 0.5B_L \cdot \overline{V}_s \qquad (5\text{-}38)$

It shows that $\bar{I}_{line\_post\_fault}$ is increased, compared with the current through one of the two pre-fault transmission lines ($\bar{I}_{line\_pre\_fault} = 1014.9\angle -1.75$, see section 5.2).

And, the power through the sound line (i.e., out of Bus S) is

$$S_{BUS\_S} = \bar{V}s \cdot (\bar{I}_{ser})^* == 468.9 + j95.92 \quad \text{(MW, MVar)} \tag{5-39}$$

Thus the three-phase active power transmitted through the sound transmission line (3*468.9 MW) is greater than that through the two pre-fault transmission lines (3*466 MW)

(6) Refer to Figure 5.3b, Table 5.7, (5-34) and (5-37). The steady-state value $\bar{I}_{sh}$ (t = 6.0 s):

$$\bar{I}_{sh} = \bar{I}_g - \bar{I}_{sh\_com} - \bar{I}_{ser} = 613.04\angle -82.75 \text{ (A)} \tag{5-40}$$

Then, the three-phase power into the two RPSTs is

$$\begin{aligned} S_{RPSTs} &= 2 \cdot 3 \cdot \bar{V}r \cdot (\bar{I}_{sh2})^* = 6(\bar{V}g \cdot (\bar{I}_{sh})^* \cdot e^{j2\gamma} - \left|\frac{\bar{I}_{sh} \cdot e^{j\gamma}}{T_{sh}}\right|^2 \cdot Z_{sh}) \\ &= 107.8 + j766.2 \qquad \text{(MW, MVar)} \\ &= 773.8\angle 82.0 \qquad \text{(MVA)} \end{aligned} \tag{5-41}$$

Comparing (5-41) with the total capacity of the two RPSTs in Table 5.3, we find the two machines are overloaded. Similarly, the shunt and the series transformers are also overloaded.

(7) Referring to Table 5.6 and the above results, we have

- $\overline{V}_{ser}$ leads $\overline{I}_{ser}$ by 79.77 deg. (78.61-(-1.16))
- $\overline{V}_s$ leads $\overline{V}_g$ by 10.48 deg. (10.40-(-0.08))
- $\overline{V}_s$ leads $\overline{V}_r$ by 21.85 deg. (10.40-(-1.45))
- $\overline{V}_s$ leads $\overline{I}_{ser}$ by 11.56 deg. (10.40-(-1.16))
- $\left|\overline{V}_s\right|$ is greater than $\left|\overline{V}_g\right|$

(8) Figure 5.21 through Figure 5.24 are the curves of RMS values and angles of $\overline{V}_g$, $\overline{V}_r$ $\overline{I}_g$ and $\overline{I}_r$, and the curves of P_g, P_r, Q_g and Q_r at Bus G and Bus R. Based on these curves, the load flows at Bus G and Bus R at three instants are summarized in Table 5.7.

In Figure 5.24,

- During 0 ~ 0.4 s, the differences between P_g and P_r, Q_g and Q_r are the losses of the two transmission lines, respectively;
- During 0.4 ~ 1.0 s, the differences between P_g and P_r, Q_g and Q_r are the losses of the one transmission line without the service of RPFC and the three-phase shunt compensation, respectively;
- During 1.0 ~ 6.0 s, the differences between P_g and P_r, Q_g and Q_r are the sum of the losses of the one transmission line and the power supplied by RPFC and the three-phase shunt compensation, respectively

(9) Refer to Table 5.7 and Figure 5.25 through Figure 5.28. For the symmetrical operation, the RPFC and the three-phase shunt compensation can preserve the pre-contingency load flows as expected.

(10) Compare (5-18) and (5-19) with (5-8) and (5-9), and Figure 5.18 with Figure 5.6. The larger the pole-pair numbers of RPSTs are, the less the rotors move.

(11) Compare Figure 5.8 and Figure 5.20, Figure 5.9 and Figure 5.21,etc. The beginning part (0.4~1 s) of the transient process of the transmission system is sensitive to the rotor movement of RPST with a larger pole-pair number.

(12) Figure 5.29 shows the phasors and the control range of the RPFC.

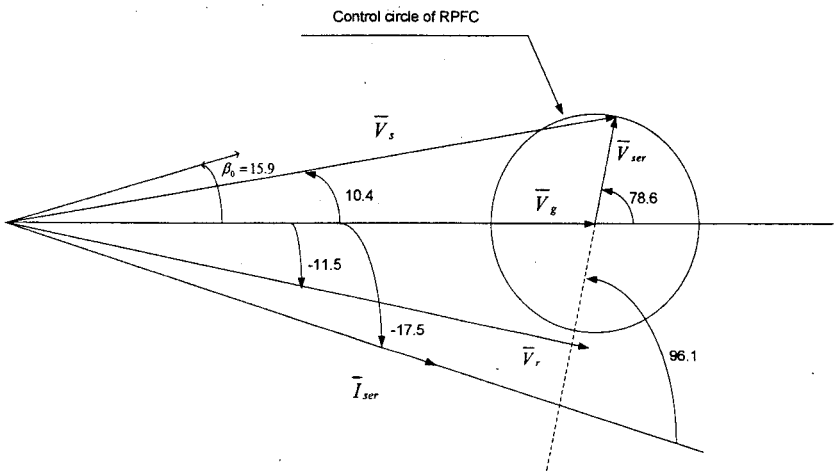

Figure 5.29 - Control range of the RPFC

Table 5.7 Phase-A load flow at Bus G and Bus R in Simulation Case 2

t (s)	At Bus G				At Bus R			
	$\overline{V}_g$ (kV / deg)	$\overline{I}_g$ (A / deg)	P_g (MW)	Q_g (MVar)	$\overline{V}_r$ (kV / deg)	$\overline{I}_r$ (A / deg)	P_r (MW)	Q_r (MVar)
0.09	229.8∠−0.1	2034∠4.15	466.0	-34.5	230.∠−11.44	2004 ∠ − 7.57	459.9	-31.0
0.39	215.7∠6.03	1892∠1.05	406.0	35.5	215.3∠−16.77	1880∠ − 4.75	396.0	-84.5
6.0	229.8∠−0.08	2034∠4.12	466.2	-33.2	230.∠−11.45	2004∠ − 7.58	460.1	-31.2

5.4 Summary

- The RPFC and the three-phase shunt compensation have been used for symmetrical operation to keeping the load flows at Bus G and Bus R the same as the pre-faulted ones, respectively (Table 5.6 and Table 5.7).
- The beginning part (0.4~1 s) of the transient process of the transmission system is sensitive to the rotor movement of the RPST with larger pole-pair number (for example, compare Figure 5.8 and Figure 5.20, Figure 5.9 and Figure 5.21,etc.).
- The larger the pole-pair numbers of RPSTs, the less the rotors move (Figure 5.6 and Figure 5.18.)
- The pole-pair numbers do not affect the steady-state values of the power system (see the operational parameters at t = 6.0 s in Table 5.6 and Table 5.7).
- The insertion of the RPFC and the three-phase shunt compensation increase the current through the sound transmission line (Line 2).

CHAPTER 6 SIMULATIONS OF A POWER SYSTEM EQUIPPED WITH THE RPFC IN ASYMMETRICAL OPERATION

6.1 Power system being simulated and its components

In this chapter, two simulations, in which the RPFC and a single-phase shunt compensation are applied to a two-line power system in asymmetrical operation, are carried out in the Matlab/Simulink environment. In the two simulations, the pole-pair numbers of each RPST are one (1) and six (6), respectively. So, we will observe not only the operation of the RPFC as a whole, but also the operation of the pole-pair numbers of the RPST from the two simulations.

Here, the term "asymmetrical operation" refers to the operation mode in which the RPFC and the single-phase shunt compensation are applied to Phase-A of the two-line power system after Phase-A of one of the two lines is opened permanently.

6.1.1 Power system being simulated

The power system to be simulated is a two-machine, two-line system. Figure 6.1a and Figure 6.2a represent the pre-contingency power systems to be simulated; Figure 6.1b and Figure 6.2b represent the post-contingency power systems to be simulated. They show that the systems are in asymmetrical operation. As for the pre-contingency power systems to be simulated, they are the same as in Figure 5.1.

The differences among Figure 5.2, Figure 6.1b and Figure 6.2b are:

- In Figure 5.2 and Figure 6.1b, we have the three-phase series transformers, while in Figure 6.2b, the single-phase transformer.
- In Figure 5.2, the three phases of the series transformer are in service, while in Figure 6.1b, only Phase-A of the series transformer is in service.

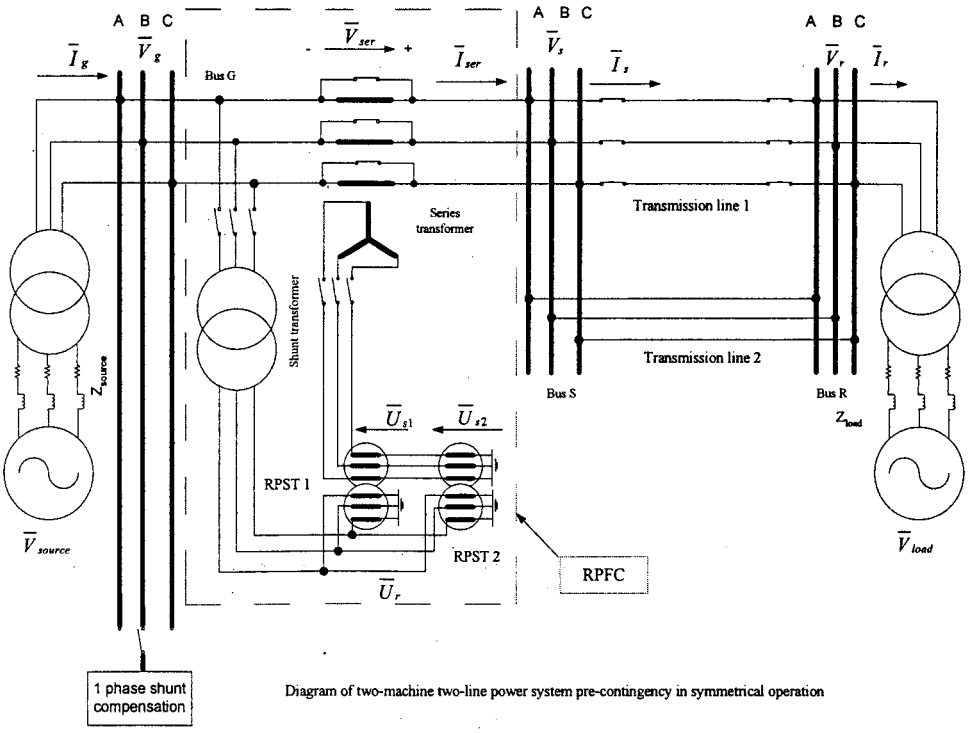

Figure 6.1a - Diagram of a two-machine two-line power system pre-contingency

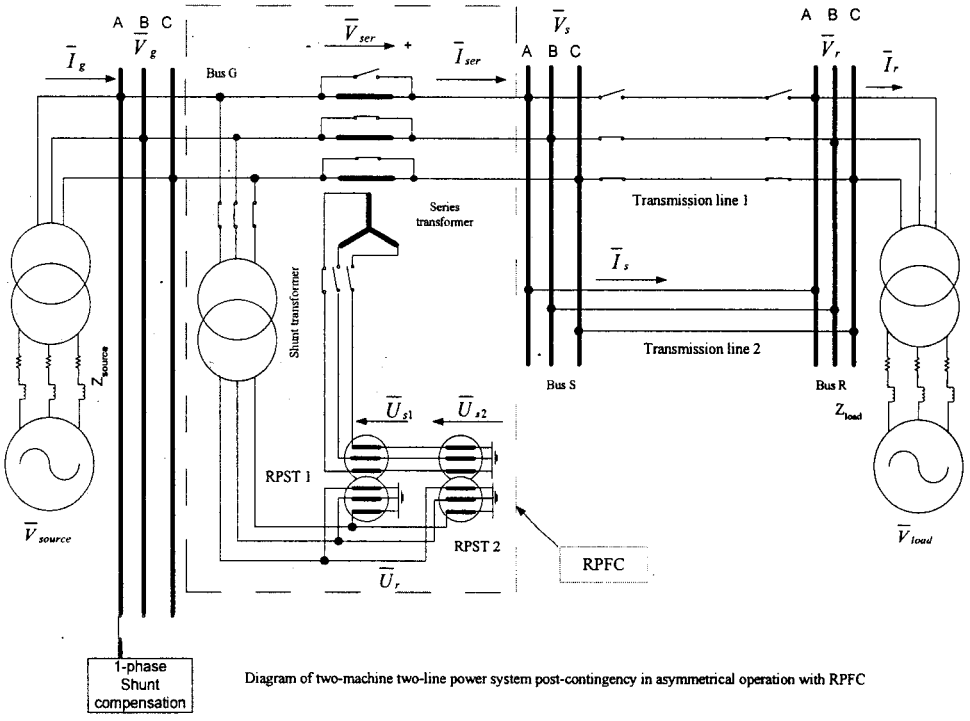

Figure 6.1b - Diagram of the power system in asymmetrical operation
(the series transformer is a three-phase transformer)

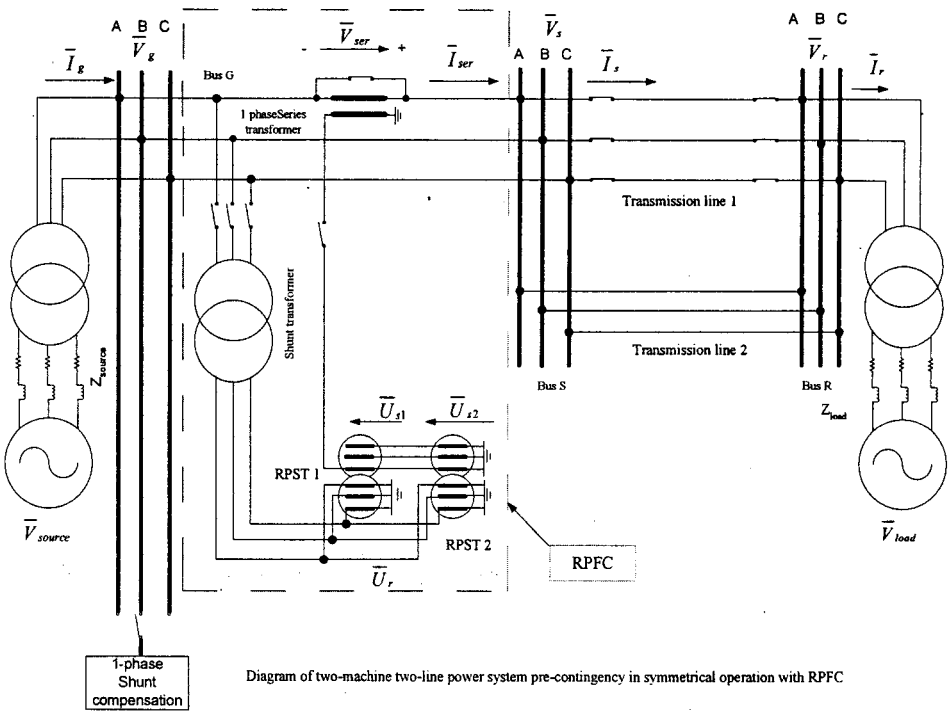

Figure 6.2a - Diagram of the power system pre-contingency
(the series transformer is a single-phase transformer)

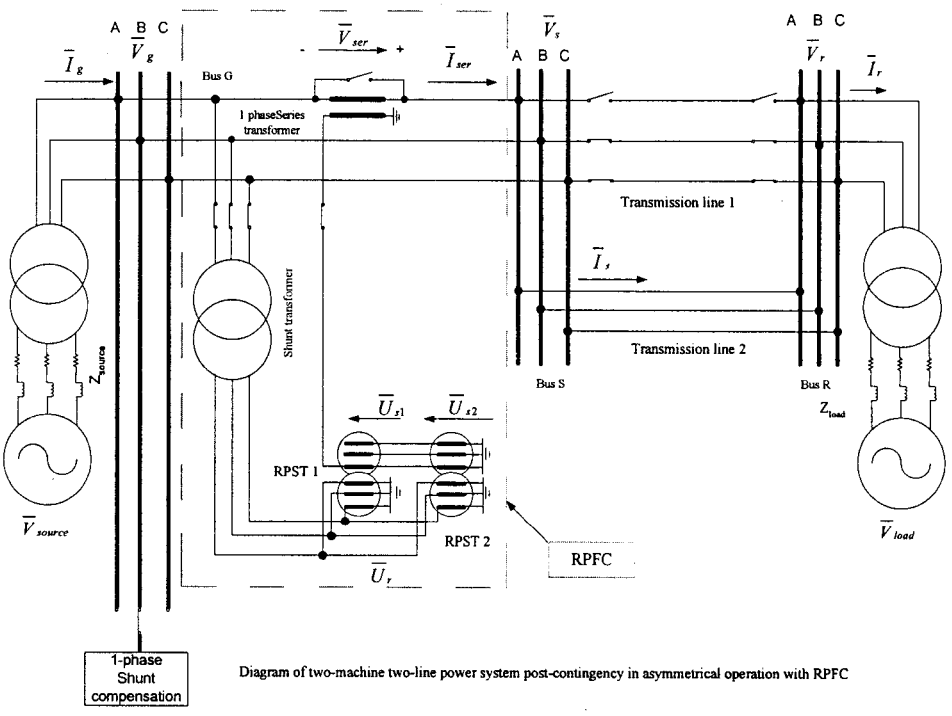

Figure 6.2b - Diagram of the power system in asymmetrical operation
(the series transformer is a single-phase transformer)

The pre-contingency power system (Figure 6.1a or Figure 6.2a) refers to two lines (Line1 and Line 2) in service; and the post-contingency power system (Figure 6.1b and Figure 6.2b) refers to Phase-B and Phase-C of Line1 and the three phases of Line 2) in service with the RPFC and a single-phase shunt compensation after Phase-A of Line 1 is opened permanently.

In Figure 6.1b and Figure 6.2b, the single-phase shunt compensation is applied to Phase-A of the power system. The power system is in asymmetrical operation mode.

6.1.2 Parameters of the electrical equipment in the power system

All the pertinent parameters of the electrical equipment in Figure 6.1a, are the same as those in Figure 5.1.

All the pertinent parameters of the electrical equipment in Figure 6.2a, are the same as those in Figure 5.1 except for the parameters of the single-phase series transformer which are shown in Table 6.1.

Table 6.1 Parameters of the single-phase series transformer

Electrical Equipment	Parameters
single-phase Series transformer	• Nominal Voltage = 69 / 20 kV • Capacity = 150 MVA • Leakage reactance Xse(p.u.) = 0.1

According Table 6.1, the real value of the leakage reactance seen from the 69 kV side is Xse= 3.174 Ω, and T_{se} = 69 / 20 = 3.45.

6.2 Equivalent circuit of the post-contingency power system

Reviewing Chapter 4, we get the equivalent circuits of Figure 6.1b and Figure 6.2b that are shown in Figure 6.3 and Figure 6.4, respectively. It should be mentioned that from the point of view of the electrical representation, the models in Figure 6.3 and Figure 6.4 are identical.

According to the theory of asymmetrical operation discussed in Chapter 2 and referring to Figure 6.3 and Figure 6.4, to keep the Phase-A load flows at Bus G and Bus R the same as those in Figure 6.1a and Figure 6.2a, the followings should be satisfied:

$$\overline{V}_{ser} = \frac{L}{N-L}(\overline{V}_g - A_0 \cdot \overline{V}_r) \tag{6-1}$$

$$\overline{I}_{sh\_com} - \overline{I}_{sh} = L \cdot C_0 \cdot \overline{V}r \tag{6-2}$$

Where,

- N = 2, L = 1
- $\overline{V}_g$ and $\overline{V}_r$ are the Phase-A load flows at Bus G and Bus R in Figure 6.1a and Figure 6.2a.

The references for Phase-A compensations, which are similar to those discussed in section 5.2, are as the following:

$$\overline{V}_{ser\_ref} = \frac{L}{N-L}(\overline{V}_g - A_0 \cdot \overline{V}_r) \tag{6-3}$$

$$\overline{I}_{es\_ref} = L \cdot C_0 \cdot \overline{V}r \tag{6-4}$$

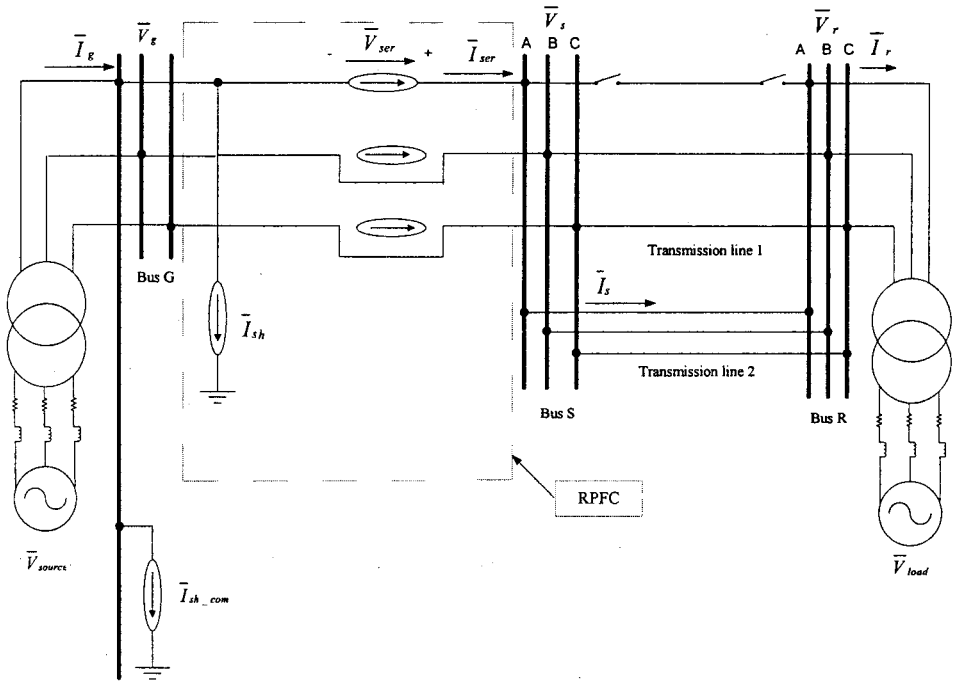

Figure 6.3 - Equivalent circuit of Figure 6.1b

(asymmetrical operation with the three-phase series transformer)

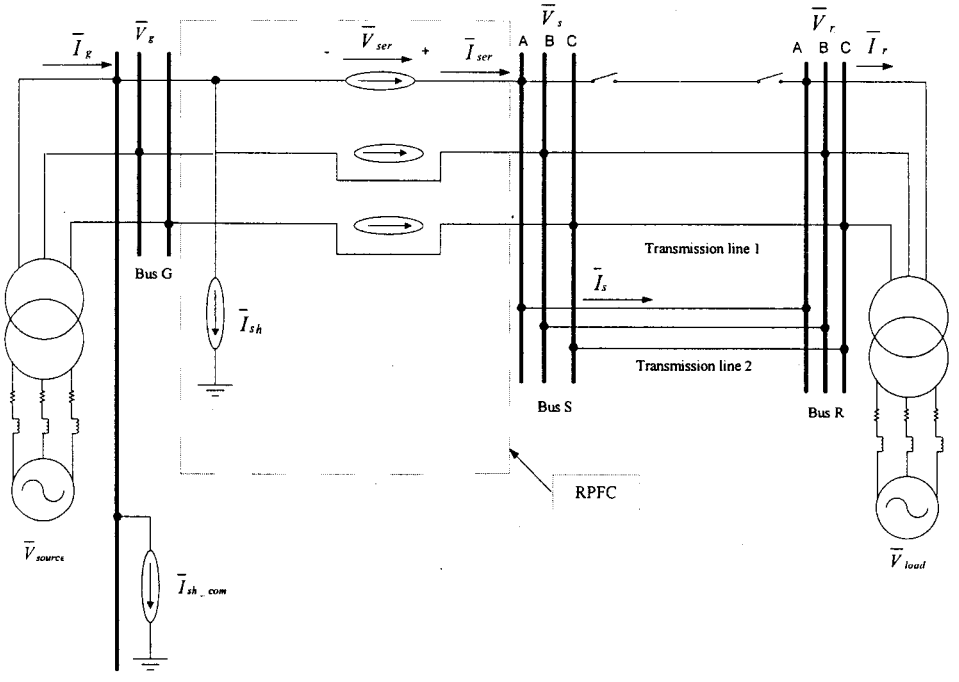

Figure 6.4 - Equivalent circuit of Figure 6.2b

(asymmetrical operation with the single-phase series transformer)

6.3 Simulation Cases

6.3.1 Description of the simulation process

The simulation model (Figure 6.5) is represented by SPS and Matlab/Simulink. Referring to Figure 6.5, the simulation process is described in Table 6.2.

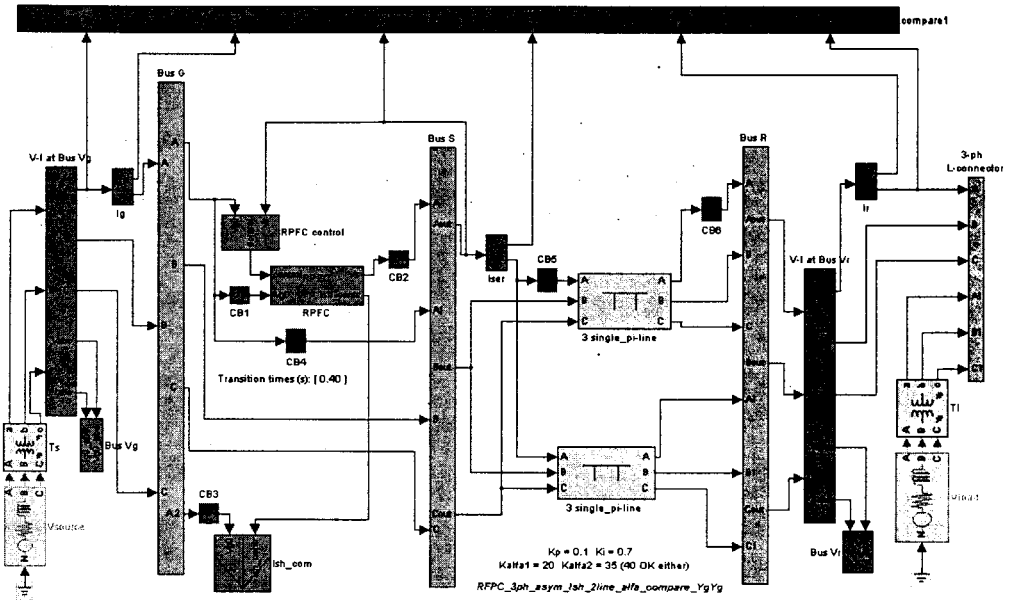

Figure 6.5 - Model represented by SPS and Simulink for Figure 6.1b and Figure 6.2b

Table 6.2 Description of the simulation process

Time(s)	Circuit-breakers in open state	Circuit-breakers in closed state	Operation of transmission lines
0.0	CB1, CB2, CB3	CB4, CB5, CB6	2 lines
0.1	CB1, CB2, CB3, CB5, CB6	CB4	1 line without RPFC
0.4	CB4, CB5, CB6	CB, CB2, CB3	1 line with RPFC

In Table 6.2, each circuit-breaker would keep its own initial state until there is a switching operation on it at the prescribed instant.

- ***Calculations for the relevant reference values***

Referring to Figure 6.1a and Figure 6.2a, the pre-contingency load flows of Phase-A at Bus G and Bus R are shown in Table 6.3. (in the forms of phasor).

Table 6.3 Phase-A load flow of the pre-contingency system simulated

At Source	At Bus G		At Bus R		At Load
$\overline{V}_{source}$ (kV/deg)	$\overline{V}_{g}$ (kV/deg)	$\overline{I}_{g}$ (A/deg)	$\overline{V}_{r}$ (kV/deg)	$\overline{I}_{r}$ (A/deg)	$\overline{V}_{load}$ (kV/deg)
$1.493 \cdot 14 \angle 53.47$	$230.8 \angle 0.$	$2034 \angle 4.11$	$230.1 \angle -11.34$	$2006 \angle -7.6$	$1.49 \cdot 69 \angle -66.8$

Based on Table 6.3, $\overline{V}_{ser\_ref}$ and $\overline{I}_{es\_ref}$ can be calculated by (6-3) and (6-4),

$$\overline{V}_{ser\_ref} = 44.9 \angle 78.52 \quad \text{kV}$$

$$\overline{I}_{es\_ref} = 205.0 \angle 78.70 \quad \text{A}$$

And, the current through each of the two A-phases of the two lines is $\overline{I}_{line\_pre\_fault} = 1014.9 \angle -1.75$ A. Where,

$$\overline{I}_{line\_pre\_fault} = 0.5(\overline{I}_{g} - \overline{I}_{2\_line\_capacitor}) = 0.5(\overline{I}_{g} - 2 \cdot 0.5 B_{L} \cdot \overline{V}_{g})$$

6.3.2 Simulation Case 3 - Asymmetrical operation with two one-pole-pair RPSTs

6.3.2.1 Results of Simulation Case 3

- In our study, the insertion of the RPFC and the shunt compensation after a contingency is to preserve the pre-contingency Phase-A load flows at Bus G and Bus R. We are interested in the voltages, currents and powers of Phase-A at the two buses during the simulation;
- Because the power system is in asymmetrical operation, we are interested in the operational parameters (i. e., voltages and currents) of the other two phases, and the sequence components of these operational parameters;
- From the point of view of compensations, we are interested in the shunt compensation I_{sh_com} and $\overline{V}_{ser}$ for Phase-A.
- From the point of view of control of the RPFC (see Figure 4.3), we are interested in δ_ref, φ_ref, $\alpha 1$ and $\alpha 2$;

Figure 6.6 to Figure 6.20 show the curves of Simulation Case 3.

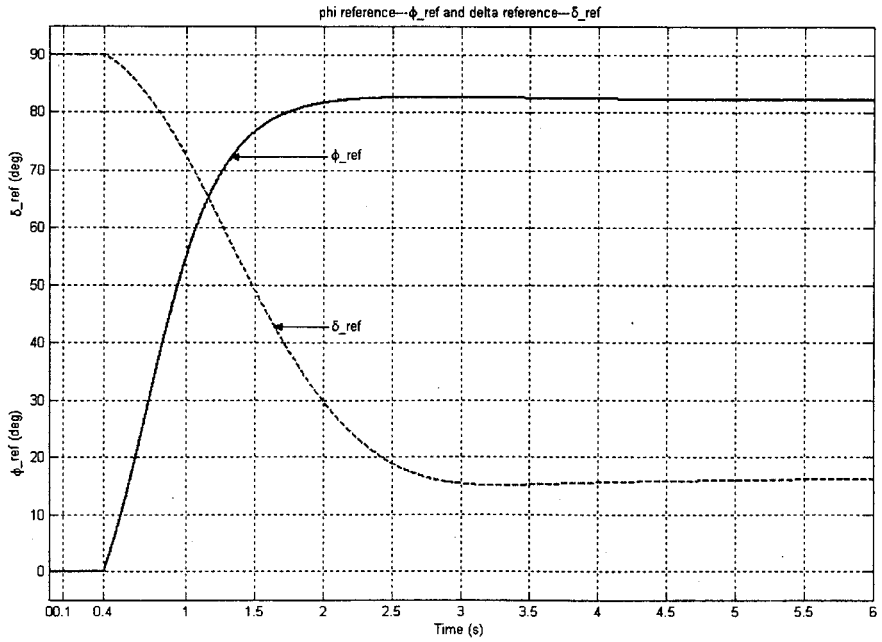

Figure 6.6 - Curves of φ_ref and δ_ref in Simulation Case 3

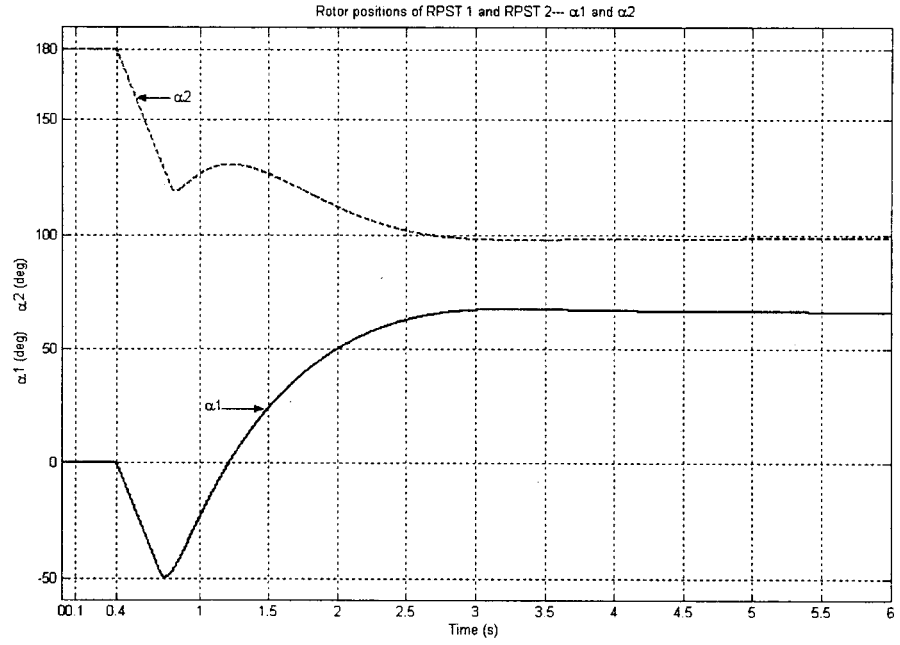

Figure - 6.7 Rotor positions of RPSTs -- α1 and α2 in Simulation Case 3

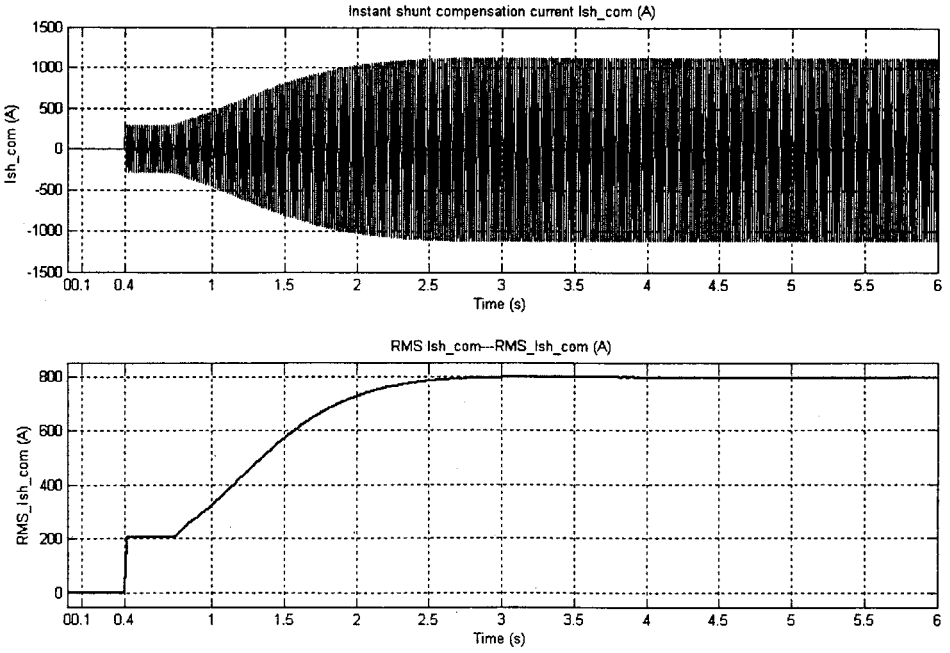

Figure 6.8 - Shunt compensation current I_{sh_com} in Simulation Case 3

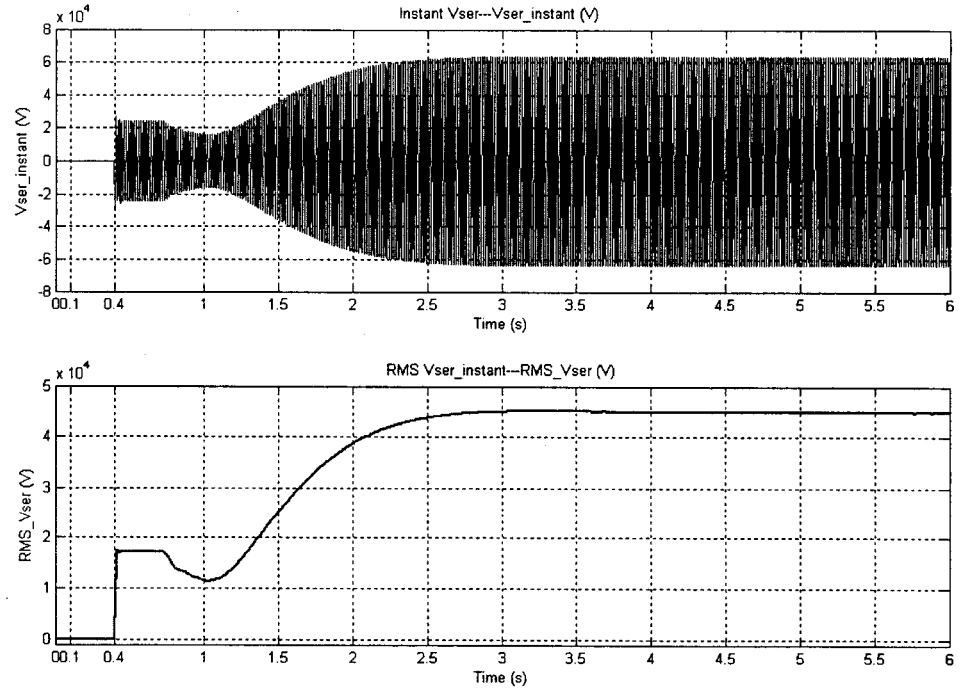

Figure 6.9 - Inserted series voltage V_{ser} in Simulation Case 3

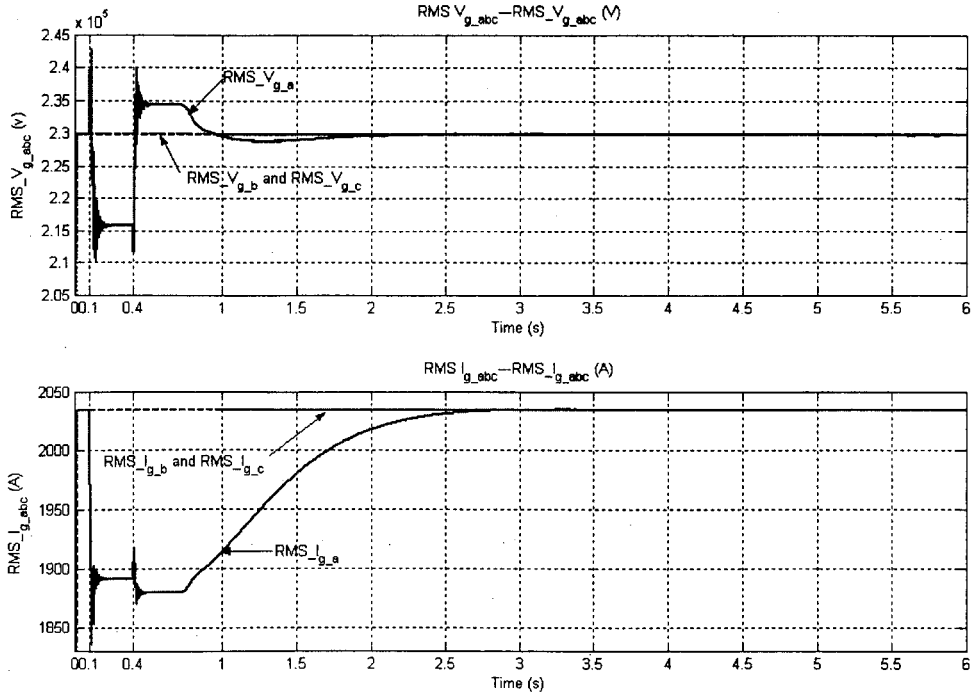

Figure 6.10 - Three-phase rms voltages and currents at Bus G in Simulation Case 3

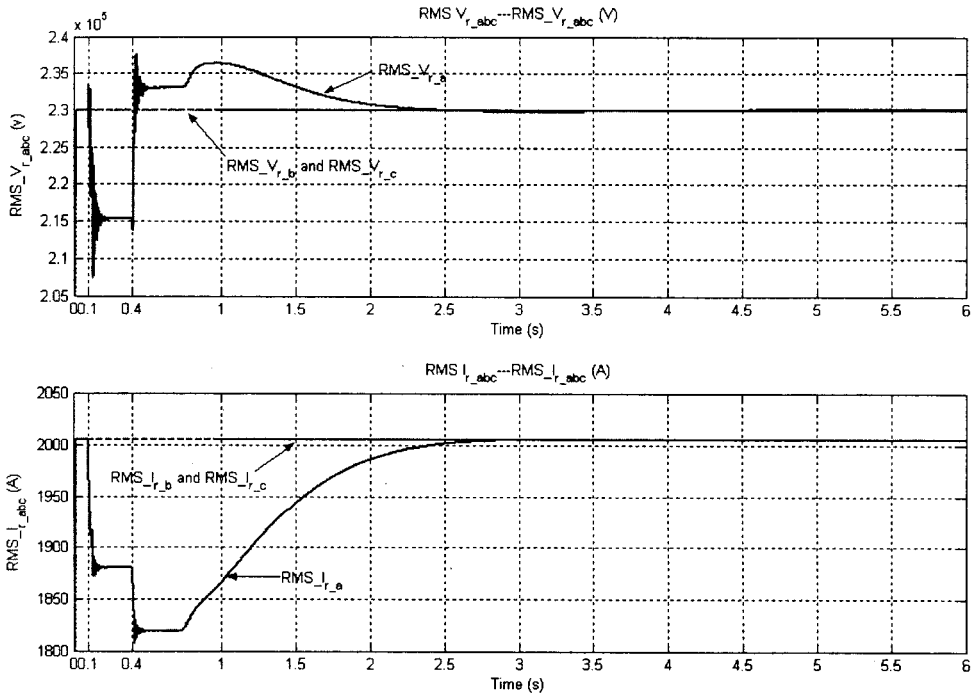

Figure 6.11 - Three-phase rms voltages and currents at Bus R in Simulation Case 3

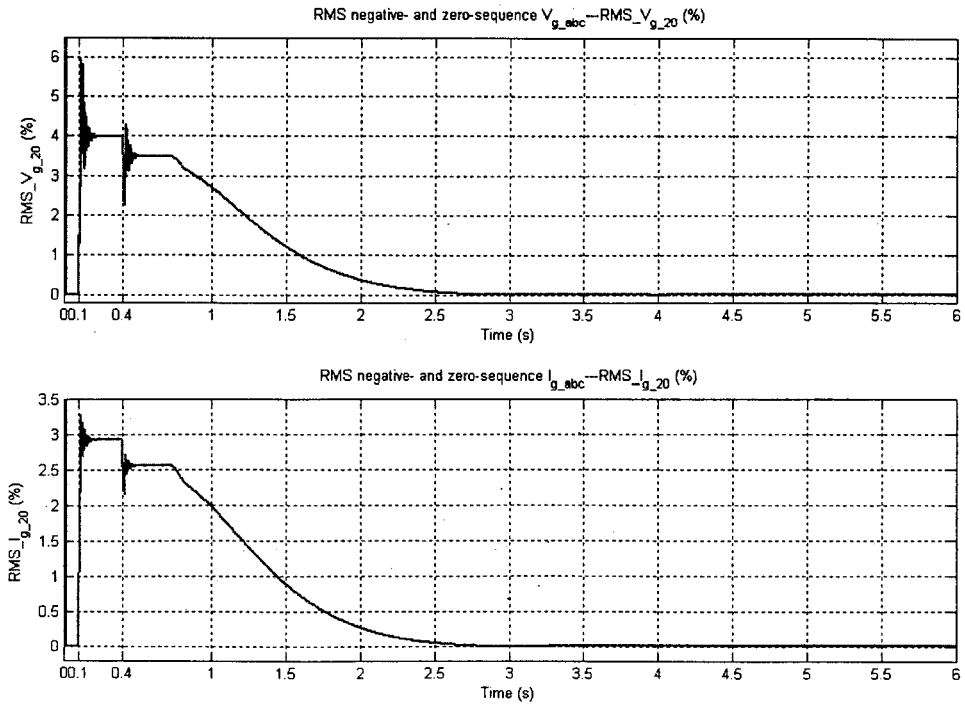

Figure 6.12 - Negative- and zero-sequence rms voltages and currents at Bus G in Simulation Case 3

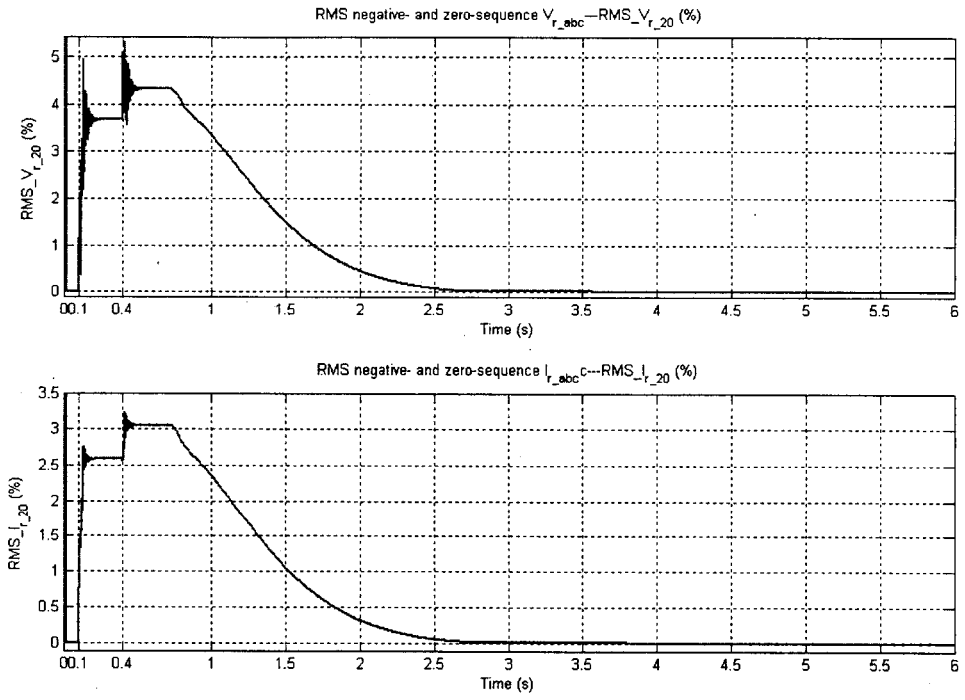

Figure 6.13 - Negative- and zero-sequence rms voltages and currents at Bus R in Simulation Case 3

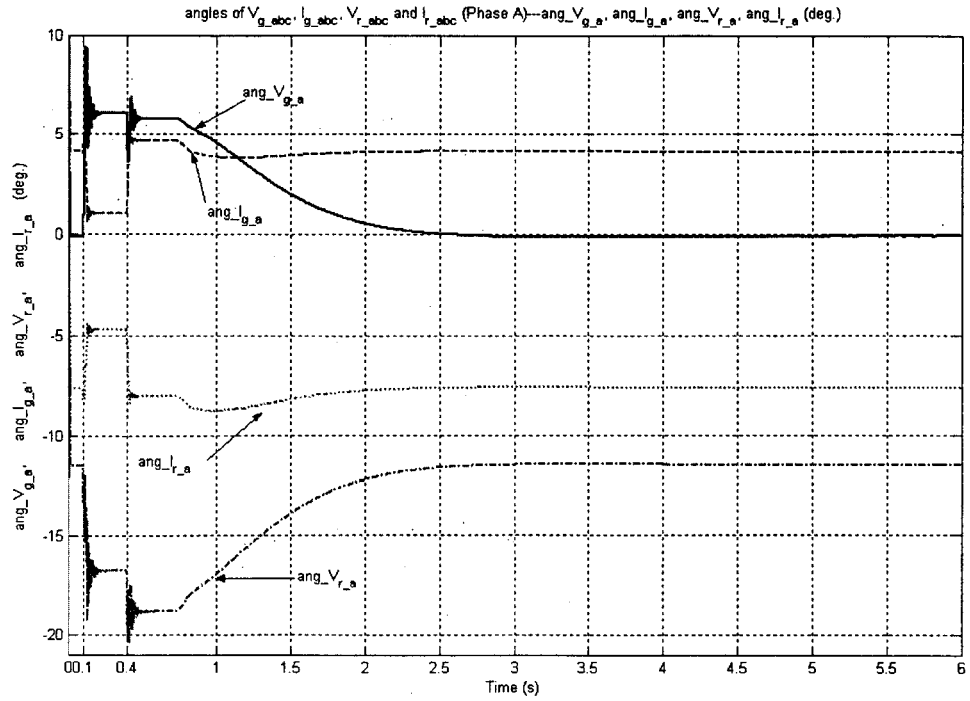

Figure 6.14 - Angles of voltages and currents of Phase A at Bus G and Bus R in Simulation Case 3

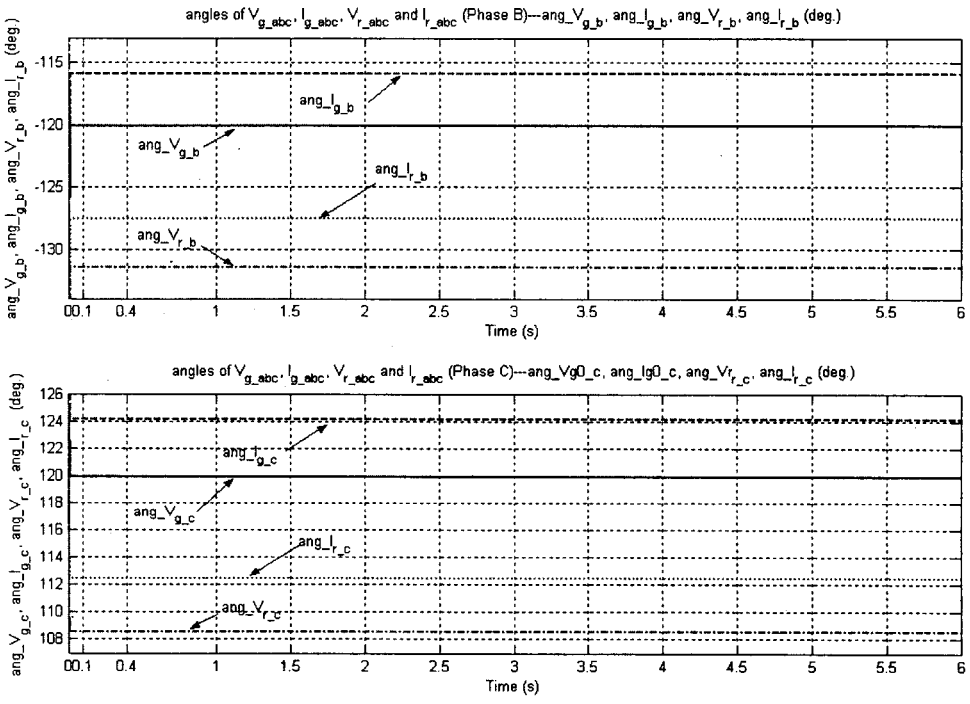

Figure 6.15 - Angles of voltages and currents of Phase B and C at Bus G and Bus R in Simulation Case 3

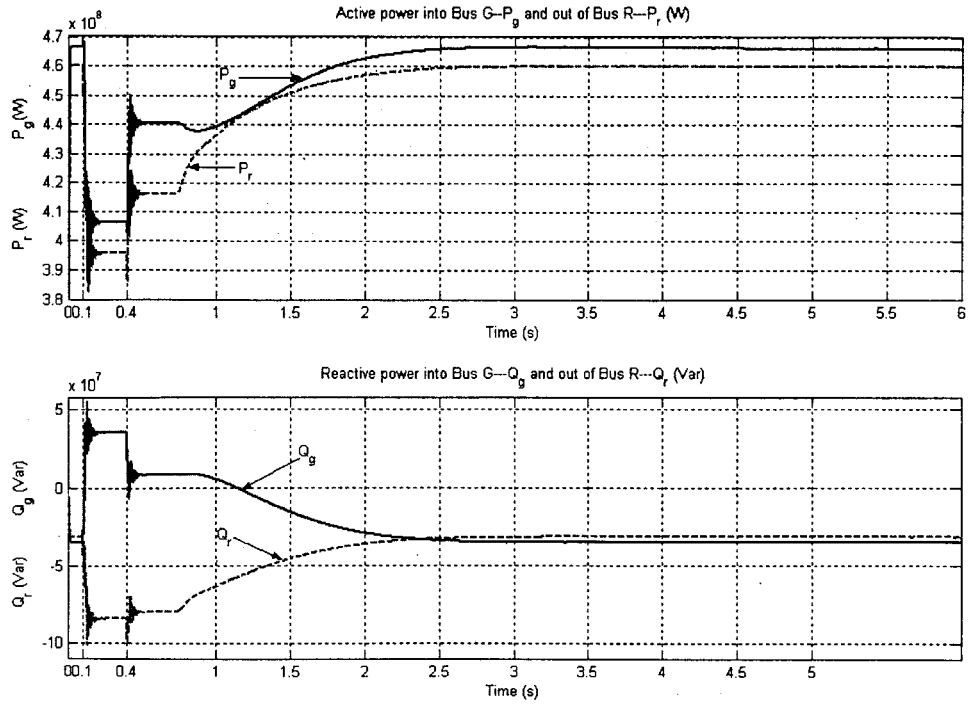

Figure 6.16 - Phase-A active and reactive powers at Bus G and Bus R in Simulation Case 3

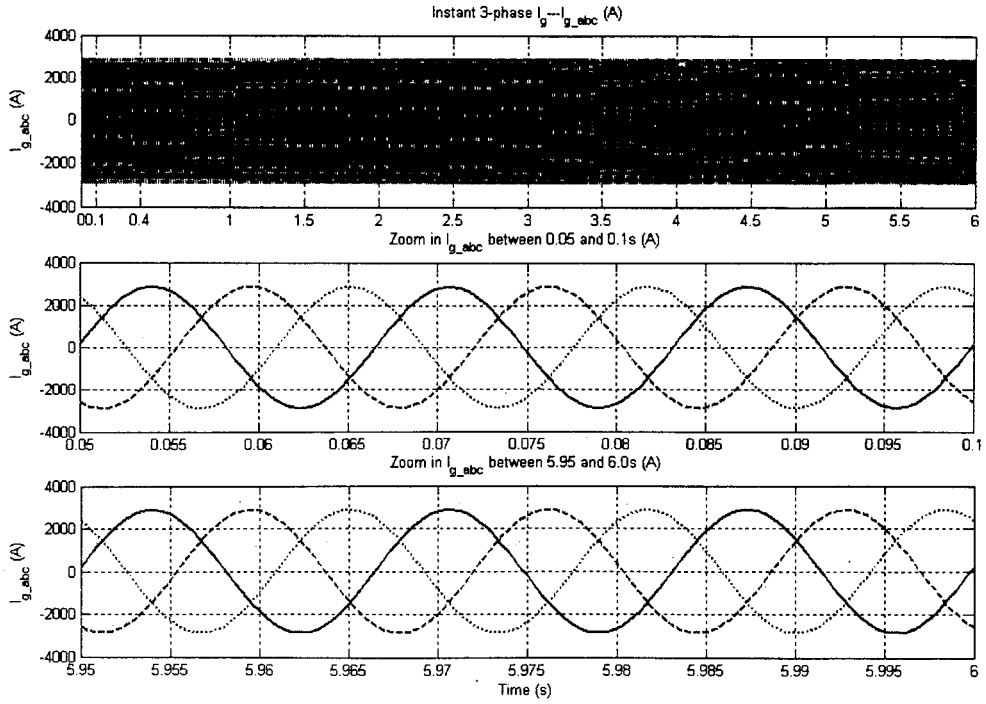

Figure 6.17 - Three-phase instantaneous currents into Bus G in Simulation Case 3

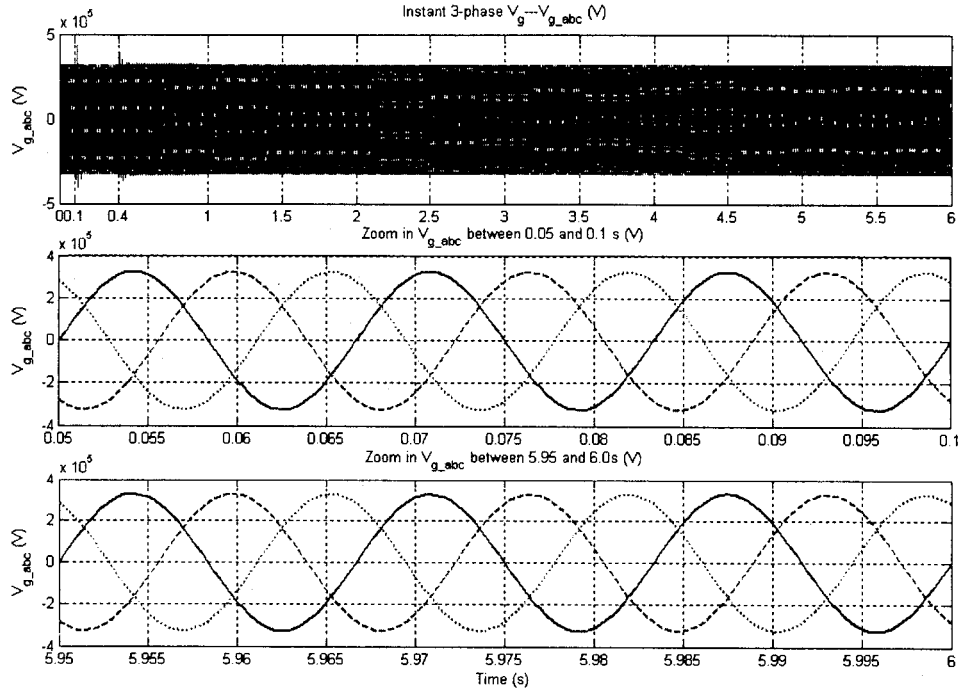

Figure 6.18 - Three-phase instantaneous voltages at Bus G in Simulation Case 3

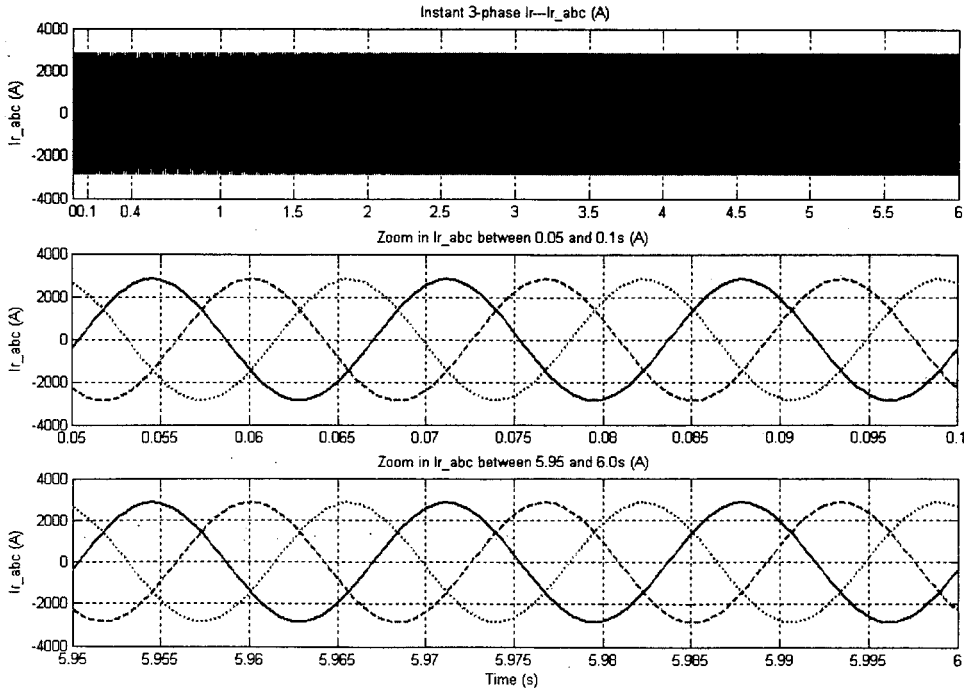

Figure 6.19 - Three-phase instantaneous currents out of Bus R in Simulation Case 3

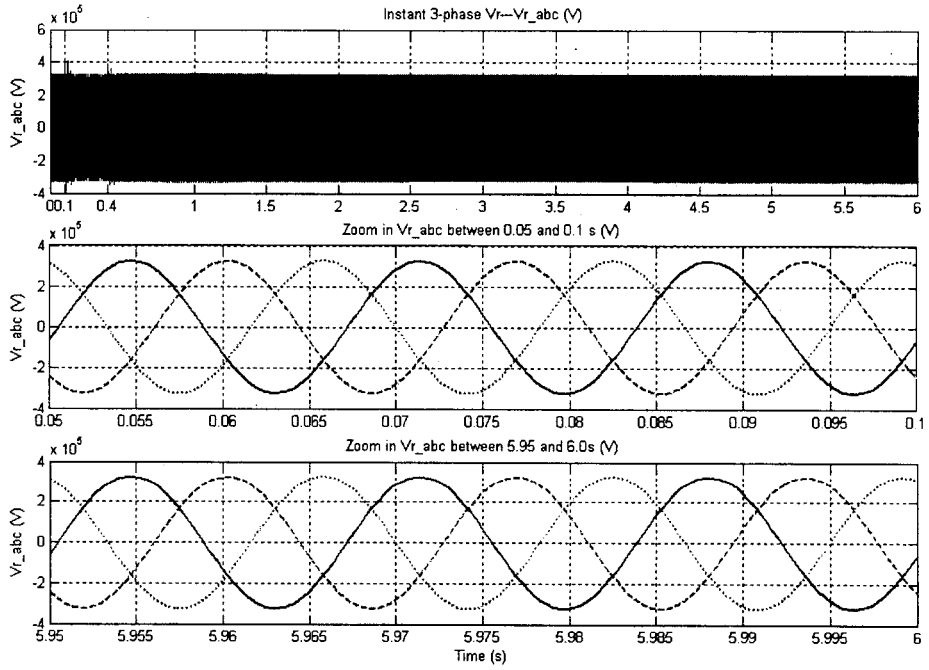

Figure 6.20 - Three-phase instantaneous voltages at Bus R in Simulation Case 3

6.3.2.2 Analysis of results of Simulation Case 3

(1) Refer to Figure 6.6. The steady-state references (t = 6.0 s) of φ_ref and δ_ref for the control of RPFC are:

$$\varphi\_ref = 82.26 \text{ deg.} \quad (6\text{-}5)$$

$$\delta\_ref = 16.24 \text{ deg.} \quad (6\text{-}6)$$

(2) Refer to Figure 6.7. The steady-state values (t = 6.0 s) of rotor positions of the two RPSTs are:

$$\alpha 1 = 66.02 \text{ deg.} \quad (6\text{-}7)$$

$$\alpha 2 = 98.49 \text{ deg.} \quad (6\text{-}8)$$

- Inserting (6-7) and (6-8) into (3-22) and (3-38), we get,

$$\delta = \frac{\alpha 2 - \alpha 1}{2} = 16.30 \text{ (deg.)} \quad (6\text{-}9)$$

$$\varphi = \theta + \gamma + \alpha = \frac{\alpha 2 + \alpha 1}{2} + \gamma + \alpha = 82.29 \text{ (deg.)} \quad (6\text{-}10)$$

It shows that the steady-state φ and δ are close to the steady-state φ_ref and δ_ref, respectively.

Note: In our project, γ and α are zeros.

- Inserting (3-37), (6-9) and (6-10) into, (3-45) and (3-46), we get,

$$T_{eq} = 1.0819 \quad (6\text{-}11)$$

$$\beta_0 = 15.95 \text{ (deg)} \quad (6\text{-}12)$$

(3) Refer to c) in Section 5.1.2 and (6-9). The two parts of the equivalent impedance of the RPFC can be calculated by (3-47) and (3-48),

$$Z_{rpfc\_c} = Z_{se} + 2 \cdot T_{se}^2 \cdot Z_{rt} = j9.375 \quad (\Omega)$$

$$Z_{rpfc\_v} = 4 \cdot T_{rt}^2 \cdot T_{se}^2 \cdot \cos^2 \delta \cdot Z_{sh} = j2.879 \quad (\Omega)$$

Then, $$Z_{rpfc} = Z_{rpfc\_c} + Z_{rpfc\_v} = j12.254 \quad (\Omega) \qquad (6\text{-}13)$$

(4) Refer to Figure 6.8 and Figure 6.9. The steady-state 1-phase shunt compensation current (t = 6.0 s), $\overline{I}_{sh\_com}$, and the injected series voltage for Phase-A, $\overline{V}_{ser}$, are:

$$\overline{I}_{sh\_com} = 794.5\angle 91.55 \text{ A} \qquad (6\text{-}14)$$

$$\overline{V}_{ser} = 44.97\angle 78.64 \text{ kV} \qquad (6\text{-}15)$$

It shows that $\overline{V}_{ser}$ is close to $\overline{V}_{ser\_ref}$ that is $44.9\angle 78.52$ kV.

Refer to Figure 6.3, Table 6.4, and (6-15). The steady-state value $\overline{V}_s$ (t = .0 s) is:

$$\overline{V}_s = \overline{V}g + \overline{V}ser = 242.64\angle 10.39 \text{ (kV)} \qquad (6\text{-}16)$$

(5) Inserting T=0.3125 (see c) in section 5.1.2), $\overline{V}_g = 229.8 \times 10^3 \angle -0.08$ (see Table 6.4), (6-9), (6-10), (6-13) and (6-15) into (3-40), we obtain

$$\overline{I}_{ser} = \frac{T \cdot |\cos\delta| \cdot \overline{V}_g \cdot e^{j\varphi} - \overline{V}_{ser}}{Z_{rpfc}} = 1980.1\angle -1.08 \quad \text{(A)} \qquad (6\text{-}17)$$

Then, the current through Phase-A of the sound line (Line 2) is $\overline{I}_{line\_post\_fault} = 2004.7\angle -4.14$ A. Where,

$$\overline{I}_{line\_post\_fault} = \overline{I}_{ser} - \overline{I}_{line\_capacitor} = \overline{I}_{ser} - 0.5B_L \cdot \overline{V}_s \qquad (6\text{-}18)$$

It shows $\bar{I}_{line\_post\_fault}$ is increased, compared with the current through one of the two pre-fault A-phases ($\bar{I}_{line\_pre\_fault} = 1014.9\angle -1.75$, see section 6.3.1).

And, the power through Phase-A of the sound line (i.e., out of Bus S) is

$$S_{BUS\_S} = \bar{V}_S \cdot (\bar{I}_{ser})^* = 471 + j95.5 \text{ (MW, MVar)} \qquad (6\text{-}19)$$

Thus, the active power (471 MW) transmitted through Phase-A of the sound line is greater than that (466 MW) through the two pre-fault A-phases.

(6) Refer to Figure 6.3, Table 6.4, (6-14) and (6-17). The steady-state value $\bar{I}_{sh}$ (t = 6.0 s):

$$\bar{I}_{sh} = \bar{I}_g - \bar{I}_{sh\_com} - \bar{I}_{ser} = 615.16\angle -83.42 \text{ (A)} \qquad (6\text{-}20)$$

Then, Phase-A power into the two RPSTs is

$$S_{RPSTs} = 2 \cdot \bar{V}r \cdot (\bar{I}_{sh2})^* = 6(\bar{V}g \cdot (\bar{I}_{sh})^* \cdot e^{j2\gamma} - \left|\frac{\bar{I}_{sh} \cdot e^{j\gamma}}{T_{sh}}\right|^2 \cdot Z_{sh})$$

$$= 32.8 + j256.6 \qquad \text{(MW, MVar)}$$

$$= 258.7\angle 82.7 \qquad \text{(MVA)} \qquad (6\text{-}21)$$

Comparing (6-21) with the third of the total capacity of the two RPSTs in Table 5.3, we find the two machines are overloaded. Similarly, the shunt and the series transformers are also overloaded.

(7) Referring to Table 5.6 and the above results, we have

- $\bar{V}_{ser}$ leads $\bar{I}_{ser}$ by 79.72 deg. (78.64-(-1.08))
- $\bar{V}_s$ leads $\bar{V}_g$ by 10.47 deg. (10.39-(-0.08))
- $\bar{V}_s$ leads $\bar{V}_r$ by 21.84 deg. (10.39-(-11.45))

- $\overline{V}_s$ leads $\overline{I}_{ser}$ by 11.47 deg. (10.39-(-1.08))
- $|\overline{V}_s|$ is greater than $|\overline{V}_g|$

(8) Figure 6.10 to Figure 6.16 are the curves of:

- The rms values and angles of three-phase $\overline{V}_g$, $\overline{V}_r$, $\overline{I}_g$ and $\overline{I}_r$;
- The rms values in percent of negative- and zero-sequence voltages and currents at Bus G and Bus R;
- P_g, P_r, Q_g and Q_r of Phase-A at Bus G and Bus R.

Based on these curves, the load flows at Bus G and Bus R at three instants are summarized in Table 6.4.

In Figure 6.16,

- During 0 ~ 0.4 s, the differences between P_g and P_r, Q_g and Q_r are the losses of Phase-A of the two transmission lines, respectively;
- During 0.4 ~ 1.0 s, the differences between P_g and P_r, Q_g and Q_r are the losses of Phase-A of the remaining transmission lines without the service of the RPFC and the single-phase shunt compensation, respectively;
- During 1.0 ~ 6.0 s, the differences between P_g and P_r, Q_g and Q_r are the sum of the losses of Phase-A of the remaining transmission lines and the power supplied by RPFC and the three-phase shunt compensation, respectively.

(9) Refer to Table 6.4 and Figure 6.17 through Figure 6.20. For A.O., the RPFC and a single-phase shunt compensation can preserve the pre-contingency load flows as expected and almost cancel the relative sequence components.

(10) The curves of the sequence components in Figure 6.12 and Figure 6.13 are identical, respectively, because of the Y_g-Y_g connections.

Table 6.4 Phase-A load flow at Bus G and Bus R in Simulation Case 3

At Bus G						
t (s)	V_{g_a}, (kV / deg.) V_{g_b}, V_{g_c}	V_{g_2}, (%) V_{g_0} (%)	I_{g_a} (A / deg.) I_{g_b} I_{g_c}	I_{g_2} (%) I_{g_0} (%)	P_g (MW)	Q_g (MVar)
0.09	229.8∠−0.1, 229.8∠−120, 229.8∠120	0.0001 0.0001	2034∠4.14, 2034∠−115.8, 2034∠124.2	0.0009 0.0011	466	-34.5
0.39	215.7∠6.03, 229.8∠−120, 229.8∠120	3.95 3.95	1892∠1.05 2034∠−115.8, 2034∠124.2	2.92 2.92	406	35.5
6.0	229.8∠−0.08, 229.8∠−120, 229.8∠120	0.01 0.01	2034∠4.11, 2034∠−115.8, 2034∠124.2	0.02 0.02	466.2	-34.2
At Bus R						
t (s)	Vr_a, Vr_b, Vr_c,	Vr_2, (%) Vr_0 (%)	Ir_a, Ir_b, Ir_c,	Ir_2, (%) Ir_0 (%)	Pr (MW) (Phase A)	Qr (MVar) (Phase A)
0.09	230.∠−11.45, 230.∠−131.5, 230.∠108.6	0.0002 0.0001	2005 ∠ − 7.57, 2005 ∠ − 127.7, 2005 ∠112.3	0.0009 0.0011	460	-31.1
0.39	215.3∠−16.78, 230.∠−131.5, 230.∠108.6	3.67 3.67	1880∠ − 4.75, 2005 ∠ − 127.7, 2005 ∠112.3	2.6 2.6	396	-84.5
6.0	230.∠−11.45, 230.∠−131.5, 230.∠108.6	0.01 0.01	2005 ∠ − 7.57, 2005 ∠ − 127.7, 2005 ∠112.3	0.01 0.01	460.1	-31.1

6.3.3 Simulation Case 4 - Asymmetrical operation with two six-pole-pair RPSTs

The main purpose of this simulation is to observe how the pole-pair number affects the transient process of the power system and performance of the RPFC itself, comparing to Simulation Case3 in which the pole-pair number of the RPST is one.

6.3.3.1 Results of Simulation Case 4

The pertinent operational parameters are the same as those in Simulation Case3 of section 6.3.2.1.

Figure 6.21 to Figure 6.35 show the concerned curves of Simulation Case 4.

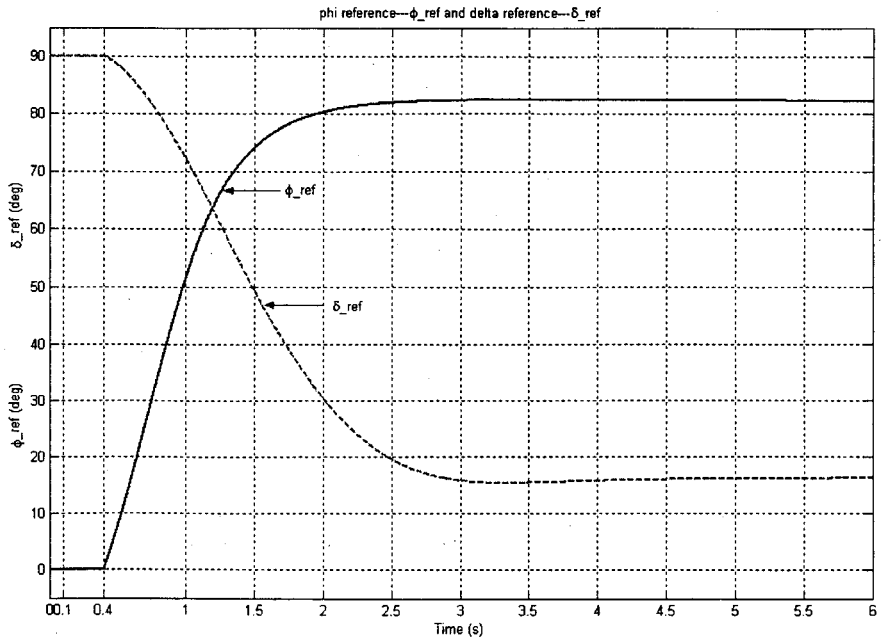

Figure 6.21 - Curves of φ_ref and δ_ref in Simulation Case4

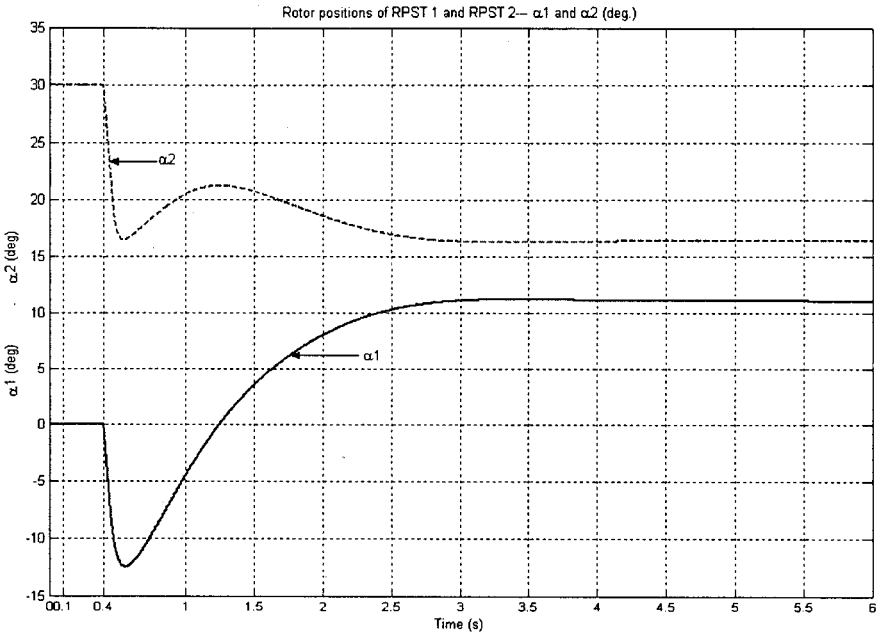

Figure 6.22 - Rotor positions of RPSTs---α1 and α2 in Simulation Case4

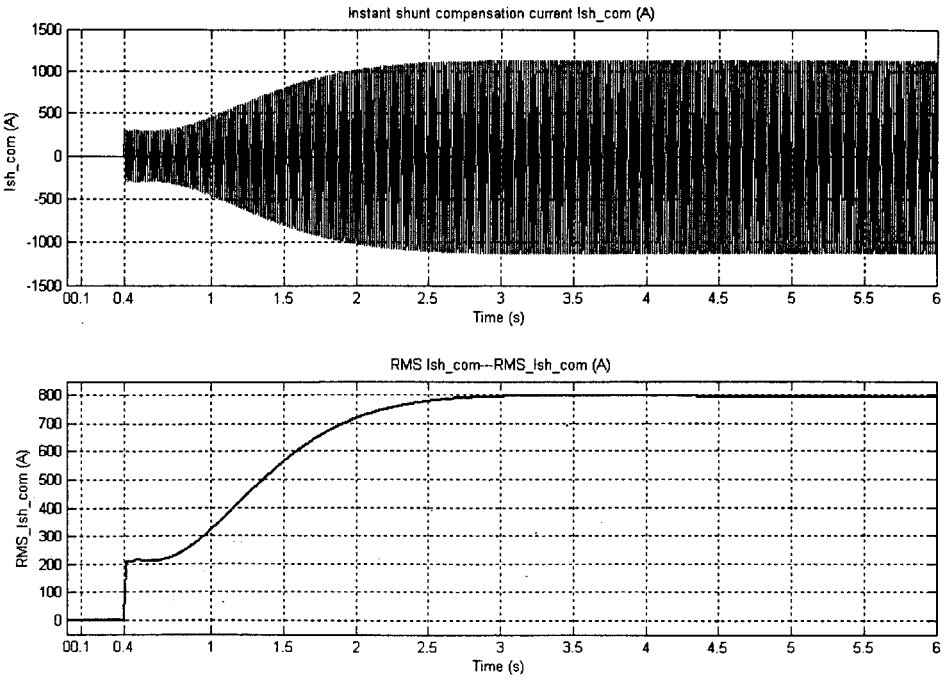

Figure 6.23 - Shunt compensation current $I_{sh\ com}$ in Simulation Case4

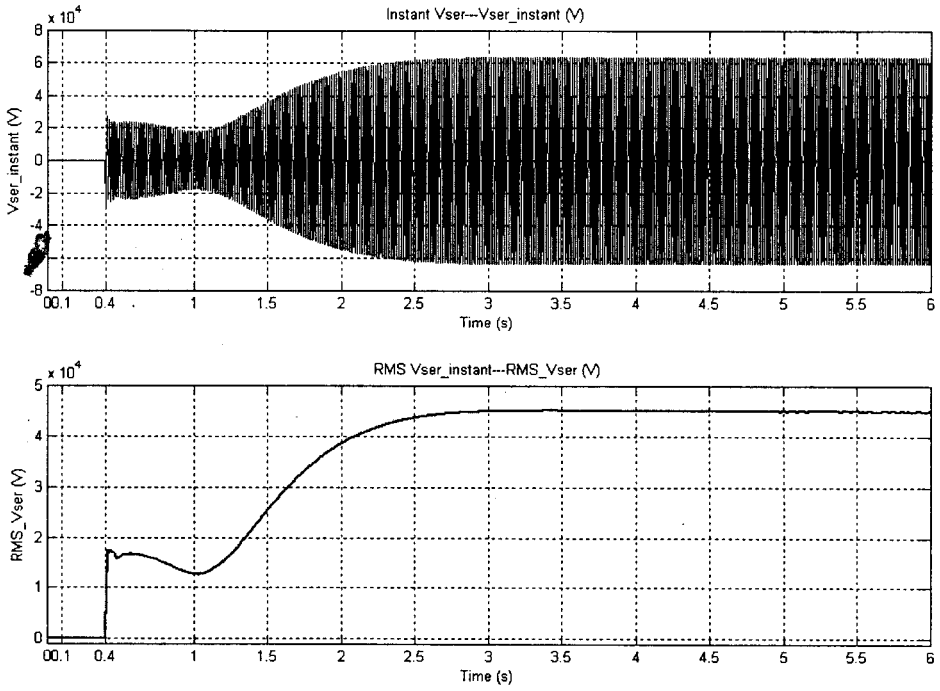

Figure 6.24 - Inserted series voltage V_{ser} in Simulation Case4

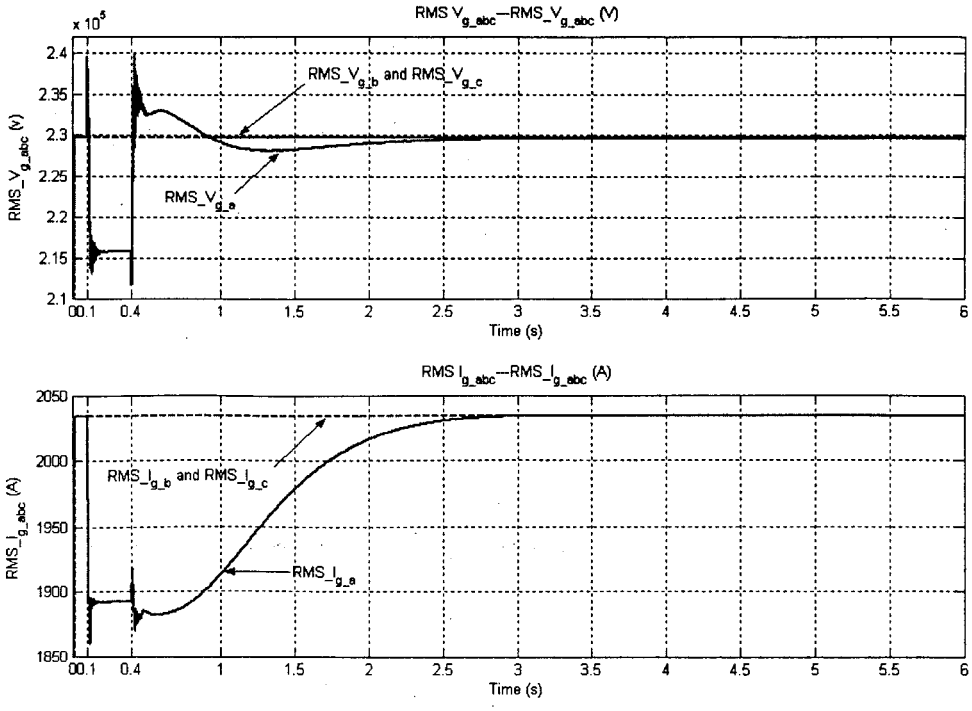

Figure 6.25 - Three-phase rms voltages and currents at Bus G in Simulation Case4

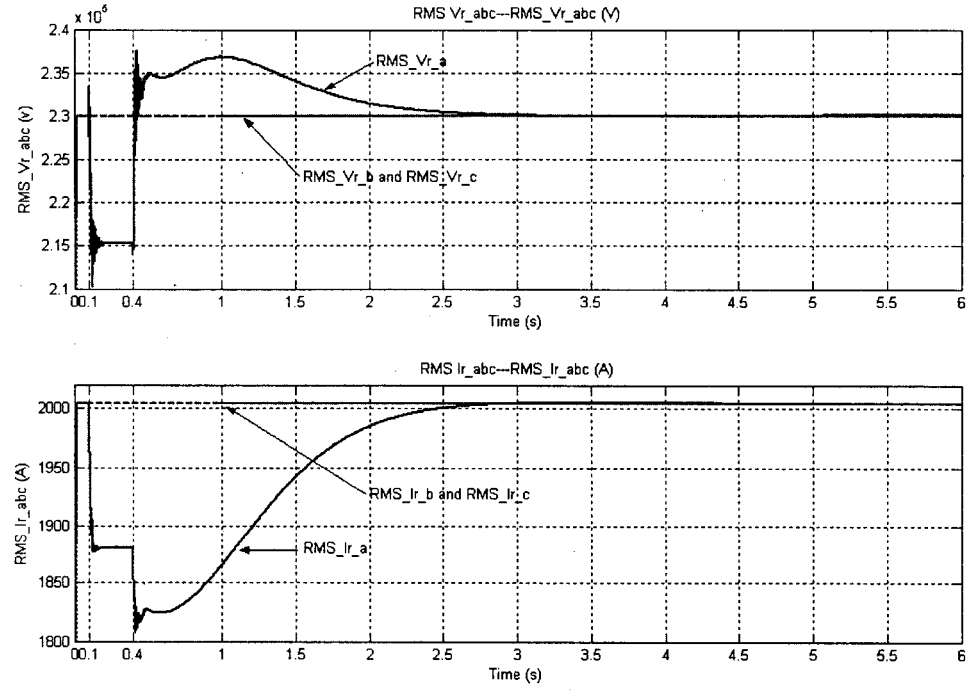

Figure 6.26 - Three-phase rms voltages and currents at Bus R in Simulation Case4

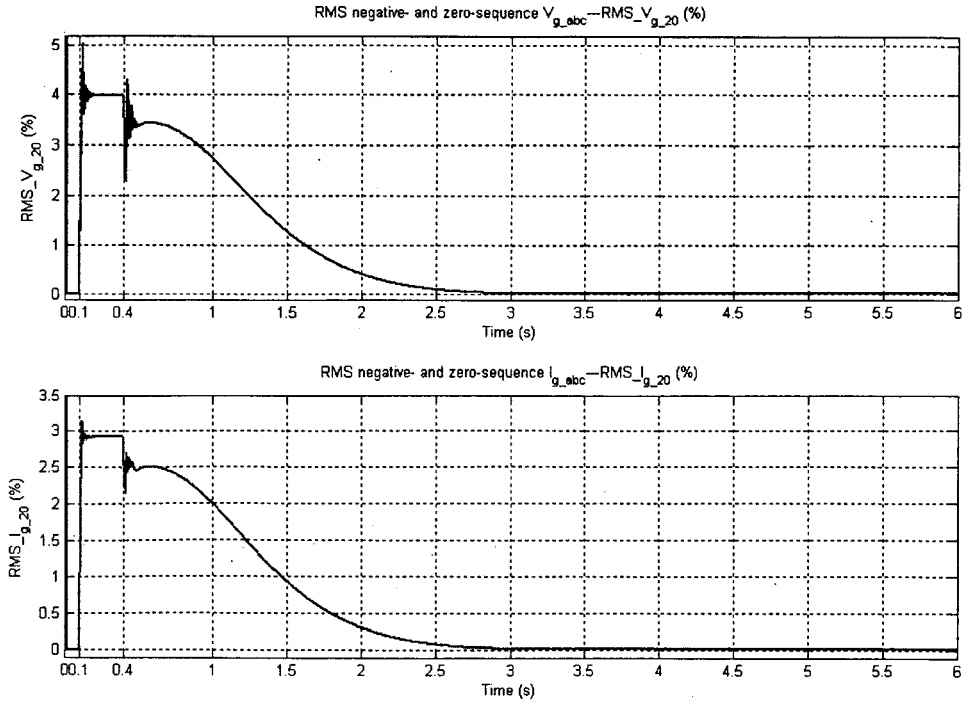

Figure 6.27- Negative- and zero-sequence rms voltages and current at Bus G in Simulation Case4

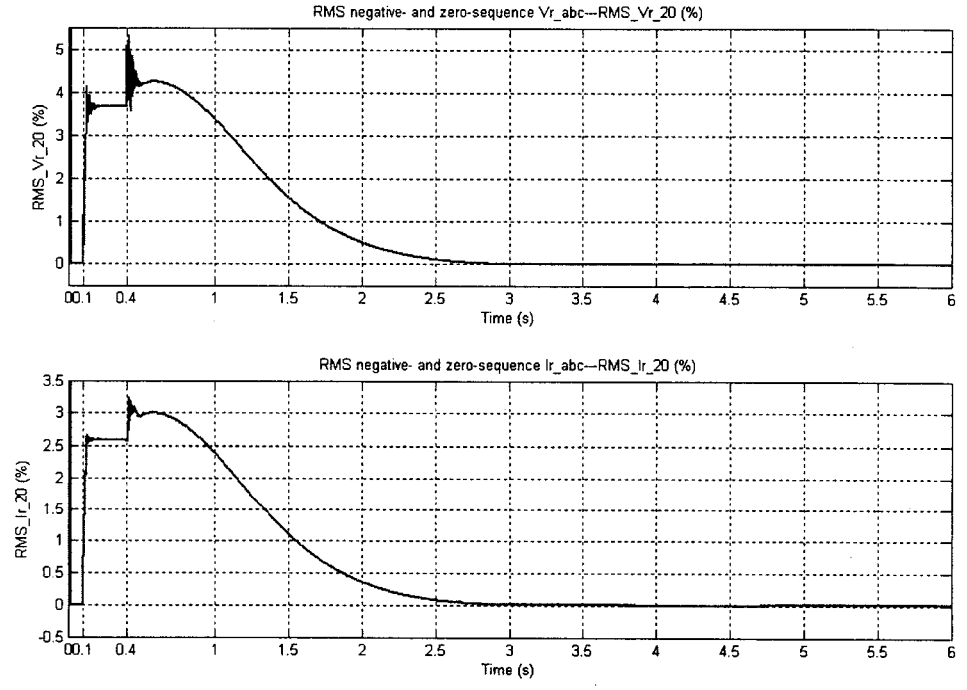

Figure 6.28 - Negative- and zero-sequence rms voltages and currents at Bus R in Simulation Case4

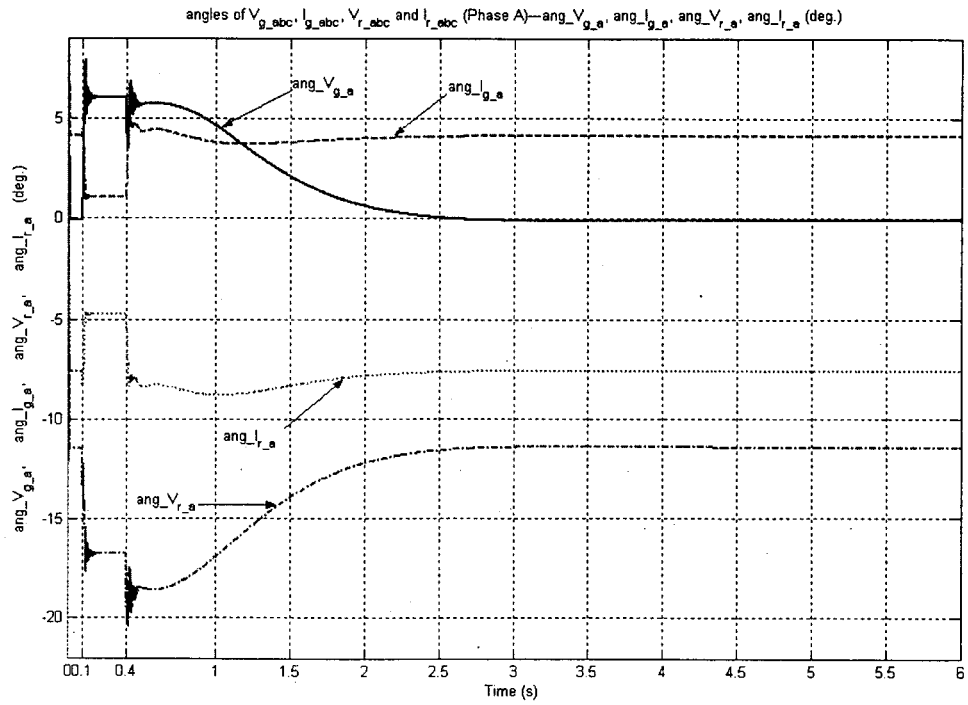

Figure 6.29 - Angles of voltages and currents of Phase A at Bus G and Bus R in Simulation Case4

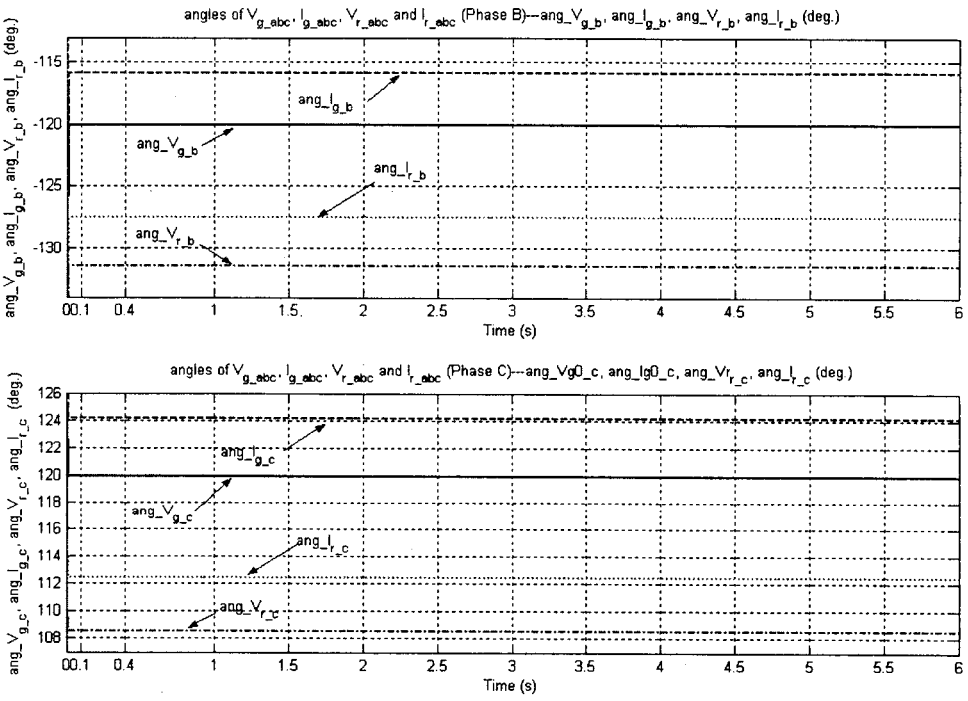

Figure 6.30 - Angles of voltages and currents of Phase B and C at Bus G and Bus R in Simulation Case4

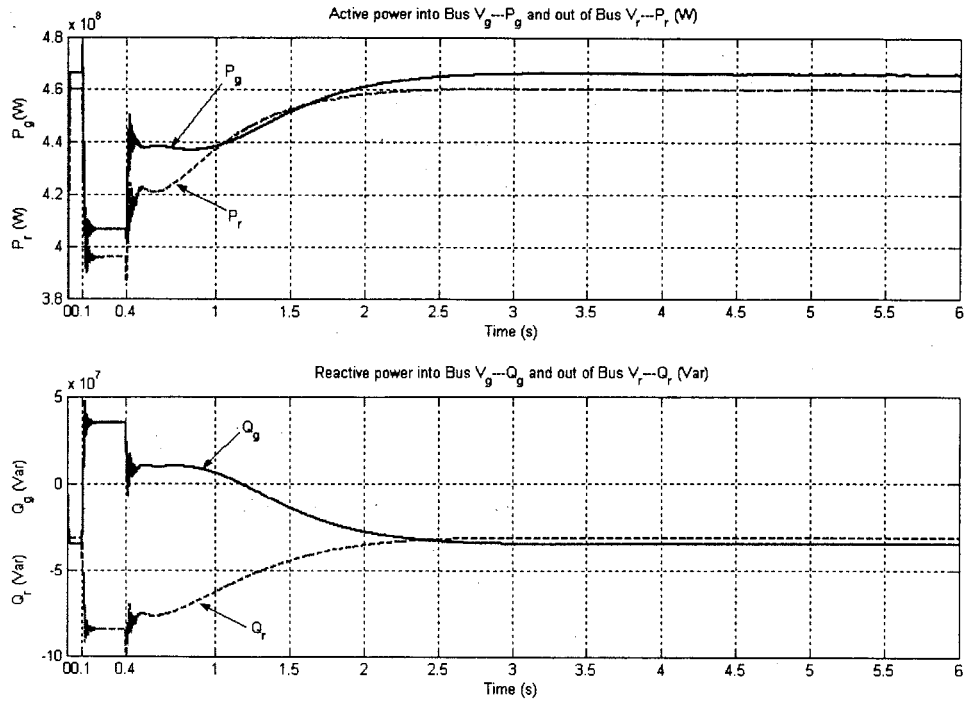

Figure 6.31- Phase-A active and reactive powers at Bus G and Bus R in Simulation Case4

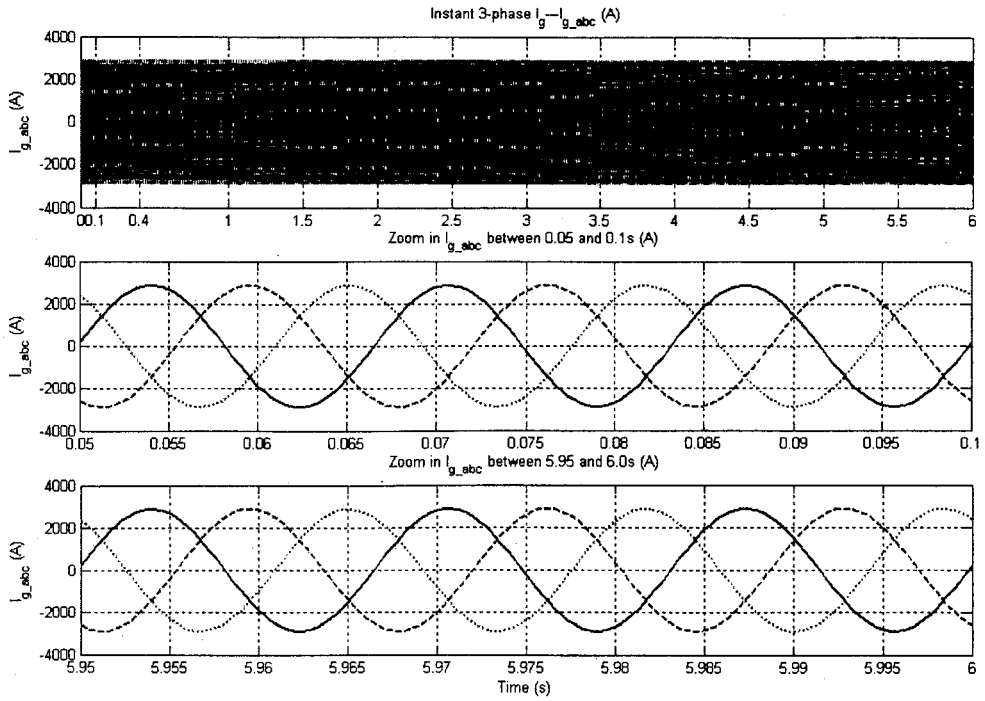

Figure 6.32 - Three-phase instantaneous currents into Bus G in Simulation Case4

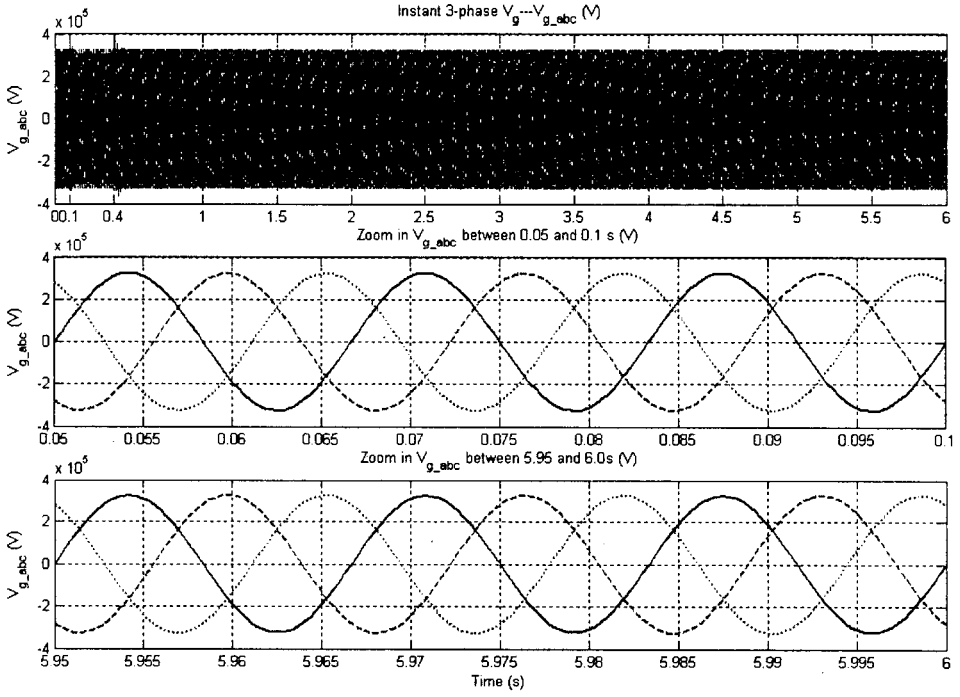

Figure 6.33 - Three-phase instantaneous voltages at Bus G in Simulation Case4

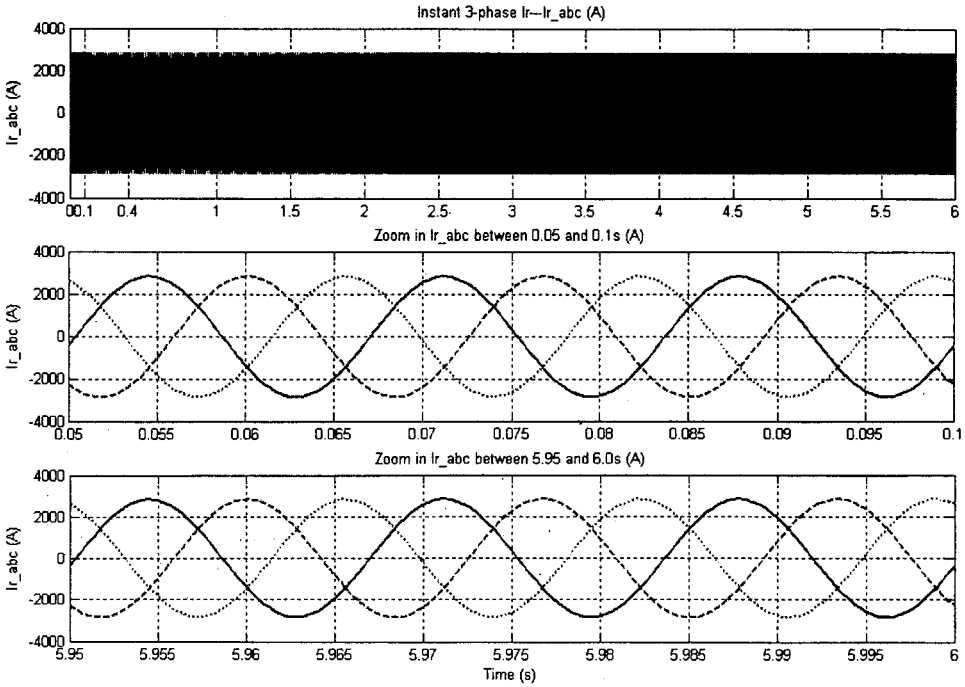

Figure 6.34 - Three-phase instantaneous currents out of Bus R in Simulation Case4

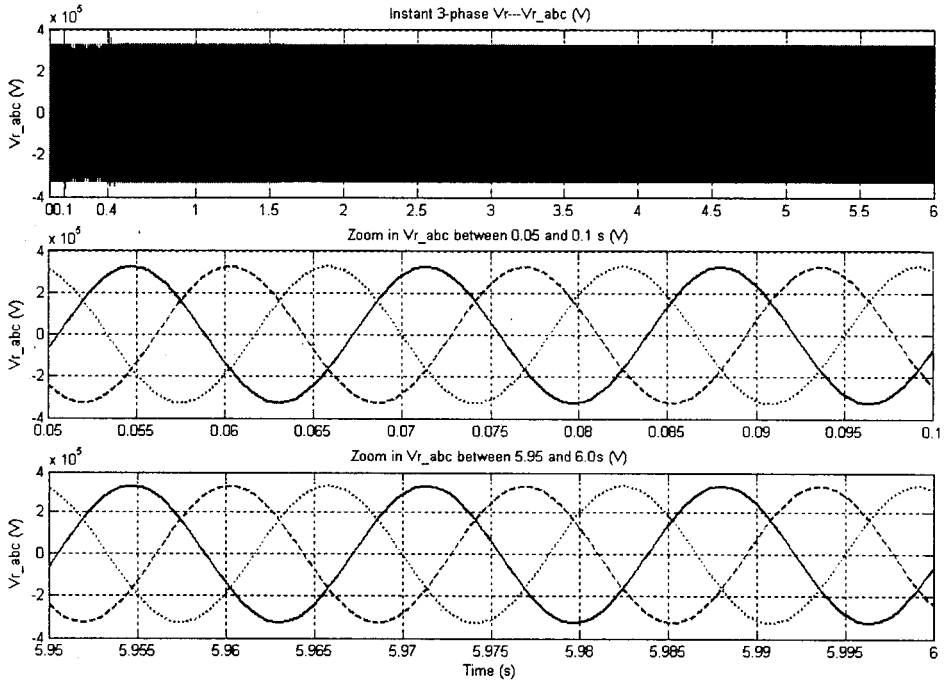

Figure 6.35 - Three-phase instantaneous voltages at Bus R in Simulation Case4

6.3.3.2 Analysis of results of Simulation Case 4

(1) Refer to Figure 6.21. The steady-state references (t = 6.0 s) of φ_ref and δ_ref for the control of RPFC are:

$$\varphi\_ref = 82.17 \text{ deg.} \quad (6\text{-}22)$$

$$\delta\_ref = 16.24 \text{ deg.} \quad (6\text{-}23)$$

(2) Refer to Figure 6.22. The steady-state values (t = 6.0 s) of rotor positions of the two RPSTs are:

$$\alpha 1 = 10.99 \text{ deg.} \quad (6\text{-}24)$$

$$\alpha 2 = 16.40 \text{ deg.} \quad (6\text{-}25)$$

Note: the pole-pair number is 6.

- Reviewing the **Note** in Section 3.7, we multiply (6-24) and (6-25) by 6, then insert them into (3-22) and (3-38), we get,

$$\delta = \frac{\alpha 2 - \alpha 1}{2} = 16.23 \text{ (deg.)} \quad (6\text{-}26)$$

$$\varphi = \theta + \gamma + \alpha = \frac{\alpha 2 + \alpha 1}{2} + \gamma + \alpha = 82.17 \text{ (deg.)} \quad (6\text{-}27)$$

It shows that the steady-state φ and δ are close to the steady-state φ_ref and δ_ref, respectively.

Note: In our project, γ and α are zeros.

- Inserting (3-37), (6-26) and (6-27) into, (3-45) and (3-46), we get,

$$T_{eq} = 1.0825 \quad (6\text{-}28)$$

$$\beta_0 = 15.94 \text{ (deg)} \quad (6\text{-}29)$$

(3) Refer to c) in Section 5.1.2 and (6-26). The two parts of the equivalent impedance of the RPFC can be calculated by (3-47) and (3-48),

$$Z_{rpfc\_c} = Z_{se} + 2 \cdot T_{se}^2 \cdot Z_{rt} = j9.375 \quad (\Omega)$$

$$Z_{rpfc\_v} = 4 \cdot T_{rt}^2 \cdot T_{se}^2 \cdot \cos^2 \delta \cdot Z_{sh} = j2.88 \quad (\Omega)$$

Then, $$Z_{rpfc} = Z_{rpfc\_c} + Z_{rpfc\_v} = j12.255 \quad (\Omega) \qquad (6\text{-}30)$$

(4) Refer to Figure 6.23 and Figure 6.24. The 1-phase steady-state shunt compensation current (t = 6.0 s), $\overline{I}_{sh\_com}$, and the injected series voltage for Pase-A, $\overline{V}_{ser}$, are:

$$\overline{I}_{sh\_com} = 794.16\angle 91.51 \text{ A} \qquad (6\text{-}31)$$

$$\overline{V}_{ser} = 45.02\angle 78.73 \text{ kV} \qquad (6\text{-}32)$$

It shows that $\overline{V}_{ser}$ is close to $\overline{V}_{ser\_ref}$ that is $44.9\angle 78.52$ kV.

Refer to Figure 6.3, Table 6.5, and (6-32). The steady-state value $\overline{V}_s$ is:

$$\overline{V}_s = \overline{V}g + \overline{V}ser == 242.59\angle 10.41 \text{ (kV)} \qquad (6\text{-}33)$$

(5) Inserting T=0.3125 (see c) in section 5.1.2), $\overline{V}_g = 229.8 \times 10^3 \angle -0.08$ (see Table 6.5), (6-26), (6-27), (6-30) and (6-32) into (3-40), we obtain

$$\overline{I}_{ser} = \frac{T \cdot |\cos\delta| \cdot \overline{V}_g \cdot e^{j\varphi} - \overline{V}_{ser}}{Z_{rpfc}} = 1970.8\angle -1.64 \quad \text{(A)} \qquad (6\text{-}34)$$

Then, the current through Phase-A of the sound line (Line 2) is $\overline{I}_{line\_post\_fault} = 1996.5\angle -4.7$ A. Where,

$$\overline{I}_{line\_post\_fault} = \overline{I}_{ser} - \overline{I}_{line\_capacitor} = \overline{I}_{ser} - 0.5B_L \cdot \overline{V}_s \qquad (6\text{-}35$$

It shows $\bar{I}_{line\_post\_fault}$ is increased, compared with the current through one of the two pre-fault A-phases ($\bar{I}_{line\_pre\_fault} = 1014.9\angle -1.75$, see section 6.3.1).

And, the power through Phase-A of the sound line (i.e., out of Bus S) is

$$S_{BUS\_S} = \bar{V}s \cdot (\bar{I}_{ser})^* = 478 + \text{j}99.8 \quad \text{(MW, MVar)} \qquad (6\text{-}36)$$

Thus, the active power (478 MW) transmitted through Phase-A of the sound line is greater than that (466 MW) through the two pre-fault A-phases.

(6) Refer to Figure 6.3, Table 6.5, (6-31) and (6-34). The steady-state value $\bar{I}_{sh}$ (t = 6.0 s):

$$\bar{I}_{sh} = \bar{I}_g - \bar{I}_{sh\_com} - \bar{I}_{ser} = 597.2\angle -82.34 \quad \text{(A)} \qquad (6\text{-}37)$$

Phase-A power into the two RPSTs is

$$\begin{aligned} S_{RPSTs} = 2 \cdot \bar{V}r \cdot (\bar{I}_{sh2})^* &= 6(\bar{V}g \cdot (\bar{I}_{sh})^* \cdot e^{j2\gamma} - \left|\frac{\bar{I}_{sh} \cdot e^{j\gamma}}{T_{sh}}\right|^2 \cdot Z_{sh}) \\ &= 37.0 + j249.2 \qquad \text{(MW, MVar)} \\ &= 251.9\angle 81.6 \qquad \text{(MVA)} \end{aligned} \qquad (6\text{-}38)$$

Comparing (6-38) with the third of the total capacity of the two RPSTs in Table 5.3, we find the two machines are overloaded. Similarly, the shunt and the series transformers are also overloaded.

(7) Referring to Table 5.6 and the above results, we have

- $\overline{V}_{ser}$ leads $\overline{I}_{ser}$ by 96.19 deg. (78.73-(-17.55))
- $\overline{V}_s$ leads $\overline{V}_g$ by 10.49 deg. (10.41-(-0.08))
- $\overline{V}_s$ leads $\overline{V}_r$ by 21.86 deg. (10.41-(-11.45))
- $\overline{V}_s$ leads $\overline{I}_{ser}$ by 27.96 deg. (10.41-(-17.55))
- $\left|\overline{V}_s\right|$ is greater than $\left|\overline{V}_g\right|$

(8) Figure 6.25 to Figure 6.31 are the curves of:

- The rms values and angles of three-phase $\overline{V}_g$, $\overline{V}_r$, $\overline{I}_g$ and $\overline{I}_r$;
- The rms values in percent of negative- and zero-sequence voltages and currents at Bus G and Bus R;
- P_g, P_r, Q_g and Q_r of Phase-A at Bus G and Bus R.

Based on these curves, the load flows at Bus G and Bus R at three instants are summarized in Table 6.5.

In Figure 6.31,

- During 0 ~ 0.4 s, the differences between P_g and P_r, Q_g and Q_r are the losses of Phase-A of the two transmission lines, respectively;
- During 0.4 ~ 1.0 s, the differences between P_g and P_r, Q_g and Q_r are the losses of Phase-A of the remaining transmission lines without the service of the RPFC and the single-phase shunt compensation, respectively;
- During 1.0 ~ 6.0 s, the differences between P_g and P_r, Q_g and Q_r are the sum of the losses of Phase-A of the remaining transmission lines and the power supplied by the RPFC and the three-phase shunt compensation, respectively.

(9) Refer to Table 6.5 and Figure 6.32 through Figure 6.35. For asymmetrical operation, the RPFC and a single-phase shunt compensation can preserve the pre-contingency load flows as expected and make the relative sequence components in an acceptable margin.

(10) The curves of the sequence components in Figure 6.27 and Figure 6.28 are identical, respectively, because of the Y_g / Y_g connections.

(11) Compare (6-24) and (6-25) with (6-7) and (6-8), and Figure 6.22 with Figure 6.7. The larger the pole-pair numbers of RPSTs, the less the rotors move.

(12) Compare Figure 6.9 and Figure 6.24, Figure 6.10 and Figure 6.23, etc. The beginning part (0.4~1 s) of transient process of transmission system is sensitive to the rotor movement of the RPST with a larger pole-pair number.

Table 6.5 Phase-A load flow at Bus G and Bus R in Simulation Case 4

At Bus G						
t (s)	V_{g_a}, (kV / deg.) V_{g_b}, V_{g_c}	V_{g_2}, (%) V_{g_0} (%)	I_{g_a} (A / deg.) I_{g_b} I_{g_c}	I_{g_2} (%) I_{g_0} (%)	P_g (MW)	Q_g (MVar)
0.09	229.8∠−0.1, 229.8∠−120, 229.8∠120	0.0001 0.0001	2034∠4.14, 2034∠−115.8, 2034∠124.2	0.0009 0.0011	466	-34.5
0.39	215.7∠6.03, 229.8∠−120, 229.8∠120	3.95 3.95	1892 / 1.05, 2034∠−115.8, 2034∠124.2	2.92 2.92	406	35.5
6.0	229.8∠−0.08, 229.8∠−120, 229.8∠120	0.01 0.01	2034∠4.11, 2034∠−115.8, 2034∠124.2	0.02 0.02	466.2	-34.2
At Bus R						
t (s)	Vr_a, Vr_b, Vr_c,	Vr_2, (%) Vr_0 (%)	Ir_a, Ir_b, Ir_c,	Ir_2, (%) Ir_0 (%)	Pr (MW) (Phase A)	Qr (MVar) (Phase A)
0.09	230.∠−11.45, 230.∠−131.5, 230.∠108.6	0.0002 0.0001	2005 ∠ − 7.57, 2005 ∠ − 127.7, 2005 ∠112.3	0.0009 0.0011	460	-31.1
0.39	215.3∠−16.78, 230.∠−131.5, 230.∠108.6	3.67 3.67	1880∠ − 4.75, 2005 ∠ − 127.7, 2005 ∠112.3	2.6 2.6	396	-84.5
6.0	230.∠−11.45, 230.∠−131.5, 230.∠108.6	0.01 0.01	2005 ∠ − 7.57, 2005 ∠ − 127.7, 2005 ∠112.3	0.01 0.01	460.1	-31.1

6.4 Summary

- The RPFC and a single-phase shunt compensation have been used for asymmetrical operation, preserving the pre-contingency load flows at Bus G and Bus R, respectively, and making the negative- and zero-sequences voltages and currents in an acceptable margin (Table 6.4 and Table 6.5).
- The beginning part (0.4~1 s) of the transient process of the transmission system is sensitive to the rotor movement of the RPST with large pole-pair number (for example, compare Figure 6.9 and Figure 6.24, Figure 6.10 and Figure 6.23, etc.).
- The larger the pole-pair numbers of the RPSTs, the less the rotors move (Figure 6.7 and Figure 6.22)
- The pole-pair numbers do not affect the steady-state values of the power system (see the operational parameters at t = 6.0 s in Table 6.4 and Table 6.5)
- The insertion of the RPFC and the single-phase shunt compensation increase the current through Phase-A of the sound transmission line (transmission line 2).

CHAPTER 7 CONCLUSION

The need for increasing transmission capacity has received a certain impetus nowadays mainly because of the environmental process involved in building new transmission lines and the difficulty of apportioning the cost in a deregulated environment. The Rotary Power Flow Controller (RPFC) is an alternative approach to meet the need instead of building new transmission lines or installing classical series compensation or installing FACTS devices.

In this Master dissertation, Asymmetrical Operation (A.O.) of an electric power system is defined as the operation of three-phase equipment as three single-phase elements operating separately.

The asymmetrical operation of a power system provides practical and economical solutions to increase the capacity of the power transmission system. When one phase of a line is broken, we can preserve the angles and amplitudes of voltages and currents at the both ends, i.e., sending- and receiving-ends, of the line, by taking the appropriate corrective measures.

The developed theory is used to determine the conditions in which the respect of criteria of conservation of the angles and amplitudes of voltages and currents is guaranteed when one phase or three phases of a line is (are) lost.

An RPFC consists of a shunt and a series transformers, and two series-connected rotary phase-shifting transformers (RPSTs) that are wound-rotor induction machines in the standstill operation mode. Its equivalent circuit can be represented by an induction machine in the standstill operation mode, whose turn-ratio of the stator-winding over the rotor-winding, angle between the stator- and rotor-windings' axes, and impedance, are functions of the rotor positions of the two-series connected RPSTs of the RPFC.

The RPFC has been molded by a voltage source in series and an inductive current source in parallel with the power system. Its control system is a two-inputs-two-outputs system that consists of two independent sets of proportional / integral (PI) and closed-loop system. The co-ordination among the parameters of the control system is very important for the successful RPFC operation.

The particular cases invested in this Master dissertation deal with a transmission system consisting of two lines in the same corridor where one phase or three phases of one of the two lines is or are out of service. The system that has been simulated is implemented in the Matlab/Simulink and SPS (Simulation-Power-System developed by l'Institut de Recherche d'Hydro Quebec).

The RPFC as series compensation has been used not only in symmetrical operation, but also in asymmetrical operation of the power system.

The simulation results have shown that the RPFC and a three- or single-phase shunt compensation can preserve the angles and amplitudes of voltages and currents at the both ends when three phases or one phase of a line are or is broken, respectively. But, the improper coordination between the shunt- and series-transformers' ratios resulted in the RPFC not reaching its expected performance criteria.

The beginning part (0.4~1 s) of the transient process of the transmission system is sensitive to the rotor movement of the RPST with a larger pole-pair number. The larger the pole-pair numbers are, the less the rotors move. But, The pole-pair numbers do not affect the steady-state values of the power system.

For the symmetrical operation, the insertion of the RPFC and the three-phase shunt compensation increase the current through the sound transmission line, while for the asymmetrical operation (for example, Phase-A of one of the transmission lines is opened due to a fault), the insertion of the RPFC and the single-phase shunt compensation increase the current(s) through the A-phase(s) of the sound transmission lines.

- **Future work**

  - ✓ A new set of parameters applied to the developed control system of the RPFC in this study should be investigated for the case where their connections of step-up and step-down transformers are Δ-Y_g and Y_g-Δ
  - ✓ Simulations in the discrete-time system are recommended
  - ✓ Simulation of reversing the transmitted powers through the transmission lines
  - ✓ Modeling of components of the Rotary Phase Shift Transformer (RPST)

References

[1] Chapman, Stephen J., (1985). Electric Machinery Fundamentals, McGraw- Hill Book Company.

[2] Fujita, H. et al, (Aug. 2000). Power Flow Controller Using Rotary Phase-Shifting Transformers, Paper 37-102, CIGRE Session, Paris.

[3] Fujita, H. et al, (2000). Basic Characteristics of a Rotary Power Flow Controller, Proc. IEEE/PES Winter Meeting, Singapore, 1477-1482.

[4] Fujita, H. et al, (2001). Modeling and Dynamic Performance of A Rotary Power Flow Controller, Proc. IEEE/PES Winter Meeting, Columbus, Ohio, 599- 604.

[5] Fujita, H. et al, (2001). Simulator Model of Rotary Power Flow Controller, Proc. IEEE/PES, Summer Meeting, 1794-1797.

[6] Gyugyi, L., (April 1988). Unified Power Flow Control Concept for Flexible AC Transmission Systems, IEE Proceedings, Vol. 76, No.4.

[7] Gyugyi, L., et al, (April 1995). Unified Power Flow Controller: A new Approach to Power Transmission Control, IEEE Transaction on Power Delivery, Vol.10, No.2, 1085-1097.

[8] Hingorani, Narain G., Gyugyi, Laszlo, (2000). Understanding FACTS, The Institute of Electrical and Electronics Engineers, Inc.

[9] Jacobs, O.L.R., (1974). Introduction to Control System, Oxford University Press.

[10] Kang,Y.L., Shrestha, G.B., Lie, T.T., (2000). Improvement of Power System Dynamic Performance with the Magnitude and Phase Angle Control of Static Phase-Shifter, Electric Power System Research, 121-128.

[11] Kosow, Irving L., (1991). Electric Machinery and Transformers, 2nd Edition, Prentice-Hall.

[12] Larsen, Einar V., (Nov.1998), Power Flow Control with Rotary Transformers, US Patent 5,841,267.

[13] Larsen Einar V., (July 1999). A Classical Approach to Constructing A Power Flow Controller, Proc. IEEE/PES Summer Meeting, Edmonton, Canada, 1192 – 1195.

[14] Mathur, R.M., Basati, R.S., (May 1981). A Thyristor Controlled Static Phase-Shifter for AC Power Transmission, IEEE Transaction on Power Apparatus and Systems, Vol. PAS-100, No.5, 2650-2655.

[15] Norozian, M., Ãnbquist, L., Ghandhari, M., Andersson, G., (October 1997). Improving Power System Dynamics by Series-Connected FACTS Devices, IEEE Transactions on Power Delivery, Vol. 12, No.4, 1635-1641.

[16] Norozian, M., Andersson, G., (July 1993). Power Flow Control by Use of Controllable Series Components, IEEE Transaction on Power Delivery, Vol. 8, No.3, 1420-1429.

[17] Ooi, Boon Teck, Dai, Shu Zu, Wang, Xiao, (April 1992). A Solid-State Capacitive Reactance Compensators, IEEE Transaction on Power Delivery, Vol. 7, No.2, 914-917.

[18] Ooi, Boon Teck, Dai, Shu Zu, Galiana, Francisco D., (April 1993). A Solid-State PWM Phase-Shifter, IEEE Transaction on Power Delivery, Vol. 8, No.2, 573-579.

[19] Richardson, Donald V., (1978). Rotating Electric Machinery and Transformer, Technology, Prentice-Hall Company.

[20] Sana Abdou-Rahmanni, (2001). Exploitation Asymétrique des Réseaux de Transport d'Énergie Électrique, Ph. D thesis, École Polytechnique de Montréal.

[21] Sana, A.-R., McGillis, D.T., Marceau R.J., Do, X.D., Olivier, Guy, (May 2000). Asymmetrical Operation of Corridor With One Single Line, Proceedings, IEEE-CCECE'2000, Halifax, NS, Canada, 936-939.

[22] Sana, A.-R., McGillis, D.T., Marceau R.J., Do, X.D., Todde, C., (June 1999). On the Asymmetrical Operation of Transmission Systems, Proceedings of CIGRE Symposium on Working Plant and Systems Harder,London, U.K.

[23] Sana, A.-R., Marceau R.J., Todde, C., Do, X.D., Mahseredian, J., Joos,G., (May, 1998). L'Exploitation Asymétrique des Réseaux de Transport d'Énergie Électrique, Proceedings, IEEE-CCECE'98, , Waterloo, Ontario, 485-488.

[24] Sarma, Mulukutla S., (1985). Electric Machines Steady-State Theory and Dynamic Performance, WM.C. Brown Publishers.

[25] Sen, Kalyan K., (January 1998). SSS – Static Synchronous Series Compensator: Theory, Modeling, and Applications, IEEE Transactions on Power Delivery, Vol. 13, No.1, 241-246.

[26] Todde, C., Marceau R.J., McGillis, D.T., Lefebvre, S., Sana, A.-R., (May 1999). An Investigation into the Compensation of Asymmetrical Systems, Proceedings, IEEE-CCECE'99, Edmonton, Alberta, 187-1190.

Appendix **Sum of vector $e^{j\alpha 1}$ and vector $e^{j\alpha 2}$**

The sum of vector $e^{j\alpha 1}$ and vector $e^{j\alpha 2}$ is illustrated in Figure 3.7.

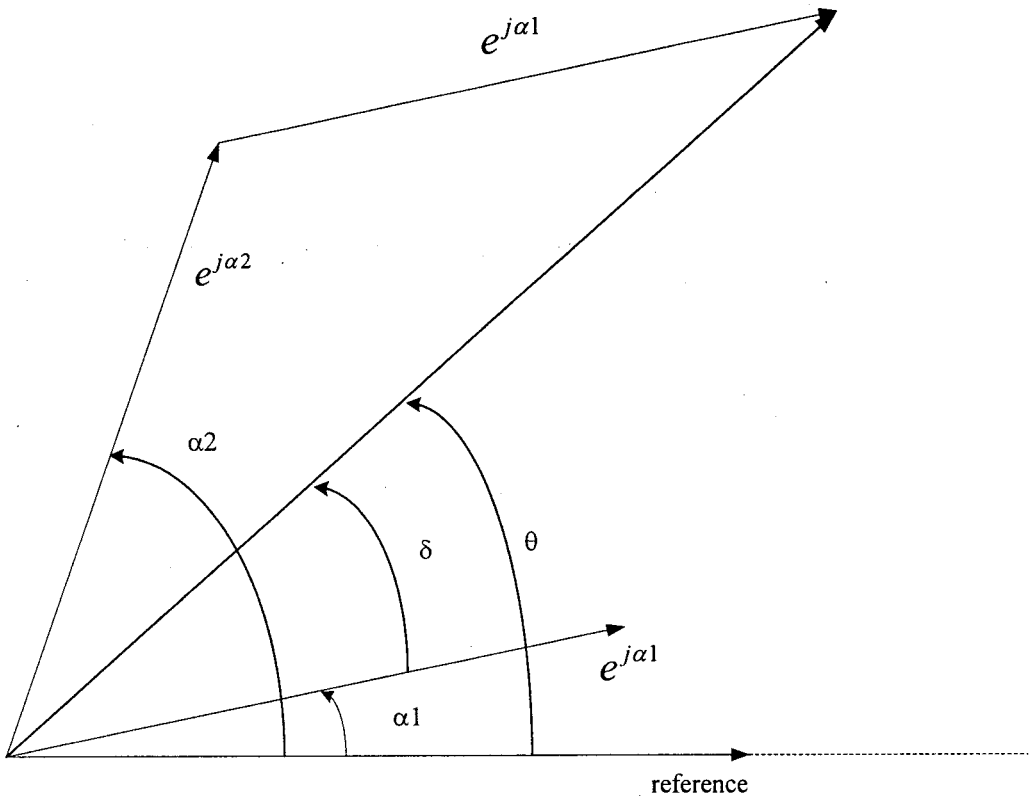

$$e^{j\alpha 1} + e^{j\alpha 2} = 2\left|\cos\delta\right|e^{j\theta}$$

$$e^{-j\alpha 1} + e^{-j\alpha 2} = 2\left|\cos\delta\right|e^{-j\theta}$$

where $\delta = \dfrac{\alpha 2 - \alpha 1}{2}$, $\theta = \dfrac{\alpha 2 + \alpha 1}{2}$